LIBRARY
Michigan State
University

This is to certify that the
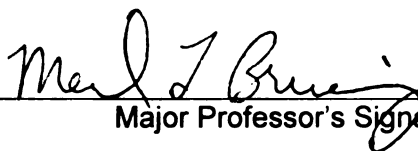dissertation entitled

Characterization and Manipulation of Vesicles Formed from
1,2-Butylene Oxide/ Ethylene Oxide Diblock Copolymers

presented by

John Keith Harris

has been accepted towards fulfillment
of the requirements for the

_____Ph.D._____   degree in   ___Department of Chemistry____

_____
Major Professor's Signature

_____December 5, 2003_____

Date

PLACE IN RETURN BOX to remove this checkout from your record.
TO AVOID FINES return on or before date due.
MAY BE RECALLED with earlier due date if requested.

DATE DUE	DATE DUE	DATE DUE

CHARACTERIZATION AND MANIPULATION OF VESICLES FORMED FROM 1,2-BUTYLENE OXIDE/ ETHYLENE OXIDE DIBLOCK COPOLYMERS

By

John Keith Harris

A Dissertation

Submitted to
Michigan State University
in partial fulfillment of the requirements
for the degree of

DOCTOR OF PHILOSOPHY

Department of Chemistry

2003

ABSTRACT

CHARACTERIZATION AND MANIPULATION OF VESICLES FORMED FROM 1,2-BUTYLENE OXIDE/ ETHYLENE OXIDE DIBLOCK COPOLYMERS

By

John Keith Harris

Vesicular structures are promising materials for encapsulation applications, and vesicles composed from block copolymers are especially attractive in this regard because of their cost, purity, tunability and stability. However, vesicle formation generally requires specialized procedures. This dissertation demonstrates that 1,2-butylene oxide/ ethylene oxide di-block copolymers spontaneously form μm-sized, multi-lamellar vesicles ("onions") over a broad range of copolymer concentrations upon simple mixing with water. Slow copolymer hydration without agitation produces giant vesicles with diameters greater than 0.1 mm.

This behavior is consistent with a geometric argument that asserts vesicle formation is preferred only when the proper ratio of hydrophobe volume to the product of head group area and hydrophobe length is achieved. The relatively large volume to length ratio of the butylene oxide hydrophobe is critical to vesicle formation, but formation also depends on the ethylene oxide head group length. For BO block lengths 15 units or less, BO/EO copolymers with EO blocks between 5 and 15 units long spontaneously form large

MLVs upon simple mixing with water. EO lengths greater than 15 result in small vesicles or no vesicles at all. We also found that EO block length polydispersity strongly affects structure formation. Substitution of an SO_3^- group for the EO block produced small vesicles, further evidence that the BO geometry is key. For BO/EO copolymers with BO block lengths of 15 to 25 units, ultra-sonication is required for vesicle formation, and the resulting structures have diameters of about 70 nm.

BO/EO MLVs formed by hand-shaking have shelf lives of over 2 years and survive thermal cycling, mild sonication and moderate shear. In contrast, extrusion of the same dispersion through a porous membrane reduces vesicle sizes, although final structure diameter is independent of shear rate and the pore size used for extrusion. Vesicle formation is reversed by thermal cycling. Ultra-sonication also reduces structure diameter.

Copolymer composition was analyzed using nuclear magnetic resonance (NMR), gel permeation chromatography (GPC) and mass spectrometry (MS). Vesicle capacity for encapsulating both hydrophobic and hydrophilic materials was explored. Phase diagrams were prepared of the copolymer, a model hydrophobe and water. The release rate of an encapsulated hydrophile was also studied. Structures were characterized using plane-polarized light microscopy, dynamic light scattering and cryogenic scanning electron microscopy.

To Sharon, my "pearl of great price".

All the wonderful events of my life have happened with you at my side.

ACKNOWLEDGEMENTS

TABLE OF CONTENTS

Chapter 1. Introduction to Vesicle Formation

Chapter 2. Synthesis and Characterization of 1,2-Butylene Oxide/ Ethylene Oxide Diblock Copolymers

Chapter 3. Effect of Butylene Oxide and Ethylene Oxide

Block Length on Structure Formation

Chapter 4. Vesicle Characterization and Stability

Chapter 5. Spontaneous Vesicle Formation from

Poly(1,2-Butylene Oxide) Sulfate Oligomers

Chapter 6. Summary and Future Work

Appendix A   Geometric Limitations Imposed by Surfactant Packing Shape

Appendix B   Processing the Mass Spectrometry Data

List of Schemes

List of Tables

List of Figures

Chapter 1

Introduction to Vesicle Formation

1.1 *Molecular Self-assembly and Overview of the Dissertation*

Micrometer- and nanometer-sized structures are employed in applications ranging from material modification to encapsulation. Nevertheless, synthesis of micro- or nano-structures such as exfoliated clays, inorganic nanoparticles, carbon nanotubes, hollow latexes, and hollow polyelectrolyte spheres is generally labor or energy intensive.[1-4] Development of systems that self-assemble at the molecular level to yield such structures should significantly reduce the effort required to produce large quantities of micro- and nano-materials.[5] Such self-assembly systems could be driven either kinetically or thermodynamically.

A thermodynamic mechanism for molecular self-assembly already exists for selected molecules and offers several advantages over conventional processes for micro- and nano-structure generation. The process is an equilibrium condition, however, and requires careful control over molecular architecture and environmental conditions to function correctly. Because the self-assembled structure is the preferred molecular state, these compounds generally have high yields and reduced levels of waste material. Self-assembly also provides fine control over material properties because structure formation is governed at the molecular level, where small changes can dramatically alter structure energies and geometries.[6,7] This allows tailoring of structure properties (i.e., size, shape or durability) using only slight changes in environment or molecular composition. Additionally, because the desired structure is the preferred molecular arrangement, minimal defects occur leading to improved material properties.[8]

1

While development of a self-assembling system requires careful control of molecular architecture and environmental conditions, numerous examples of such systems exist. In nature, phospholipids self-assemble into vesicles, the protective membranes that house biological cells and protect them from a hostile environment. Phospholipids form an encapsulating molecular bilayer that is robust, flexible and self-repairing. The bilayer can also be perm-selective, allowing for controlled transmembrane transport, and modification of vesicle surfaces permits partitioning of structures into selected environments such as specific biological domains or organs. These properties make vesicles ideal candidates for a host of encapsulation applications including improved drug solubility, increased "release-rate" control, enhanced biological imaging techniques, and artificial cells for oxygen transport or artificial photosynthesis.[9-13] Vesicular structures have also been used as additives for modification of polymer material properties.[14]

Unfortunately, phospholipids have inherent operational limitations as well as processing constraints. Synthesis and purification of these materials is costly, and vesicle formation often requires additives and development of highly specific formulations. Structure generation can also be laborious and time consuming. Finally, phospholipid structures frequently have limited stability during exposure to thermal variations, salinity changes, shear or organic solvents.

In an effort to overcome the limitations of phospholipids, this work explores the use of selected diblock copolymers as vesicle-forming materials. Synthesis and purification of copolymers is often straightforward and can yield larger quantities of materials more quickly and at relatively lower cost than phospholipids. Rapid synthesis

2

also means that the effects of changes in monomer or block lengths on structure stability can be evaluated faster and more thoroughly and, once understood, these compositional changes should allow for tailoring of vesicle properties for specific applications. Specifically, this dissertation examines the formation of vesicles by a series of 1,2-butylene oxide/ ethylene oxide diblock copolymers. Copolymer synthesis is rapid and versatile, and allows for accurate control of block lengths. Moreover, 1,2-butylene oxide/ ethylene oxide (BO/EO) copolymers are innocuous, bio-compatible and inexpensive.

This dissertation is divided into six chapters. The first provides background information on the nature of surfactants, the driving force behind self-assembly, and the model that I use to explain the impact of the BO/EO copolymer geometry on structure formation. Chapter 2 then focuses on copolymer synthesis and characterization, while Chapter 3 examines the effect of block lengths and formation processes on structure formation. In Chapter 4, I discuss structure stability with respect to thermal and mechanical stresses, methods of altering the mean particle size and vesicle release rates. To better understand vesicle formation, I also prepared sulfonated butylene oxide oligomers, and Chapter 5 presents the vesicle-forming properties of these materials. Chapter 6 examines the conclusions of this work and proposes future research directions.

I chose 1,2-butylene oxide/ ethylene oxide diblock copolymers based on a fundamental understanding of the driving forces behind self-assembly and structure formation. To help explain this project and its goals, I present below a brief description of these forces and their effects on self-assembly. Section 1.2 discusses the fundamental interactions involved in solvation. In Sections 1.3 through 1.5, I address the driving forces behind surfactancy, self-assembly and structure formation. I describe the impact

of molecular geometry on structure size and shape in Section 1.6, and Section 1.7 discusses the nature of vesicles; their properties, uses and limitations. I then show how others have used di- and tri-block copolymers to form self-assembled structures in Section 1.8. Finally, in light of these topics, Section 1.9 presents my reasoning for selecting 1,2-butylene oxide/ ethylene oxide copolymers for vesicle formation and the experimental course I pursued.

1.2 *Solvent-solute Interactions and Pair Potentials*

A heuristic principle of solvent-solute interactions is that "likes dissolve likes". From a thermodynamic perspective, this translates into a comparison of solute-solute and solvent-solvent interactions with solvent-solute interactions. The net force between any two molecules is called the pair potential and reflects the sum of the attractive and repulsive forces that exist between them. The similarity of the solute-solute and solvent-solvent pair potentials is the overriding factor determining solubility.

Israelachvili discusses pair potentials and the two dominant types of intermolecular forces that produce them.[15] The first forces are the electrostatic interactions that arise from fixed charges or permanent dipoles in the molecules. These forces act over short ranges and adhere to typical coulombic laws governing the interactions of charged species. The second forces result from induced dipoles and also extend over only a few Å.

If the solvent pair potential is comparable to the solute pair potential, solvation can occur spontaneously because the solute-solvent pair potential will likely be comparable to both the solute and solvent pair potentials, and entropy will drive

dissolution. Solute dissolution can affect the system free energy however, by changing the solute-solute or solvent-solvent pair potentials. For example, the solute molecule may be of sufficient size that it allows the solvent molecules to pack in a more efficient manner than occurs in pure solvent. The solution is then at a lower energy state than when either component was pure and solvation is generally observed as an exothermic reaction such as dissolving $MgSO_4$ in water. Systems such as this are extremely stable because there is no incentive for solute aggregation due to the high free energy costs.

Conversely, if the solute pair potential is lower than the solvent pair potential, solvation can occur only while additional energy, e.g., stirring, is provided. For instance, if the solvent molecules interact in a specific manner, such as a dipole-dipole orientation, and the solute molecule disrupts the "order" of the solvent system, then distributing the solute throughout the solvent would require an increase in the internal energy of the solution, an undesirable outcome. Therefore the lowest energy state occurs when the solute molecules are interacting with the fewest solvent molecules. Solutions produced from these solute-solvent systems would be precarious at best, because any loss of energy could initiate solute coalescence and lead to phase separation. Therefore, these systems generally require constant agitation or the solution transitions to a dispersion.

Finally, the solvent may induce some change in the solute dipole (or vice versa) that alters the net force between similar molecules. For example, ionization of the solute would convert the pair potential, which may have been mildly attractive in the uncharged state, to repulsive. Likewise molecules that had not been particularly polar when pure, may become polarized in the presence of selected solvents. Polyethers, for instance, become much more polar when dissolved in water than in their neat form. In this

5

manner, the solvent can create a physical change in the solute that alters the solute-solute pair potential.

To summarize, molecules vary chiefly in their polarity, or polarizability, which affects their tendency to interact. Aliphatic groups, like alkanes, have low polarizability and low interaction potentials, while water, which is highly polar, has a strongly attractive pair potential. In general, the more polar or polarizable a solute, the more polar the corresponding solvent must be for solvation to occur. As differences in polarity between solvent and solute increase, the solute solubility decreases.

It should be noted that the interaction potentials do not require homogeneity of the solute molecules. A sufficiently large solute could contain a polar, non-polar and polarizable group within the same molecule. The solvent molecules would interact with each group differently, generating a range of intermolecular forces that vary with the group polarity. In fact, molecules with different "groups" possess interesting and desirable properties.

1.3 *Amphiphiles and the Critical Micelle Concentration*

If the solute molecule is not homogenous with respect to polarity, that is, there are portions of the molecule that differ significantly in polarity from other portions of the same molecule, then solvent selection becomes more challenging. Molecules such as this are referred to as amphiphilic indicating that they are composed of at least two dissimilar fractions that prefer different solvents. These fractions are respectively labeled lyophilic ("solvent-loving") and lyophobic ("solvent-fearing") depending on the solvent used. With respect to water, the hydrophile is the polar group, typically ionic, but any

functional group that provides hydrogen-bonding sites will suffice. The hydrophobe is frequently an alkane, but any poorly polarizable group can serve this function. The hydrophile and hydrophobe are commonly referred to as the "head" and "tail", respectively, of the amphiphile.

Most amphiphilic molecules are not readily soluble in water.[16] Instead, upon mixing with water the amphiphile migrates to a surface, such as the air-water interface, where the hydrophobe can be displaced, at least partially, from the aqueous medium. Because of this tendency to move to a surface, amphiphiles are also called "surfactants". Once the interface is saturated with surfactant, however, any additional molecules must remain in the aqueous phase.

Amphiphile solubility is a function of its size and polarity. If the hydrophobe is sufficiently large, or if the concentration of amphiphiles is sufficiently high, it becomes thermodynamically unfavorable for the molecules to be dissolved in the aqueous phase. In this case, to minimize contact between the two incompatible components, i.e. the hydrophobe and water, the amphiphiles begin to assemble into structures. Once structure formation begins, the level of "free" surfactant, or monomer, in the system remains constant and all additional surfactant is incorporated into structures, or micelles. The concentration at which structures begin to form is called the critical micelle concentration, or CMC.

The CMC is determined by tracking specific physical phenomena of the system such as turbidity or surface tension as a function of surfactant concentration. However, regardless of the technique employed, CMC determinations have an inherent level of uncertainty and are somewhat method-dependent.[17] Examination of more than one

system property may be required to obtain precise CMC values. Nonetheless an approximate CMC value is usually sufficient for self-assembly studies.

In aqueous systems, a balance of three physical properties determine the CMC (Figure 1.1). The hydrophobe insolubility is balanced against the hydrophile solubility, which is dependent on factors such as the hydrophile-water pair potential, the number and accessibility of hydrogen-bonding sites, and hydrophile-hydrophile interactions.[18] Additionally, repulsive interactions between head groups will increase surfactant solubility, while attractive interactions reduce solubilization and facilitate longer range interactions such as gel formation or other rheological changes. In general, surfactants with ionic head groups have higher CMCs than those with nonionic head groups for a given hydrophobe.[18] Increasing the magnitude of the amphiphile's hydrophilic portion will increase CMCs slightly while increasing the hydrophobic portion will significantly decrease the CMC. Micellization, however, is not due to an attraction between the
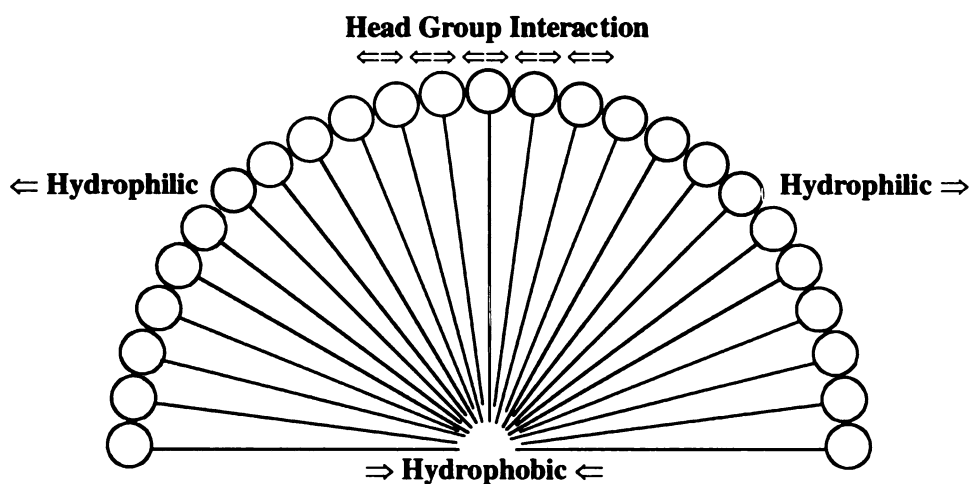
Figure 1.1. The balance of forces acting on surfactant molecules to produce micelles. (Shown as hemi-micelle).

8

hydrophobic groups. Tanford has shown that hydrophobes have about the same pair
potential with water as they do with each other,[19] which is much lower than the water pair
potential. The next section explains the driving force behind micellization.

1.4 *The Thermodynamics of Micellization*

Micellization is a thermodynamically driven process[18] and both phase-separation
and mass-action models can describe this reaction.[20] Rosen used work by Molyneux and
Birdi to present an explanation of micellization based on the phase-separation model, and
I follow that treatment here.[21,22] Equations 1.1 to 1.3 show the micellization reaction and
the chemical potentials of the surfactant in the aqueous, μ_{mon}, and micellar, μ_{mic}, phases.

$$\text{Hydrophobe}_{mon} \xleftrightarrow{\Delta} \text{Hydrophobe}_{mic} \qquad \text{eq. 1.1}$$
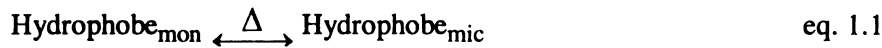
$$\mu_{mon} = \mu^{\circ}_{mon} + RT \ln a_{mon} \qquad \text{eq. 1.2}$$

$$\mu_{mic} = \mu^{\circ}_{mic} + RT \ln a_{mic} \qquad \text{eq. 1.3}$$

The chemical potential gives the total molar free energy for the molecules including the
pair potential and contributions from its thermal energy. The difference in molar free
energy between the states ($\mu_{mic} - \mu_{mon}$) is the free energy change on micellization,
ΔG°_{mic}, and is given by equation 1.4.

$$\Delta G^{\circ}_{mic} = (\mu^{\circ}_{mic} + RT \ln a_{mic}) - (\mu^{\circ}_{mon} + RT \ln a_{mon}) \qquad \text{eq. 1.4}$$

At equilibrium, $\Delta G^{\circ}_{mic} = 0$, and substitution of $K = a_{mic}/ a_{mon}$, produces equation 1.5,

$$\Delta G^{\circ}_{mic} = -RT \ln K \qquad \text{eq. 1.5}$$

where $\Delta G^{\circ}_{mic} = \mu^{\circ}_{mic} - \mu^{\circ}_{mon}$. Birdi and Molyneux also assumed that the amphiphiles
behave as a pure phase in the micelle (activity of 1) and as if at infinite dilution (activity

9

coefficient of 1) in the aqueous phase. Thus, the standard-state free energy change on micellization as a function of the surfactant concentration is given by equation 1.6, where X_{CMC} is the mole fraction of surfactant molecules dissolved in water at the CMC. (Below the CMC, micellization cannot be an equilibrium process as ΔG will be greater than zero, and once the CMC is reached, X_{CMC} is constant because all added surfactant forms micelles.)

$$\Delta G^{\circ}_{mic} = -RT \ln X_{CMC} \qquad \text{eq. 1.6}$$

Of course, ΔG°_{mic} can be expressed as a function of enthalpy, ΔH°_{mic}, and entropy, ΔS°_{mic}, changes (eq 1.7).

$$\Delta G^{\circ}_{mic} = \Delta H^{\circ}_{mic} - T\Delta S^{\circ}_{mic} \qquad \text{eq. 1.7}$$

If the micelles do not interact to facilitate or interfere with additional micelle formation, then ΔH°_{mic} and ΔS°_{mic} should be relatively constant over the temperature range examined. Thus, the derivative of ΔG°_{mic} with respect to temperature is given by equation 1.8.

$$d(\Delta G^{\circ}_{mic})/dT = -\Delta S^{\circ}_{mic} \qquad \text{eq. 1.8}$$

By monitoring the change in CMC with respect to temperature, the free energy can be used to determine the system entropy change on micellization. Likewise, if ΔS°_{mic} is held constant over the same temperature range, the change in enthalpy can be described by equation 1.9. Using these equations, the changes in free energy, enthalpy and entropy of micellization can be determined as a function of the surfactant

$$T^2 d(\Delta G^{\circ}_{mic}/T)/dT = -\Delta H^{\circ}_{mic} \qquad \text{eq. 1.9}$$

10

concentration in the system. The data from numerous studies on many types of surfactants produce a consistent pattern: negative free energy changes on micellization typically result from large positive changes in ΔS°_{mic}. Frequently the change in enthalpy, ΔH°_{mic}, is positive, but even when negative, the value of $T\Delta S^{\circ}_{mic}$ dominates the free energy change. Thus, the process of micellization is driven principally by entropy gains. How then, does molecular self-assembly lead to increased entropy in the system?

There are two explanations for this entropy increase. Aranow and Witten[23] suggest that water molecules surrounding the hydrophobe restrict its rotation about its C-C bonds. This reduces the hydrophobe's configurational entropy, forcing it to maintain an elongated and rigid shape. In a spherical micelle however, the hydrophobe is partitioned into the center of a sphere filled with other hydrophobic moieties. This should yield a configurational entropy similar to that possessed by the hydrophobe in its pure, liquid state.

The second explanation focuses on the organization of water molecules surrounding the hydrophobe.[24] Shinoda performed an extensive study of enthalpy changes that occur during micellization and concluded that at low temperatures, the presence of the hydrophobe reduces the number of hydrogen-bonding sites accessible to the water molecules surrounding it.[25] Fewer sites mean that the hydrogen-bonds that do form tend to be less flexible. This produces a rigid network of water molecules, a "pseudo-ice" state, which decreases the system entropy. Minimizing the number of water molecules in direct contact with the hydrophobe minimizes the formation of this rigid state and increases the system entropy. Thus, hydrophobe aggregation to reduce contact

11

with water is entropically highly favorable. Geometrically the structure with the smallest surface area to volume ratio is the sphere, therefore surfactants assemble in spherical structures whenever possible to minimize contact with water.

Further work by Evans[26] and Beesley et al.[27] showed that micellization requires that solvent molecules contain multiple hydrogen-bonding sites. Strong hydrogen bonds provide the driving force for cooperative interactions among solvent molecules at the hydrophobe surface. Hence, aqueous surfactant assembly is not due to attraction between hydrophobes, but rather occurs as an expression of hydrophobe expulsion by water. The hydrophobes are forced together by the strong attraction of water molecules to one another and the need to maintain the mobility of these molecules.

1.5 *Aggregation Numbers*

Section 1.4 described the entropic driving force behind micellization but said nothing of the size, shape or lifetimes of the micelles themselves. To gain a better understanding of micellar structures and any intermediate aggregates that the monomers may form, I now examine the thermodynamics of the surfactant system as a function of aggregation number.[15,19] Clint presents an in-depth discussion of the multiple equilibrium model using statistical thermodynamics.[19] To begin, I assume that the surfactant is in one of two states; a solvated monomer unit, M, or in an aggregate structure composed of N molecules, M_N, as shown in equation 1.10. In this model,

$$N M \underset{\longleftarrow}{\overset{\Delta}{\longrightarrow}} M_N \qquad\qquad \text{eq. 1.10}$$

I do not consider the aggregate as a separate phase. Equating the chemical potentials for the aggregation reaction gives equation 1.11 where I substitute "k" for "R" to indicate

that the free energies are per molecule. Note that X_N is the mole fraction of surfactant

$$N \mu^o_M + NkT \ln X_M = \mu^o_N + kT \ln (X_N/N) \qquad \text{eq. 1.11}$$

molecules in structures with aggregation number N. Thus X_N/N is the micellar

concentration of structures having aggregation number, N. Dividing equation 1.11 by N

yields equation 1.12, where $\mu^{o'}_N$ is the standard state chemical potential of a surfactant

molecule in the aggregate, rather than the aggregate itself.

$$\mu^o_M + kT \ln X_M = \mu^{o'}_N + kT/N \ln (X_N/N) \qquad \text{eq. 1.12}$$

To completely define the system, I need only remember that the total solute concentration

is given by equation 1.13 (See Figure 1.2). Solving this equation for X_N gives

$$C = X_1 + X_2 + X_3 + \ldots = \sum_{N=1}^{\infty} X_N \qquad \text{eq. 1.13}$$
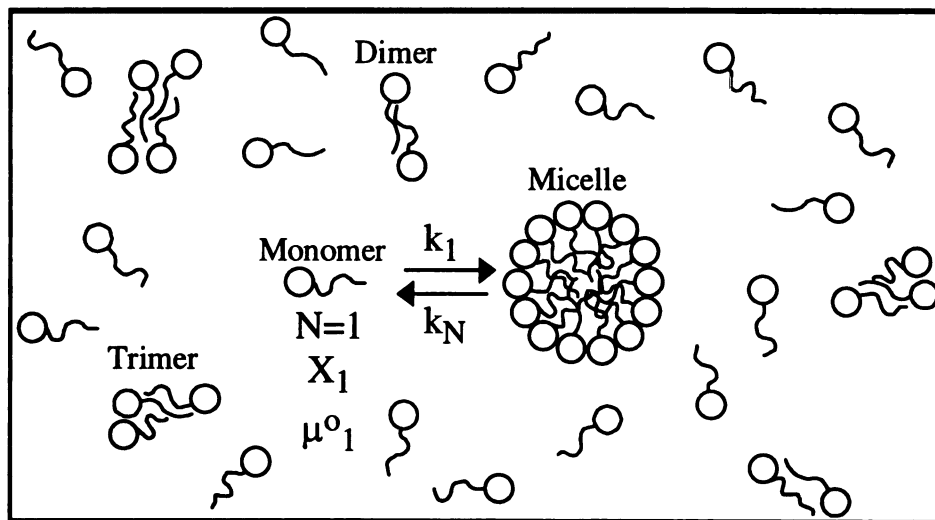
Figure 1.2. Various states of surfactant aggregation within the bulk solution. Adapted from Israelachvili, *Intermolecular and Surface Forces.*[28]

equation 1.14 which allows us to directly compare the surfactant population in each of the aggregate states as a function of surfactant concentration in the monomeric state.

$$X_N = N\{X_1 \exp[(\mu^o_1 - \mu^{o'}_N)/kT]\}^N \qquad\qquad \text{eq. 1.14}$$

This equation shows that, as expected, when $\mu^o_1 - \mu^{o'}_N = 0$, then $X_1 = X_N$ because if there is no chemical potential difference, then there is no incentive for molecular aggregation based on a decrease in entropy. Note also that increasing values of N lead to exponentially decreasing values of X_N. That is, the larger the aggregation number, the fewer such structures form. For sufficiently low monomer concentrations, X_1, we find that $X_1 \gg X_2 \gg X_3 \gg \ldots X_N$. Thus, at low concentrations, most of the molecules will be independent monomers, such that $X_1 \approx C$. Additionally, if $\mu^{o'}_N$ is relatively constant with aggregation number, entropy losses greatly favor small aggregates. Equation 1.14 also suggests that there is a threshold concentration limit at which this equation is no longer true. Since X_N cannot be > 1, as X_1 approaches the value represented by $\exp[-(\mu^o_1 - \mu^{o'}_N)/kT]$, it can increase no further. This limit in monomer concentration occurs at the CMC as shown in equation 1.15. Thus, the greater the free energy change between monomeric and micellar surfactant molecules, the lower the CMC. The CMC is dependent almost entirely on the change in chemical potential that occurs as the hydrophobe moves from the water phase to the micelle interior. The value of N at this concentration is N_{min}, the minimum number of molecules necessary to stabilize the aggregate and produce a micelle.[29]

$$CMC \approx \exp[-(\mu^o_1 - \mu^{o'}_N)/kT] \qquad\qquad \text{eq. 1.15}$$

One final aspect of this model is the relationship of enthalpy gains to micelle size. Initially, $\mu^{o'}_N$ decreases substantially with increasing N due to entropic gains associated with excluding the hydrophobe from water. However as the structure size increases, the effective surface area per molecule decreases. If the head group is ionic, a repulsion develops as head groups are forced into closer contact. As shown in Figure 1.3, the balance of attractive and repulsive head-group interactions yields a minimum free energy state at some optimum head group area, a_0. Larger spherical aggregates have head-group areas that are energetically unfavorable, and the size distribution of micelle structures is centered about structures having the optimal head-group area.
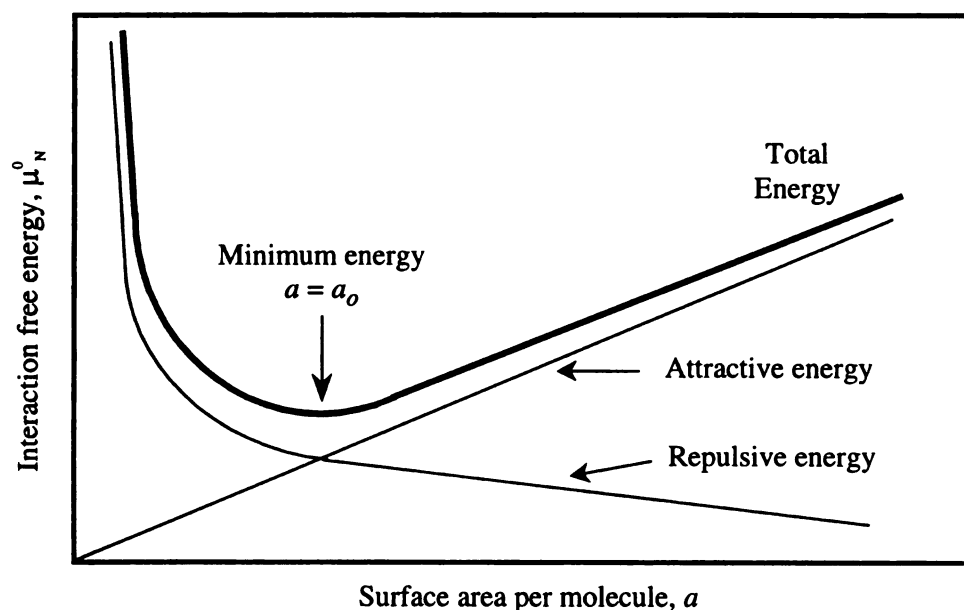
Figure 1.3. Optimum head group size as balance of attractive and repulsive forces. Adapted from Israelachvili, *Intermolecular and Surface Forces*.[28]

15

Therefore from a statistical thermodynamic approach we can see that while intermediate molecular aggregates are possible, they are not prevalent. Instead the dispersion is composed primarily of monomer until the concentration reaches a threshold level when a specific aggregate, the micelle, is formed. The model also shows the direct relationship between the chemical potential change per molecule and the CMC. Finally, this model suggests that a major factor limiting structure size is head group area.

1.6 *The Critical Packing Factor Model and Aggregate Shape*

In section 1.3, I described how amphiphilic molecules differ from typical solutes by possessing both a "solvent-loving" and "solvent-hating" portion. Section 1.4 showed that above a certain concentration these molecules form micellar structures. Structure formation is a thermodynamic process driven by the entropy gains of water as the hydrophobes are forced into a separate phase. The previous section (1.5) discussed the relationship between the aggregate size and its probability of formation. In this section I will describe how the size and shape of the hydrophobe and hydrophile influence the type (shape) of micellar structure formed. First, I will briefly describe the possible types of structures that can form, and then I will present a model explaining the factors that determine which structures form from a given surfactant.

The most commonly observed aggregate structure is the spherical micelle, though numerous other aggregate forms have been identified including elliptical, cylindrical, and worm-like micelles, discs, bilayers (continuous and discrete), and even reverse micelles (Figure 1.4).[30] Spherical micelles are dynamic structures that exist as unique entities for fractions of a second before disintegrating to form new structures milliseconds later.[19,31]

Their short lifetimes make them more reflections of a free-energy minimum than an actual organized unit. Increasing the size of the hydrophobe will decrease the CMC, and can increase the stability of structures, however, the same surfactant geometric properties must be maintained to produce spherical micelles. Typical spherical micelles have diameters slightly less than twice the length of the fully elongated hydrophobe.
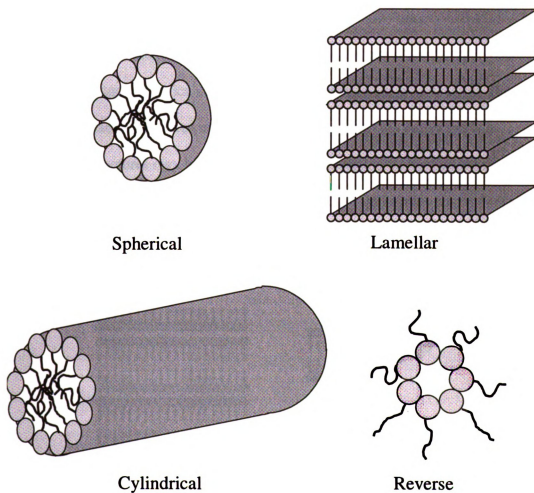
Figure 1.4. The four fundamental micellar self-assembled units.

Cylindrical micelles also have the hydrophobe partitioned to the structure center, but, because of a smaller head group, they are geometrically unable to form spheres. Instead, they produce a variety of aggregate shapes including rods, "threads" or "worms" depending on micellar length (longest dimension) and the frequency of bends in the structure. These micelles have a considerably larger aggregation number than spherical micelles and therefore tend to have longer average lifetimes.[32,33] Rod-shaped micelles must lose far more surfactant molecules before N drops below N_{min} and spontaneous disintegration of the structure takes place. Thus, while the rate of surfactant exchange between solution and cylindrical micelles is similar to that with spherical micelles, the size of the rod-shaped structures makes them exist as entities for longer periods.

Bilayer structures may be planar or flexible depending on the hydrophobe fluidity and the size and flexibility of the hydrophile (Figure 1.5). Molecules where the head group and hydrophobe diameters are nearly identical generally yield flat, planar

Rigid
Bilayer
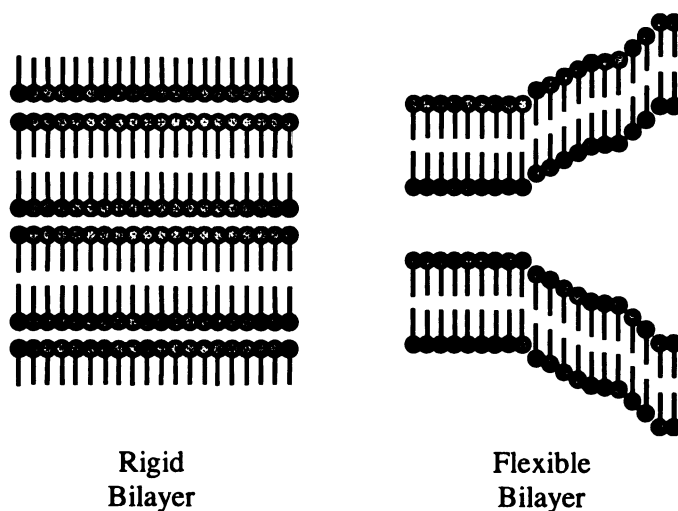
Flexible
Bilayer

Figure 1.5. Two types of aggregate bilayer structures; flexible and rigid.

structures such as micellar discs. When the head group is slightly larger than the hydrophobe, more flexible bilayers may create an extensive network, as in a bicontinuous, or sponge-phase, or may form discrete spherical structures called vesicles.For structure formation to occur, the surfactant standard state chemical potential in an aggregate must be less than that of the monomeric surfactant, $\mu^o_N < \mu^o_1$, (equation 1.15) for some value N. The value of N, while indicative of the number of monomers incorporated into each structure, does not identify the structure shape or explain why the various types of micelles form. Since self-assembly is entropically driven, one might expect that any shape that removes a similar number of hydrophobes from the aqueous phase would have a similar free energy change and therefore be equally likely to develop. This is not observed however. Instead, dispersions of "pure" surfactant (low variability in molecular composition) are typically populated by two surfactant states: the monomer and a distinct micellar structure suggesting that μ^o_N is not equal for all types of structures.

One model that describes why a single structure predominates, and defines the variables that influence the type of aggregate structures a given amphiphile will produce, is based on surfactant geometry and packing. As shown in Figure 1.1, both the hydrophobe insolubility and the hydrophile solubility significantly impact the surfactant CMC. Likewise, the shape of both the hydrophobe and the hydrophile impact the geometry of the micelle formed because of the packing constraints presented by each group. Israelachvili et al. described the constraints on micellar shape in terms of a critical packing factor (CPF), ϕ,[6] which is related to the hydrophobe volume, V, the critical chain length of the hydrophobe, l_c, and the optimum cross-sectional head group area, a_o, as

shown in equation 1.16. The value of ϕ is indicative of the type of micellar structure the amphiphile will form.

$$\phi = V / l_c \, a_o \qquad\qquad\qquad \text{eq. 1.16}$$

Figure 1.6 shows how values of V, l_c and a_o limit the possible shapes that the surfactant can assume, and thereby limit the types of aggregate structures the surfactant can form. For example, the combination of a large head group and a flexible tail of moderate length will generally produce the conical shape. If the head group shrinks, because of a change in salinity or temperature, the surfactant may form a truncated cone. Similarly, if the tail is replaced with a more bulky one, due to unsaturation or branching, its volume may increase and, again, the surfactant shape moves from conical to truncated

Conical   Truncated
Cone

Cylindrical   Inverted
Cone
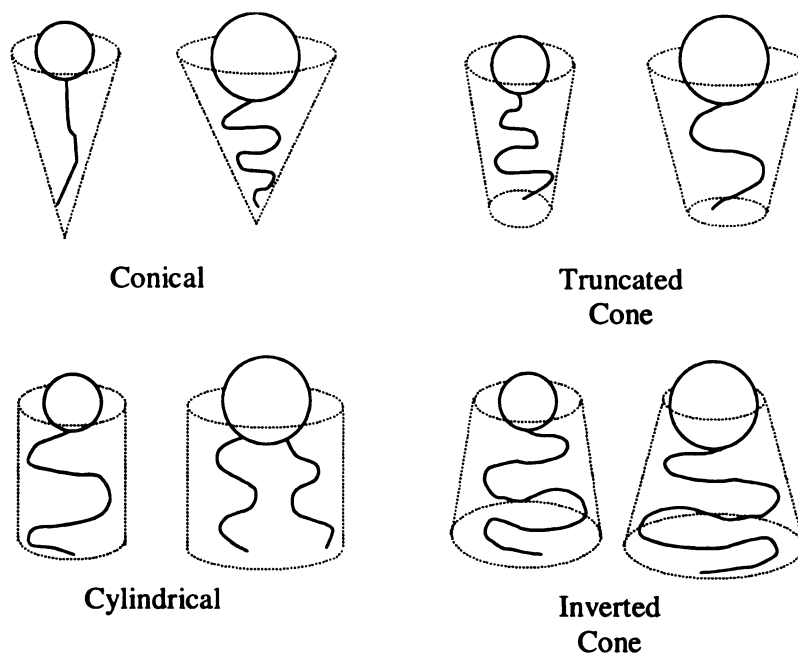
Figure 1.6. Eight basic packing configurations for various surfactant molecules in a micelle. Adapted from Israelachvili, *Intermolecular and Surface Forces.* [28]

cone. Some surfactants, like phospholipids, have multiple tails, giving the surfactant a cylindrical shape. Finally, amphiphiles with either small head groups or long or semi-rigid tails produce inverted cones. To be more quantitative, if the CPF lies between 0 and $1/3$, Israelachvili's model predicts that optimal packing will occur when the surfactant assumes a conical shape within a spherical micelle (Figure 1.6). (See Appendix A for more details on the packing factor model.) This occurs because the head group, a_o, is large and the tail group is narrow and flexible enough to allow the surfactant to form a tapered shape that readily packs into spheres. This head/ tail combination is common with mono-valent ionic surfactants having an aliphatic hydrophobe, although nonionic head groups of comparable diameter will also produce spherical and oblate micelles.

If the head group size is reduced, by the addition of salt or by blending of ionic and nonionic surfactants, or if a hydrophobe with a larger volume-to-length ratio is selected, then ϕ rises to between $1/3$ and $1/2$, and the surfactant adopts a truncated cone shape within a cylindrical micelle. These structures have a circular cross-section, but an elongated Z-axis.

When the head group diameter is similar to the hydrophobe diameter, then the CPF increases to between $1/2$ and 1, and the amphiphile molecules assume a cylindrical shape. These surfactants assemble into bilayered, or lamellar, aggregates. Lamellar structures consist of two surfactant monolayers paired such that the ends of the hydrophobes from the first layer contact the ends of the hydrophobes from the second. A CPF value closer to $1/2$ indicates a more flexible bilayer while a value near 1 indicates a planar structure (see Figure 1. 5). If the CPF value exceeds 1, reverse micelles form.

The critical hydrophobe chain length, l_c, is generally taken to be about 80 % of the tail's fully-elongated length.[34] The 20% reduction in length accounts for the normal, random movement of the tail in a liquid environment. Other variations in chain length and flexibility occur due to the twists and kinks associated with *cis* and *trans* conformations as well as the extent of saturation.

While the CPF model uses the optimum head group area, a_o, to predict structure type, the model remains valid when $a \neq a_o$, however these are metastable structures and do not represent the lowest energy state aggregates. In either case, the head group size depends on two factors: the hydrated hydrophile diameter and the extent of interaction between adjacent head groups. Ionic head groups are generally a single atom or a polyatomic complex and are treated as a point charge. They repel one another and present a slight resistance to micellization. Values of a for ionic surfactants depend on solvent ionic strength, the presence of organics, and temperature. Ionic head groups may also be influenced by the valency of the ions in solution.

Nonionic head groups, such as ethylene oxide, can interact and, under certain conditions, can form well-ordered systems. They usually contain multiple hydrophilic units rather than a single group and oppose micelle formation, but to a lesser extent than the ionic groups. (This is evidenced by the lower CMC values for surfactants with the same hydrophobe, but nonionic rather than ionic head groups.[18]) Solution salinity influences nonionic head group size, but to a lower extent than ionic groups, although nonionic groups are more temperature sensitive.

The head group area, a, depends on the model's location for the hydrophile/ hydrophobe interface. Once selected, the head group area then becomes the total

interfacial area divided by the aggregation number. While an absolute value of a is critical to some research, it is much less important to the work I will present. Instead I am primarily interested in how changes in head group size affect micellar structure. It is also important to mention that while the head group is generally modeled as a sphere, this approach is not applicable if the head "group" consists of multiple hydrophilic entities. For nonionic hydrophiles, which may be 20 times longer than a typical ionic group and consist of dozens of atoms, the head group "shape" is not obvious, and determination of head group area is complicated.

The most common head groups used in this work are ethylene oxide (EO) oligomers. The relationship between EO block length and head group area in micellar structures is not first order as it is at the air-water interface.[35] Instead, as the EO block is hydrated, it forms an expanding coil whose diameter is dependent on EO length.[36] The most pronounced changes in coil size, and hence head group area, occur with increases to shorter EO blocks. Alexandridis et al. showed that the head group area for EO_2 to EO_{10} varies with the square root of the number of EO units.[37] Thus, using an EO block as the hydrophile, one can generate various values of a_o simply by changing the block length during synthesis. The hydrophilicity of EO head groups decrease with increasing temperature due to changes to the water structure around the EO groups, changes in the hydrogen bonding to the EO groups and changes in the conformation of the EO group.[19] All contribute to reduce the EO head group area at higher temperatures. Note that Φ is inversely proportional to a_o, so decreasing the head group area is expected to produce larger structures. (See appendix A)

1.7 *Vesicles*

Vesicles form when selected surfactants self-assemble into a bilayer that curves in on itself to form a hollow, spherical nano-structure. The bilayers form closed structures to reduce contact between the water and the hydrophobic edge of the bilayer. While all bilayer structures suffer the free-energy costs of the "edge effect", only flexible lamellar structures can negotiate the bending necessary to form a closed structure and eliminate bilayer edges.

Vesicles may consist of a single or multiple bilayers (Figure 1.7). Single-bilayer vesicles are divided into three groups; small unilamellar vesicles (SUVs) with diameters of less than 100 nm, large unilamellar vesicles (LUVs) with diameters from 100 nm to 10 μm and giant unilamellar vesicles (GUVs) with diameters reported of up to approximately 5 mm.[38,39] While more time-consuming to prepare, LUVs offer an efficiency advantage over SUVs in terms of contained volume per mole of phospholipid.[40] Multi-lamellar vesicles (MLV) are composed of up to hundreds of
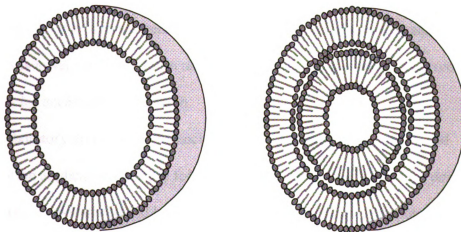
Figure 1.7. Two types of closed bilayer structures; uni-lamellar (left) and multi-lamellar (right).

concentric bilayer spheres. These structures are rarely less than 250 nm in diameter, but generally have the same upper size limits as LUVs. The separation between bilayers in an MLV is not fixed, and the number of layers contained in two MLVs of the same diameter could vary substantially.

Vesicles are of particular interest because of their encapsulation properties. They are found extensively in biological systems as cell membranes and display substantial barrier properties. The bilayer is robust, resilient and self-repairing, making these structures well suited for isolating their contents from the dispersing medium. The structure's aqueous core contains hydrophilic materials, while the bilayer interior sequesters hydrophobic while hydrophobic molecules (Figure 1.8). The bilayer can be modified for selected permeability, controlled release and system compatibility.

Although the question of whether or not vesicles are thermodynamically stable structures is debatable,[41,42] they can achieve a steady-state equilibrium with the bulk dispersion, and substantial shelf lives have been observed that range from weeks to years. While individual surfactant molecules may move laterally within a layer, the exchange rate between the two layers is generally low and the exchange rate with aqueous phase monomers is lower yet.[43] For these reasons and others, vesicles are considered ideal candidates for encapsulation research.

Laboratory preparation of vesicles was first reported by Bangham, and encapsulation applications quickly followed.[44] The use of vesicles as drug delivery agents was soon postulated and has recently received significant attention.[45,46] Fendler demonstrated the encapsulation of several amino acids and studied the effects of electrolyte and various encapsulated materials on vesicle stability.[47] Researchers have

used giant vesicles, which due to their low radius of curvature place less strain on the bilayer, as tools for studying selective transport across cell membranes.[48] Vesicles laden with contrast agents such as radiolabeled monoclonal antibodies, ferrites or paramagnetic materials, have successfully increased imaging quality in physiological studies.[49] Research has also been conducted using structures as modified solar collectors by loading the vesicles with photo-reactive materials.[9] Others have explored using vesicles as a blood substitute by packing the structures with hemoglobin.[50] Work by Meier has recently shown that modified vesicles can function as enzymatic nano-reactors.[51] Natural lipids, particularly phospholipids and lipid/ cholesterol mixtures, are the most commonly used materials for vesicle formation. A phospholipid consists of a phosphate hydrophile
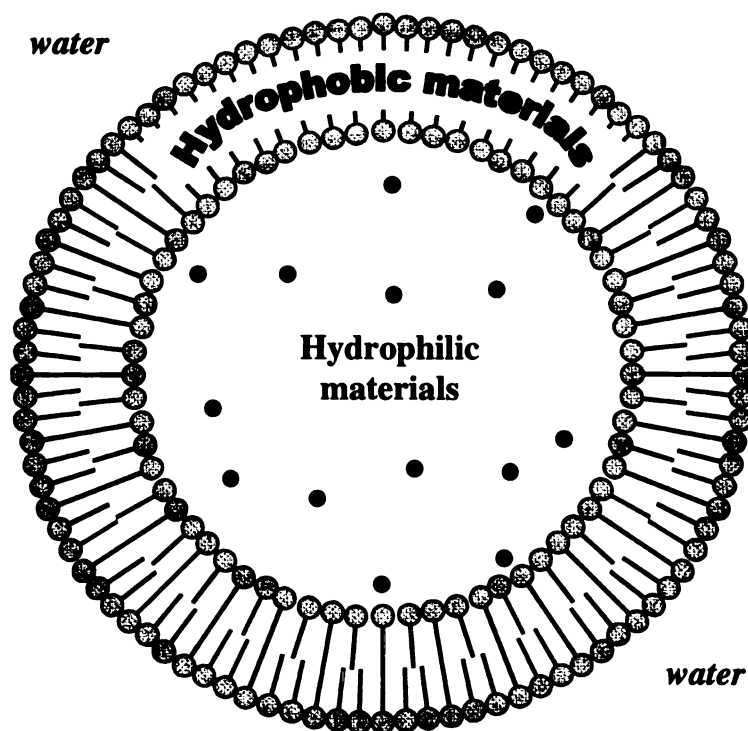
Figure 1.8. Two regions of vesicle structure are potential encapsulation areas.

and generally a diglyceride containing two similar-length aliphatic hydrophobes. Variations in hydrophobe length and saturation, as well as variations in head group substituents, produce a wide range of phospholipids. As a result, numerous vesicular structures of varying sizes and stabilities can be produced from these materials.

Vesicle generation processes are often time-consuming or elaborate.[31,40] Typically the phospholipid is mixed with other lipids or cholesterol to modify the physical characteristics of the bilayer and make vesicle formation easier. In a common preparation procedure, the mixture is dissolved in an organic solvent, filtered, cast as a film and dried (frequently freeze-dried) before phase separation of the phospholipid from the additives can occur. The dried film is then slowly hydrated with a solution of salts, buffers, and other additives and/ or stabilizers to produce structures. After initial swelling the mixture can be hand-shaken or ultra-sonicated to accelerate structure formation. More elaborate processes, which involve aggressive agitation, extensive dialysis, solvent exchange, solvent injection and even oscillating electric fields, are common. Finally, the structures are homogenized using extrusion, freeze/ thaw cycles or sonication to produce a narrow size distribution. Once homogenized, the vesicles can also be readily separated from residual materials in the aqueous phase by mechanical or gel filtration. Final structures can be characterized using aqueous size exclusion chromatography, light scattering techniques, optical microscopy, cryo-scanning electron microscopy and cryo-transmission electron microscopy.

Although formation of vesicles from phospholipids is common, lipids possess inherent chemical and mechanical limitations restricting their applicability as encapsulants.[52] Besides the preparation difficulties, the structures tend to be temperature,

shear and saline sensitive making them vulnerable in certain environments. The phosphate head group, like most ionic species, is strongly influenced by the presence of salts in the aqueous phase,[53] and certain solvents can selectively remove the additives, destabilizing the structures. The hydrophobes frequently have a phase transition temperature that limits their thermal stability as well.[31] Attempts have been made over the past four decades to improve the stability of phospholipid-based vesicles by chemical modification of the lipid and in situ polymerization of the structure.[54,55] However, these have met with limited success and have, in turn, introduced new complications to structural stability.

1.8   Block Copolymers

Some limitations of phospholipid vesicles can be overcome by using amphiphilic block copolymers as surfactants. Block copolymer synthesis can be a simple, well-understood process that involves a single step per block, and typical syntheses have high yields and do not require extensive product purification. Thus, in most cases, copolymers are much less expensive than phospholipids. Block copolymers can also be synthesized with specific physical properties, such as morphology or melting point, by selecting the appropriate hydrophobic or hydrophilic monomer. The asset of copolymers which is of most interest to this work, however, is the ability to produce surfactants with varying geometric shapes by appropriate selection of monomer type and block length.

Block copolymer surfactants can form a variety of aggregate structures. Using a solvent exchange method, Laibin and Eisenberg showed that polystyrene/ poly(acrylic acid) diblock compositions form a myriad of structures and complex shapes in an

aqueous system.[56] Alexandridis studied ethylene oxide/ propylene oxide/ ethylene oxide

(EO/PO/EO) mixtures in xylene/ water systems and found numerous aggregate structures

such as spherical and rod-shaped micelles, lamellae and reverse micelles.[57] Ding and Liu

produced vesicles in solvent mixtures of THF and hexane using polyisoprene/ poly(2-

cinnamoylethyl methacrylate),[58] and Meier prepared vesicles in water with several siloxyl

containing copolymers.[59] Using poly(amino acids), Tirrell has produced materials that

form vesicles, as well as other structures, in water.[60] In spite of these successes,

preparation of a copolymer specifically for vesicle formation is not trivial.

There remains an unmet need for a material which is easy to synthesize, bio-

compatible and which forms structures without the need for solvents. The ideal

compound could be tailored to produce range of structure sizes for various applications.

A copolymer that would allow for preparation of elevated vesicle concentrations would

advantageous as well. Additionally, improved stability, high loading capacities and

increased release rate control would be beneficial in any encapsulation application.

1.9   *1,2-Butylene oxide/ Ethylene oxide Diblock Copolymers*

The previous examples show that both ionic and nonionic surfactants can form

vesicles, however nonionic surfactants offer several advantages over ionic materials.

Nonionic copolymers demonstrate lower pH and saline sensitivity than ionic surfactants,

and vesicles produced from nonionic copolymers would be expected to show this same

reduced sensitivity.[61] Nonionic amphiphiles generally have lower CMCs, so vesicles can

be prepared at lower concentrations with a higher fraction of surfactant in the structures.

Ethoxylated copolymers have inherent biocompatibility, making them appealing as drug

delivery agents.[62] Finally, the head group size of an ethoxylated material can be easily altered by adjusting the ethoxylate block length during synthesis.[61]

Several groups examined structure formation with ethoxylated copolymers. Maskos and Harris demonstrated vesicle formation from 1,2-butadiene/ ethylene oxide copolymers and successfully cross-linked these structures after formation.[63] Discher et al. demonstrated large vesicle formation from ethyl ethylene/ ethylene oxide diblock copolymers and showed that these structures display mechanical stabilities 10 times greater than phospholipid-based structures.[64] Alexandridis studied butylene oxide/ ethylene oxide (BO/EO) diblock copolymers and found that they formed more than six different structural phases in a ternary copolymer/ water/ xylene system, although no vesicles were observed,[65] while Booth focused on using BO/EO copolymers as gel formers for possible application as drug delivery agents.[66,67] He extensively explored BO/EO micellar behavior, however he consistently worked with materials that have a larger head group than the CPF model predicts will form vesicles.

The 1,2-butylene oxide (BO) group offers several advantages as a hydrophobe. A BO unit displays about the same free energy change on micellization as a methylene group making it a substantial hydrophobe.[68] Hydrophobe length can be controlled using anionic polymerization and the BO block remains a liquid at molecular weights of more than 3000 amu. Additionally, the BO monomer is less prone to rearrangement than propylene oxide, so control of the hydrophobe shape is superior.[69] However, the BO volume-to-length ratio is the biggest factor in choosing it as a hydrophobe.

The CPF model indicates that phospholipids form vesicles because the large volume-to-length ratio of their two-tailed hydrophobe produces a cyclindrical surfactant

geometry that promotes bilayer formation. I believe that the large volume-to-length ratio

of the BO hydrophobe can produce the same results. However, the hydrophobe must be

matched with the proper size head group for vesicle formation to occur. Therefore I

surmised that butylene oxide/ ethylene oxide diblock copolymers would be potential

vesicle formers when prepared with the correct block lengths.

This work addresses the synthesis and characterization of low molecular weight

butylene oxide/ ethylene oxide diblock copolymers and examines their ability to form

vesicles in water. Remarkably, micron-sized vesicles form upon simple mixing of certain

copolymers with water. Vesicle formation is, however, a function of block length,

particularly the EO block length, and the CPF model correlates well the vesicle-forming

properties of different copolymers. BO/EO vesicles are stable over months and even

years, and release rates from these materials are very slow. One area that I have only

begun addressing is the development of polymerizable BO/EO surfactants. Given the

simplicity of vesicle formation form BO/EO copolymers, I anticipate that these materials

may have applications in a variety of encapsulation applications.

1.10 *References*

(1)   Jacoby, M. "Nanoscale Electronics"; *Chemical and Engineering News*, September 30, 2002, pp 38-43

(2)   Borman, S. "Chemistry Highlights 2001"; *Chemical and Engineering News*, December 10, 2001, pp 45-55

(3)   Borman, S. "Chemistry Highlights 2002"; *Chemical and Engineering News*, December 16, 2002, pp 42-47

(4)   Sauer, M.; Streich, D.; Meier, W. *Advanced Materials (Weinheim, Germany)* **2001**, *13*, 1649-1651.

(5)   Tanev, P. T.; Pinnavaia, T. J. *Science (Washington, D. C.)* **1996**, *271*, 1267-1269.

(6)   Israelachvilli, J. N.; Mitchell, D. J.; Ninham, B. W. *J. Chem. Soc., Faraday Trans. 2* **1976**, *72*, 1525-1568.

(7)   Fairley, P. "Nano Technology: The Start of Something Big"; *Chemical Week*, December 12, 2001, pg 23-26

(8)   Mueller, P.; Rudin, D. O.; Tien, H. T.; Wescott, W. C. Formation and Properties of Bimolecular Lipid Membranes. In *Recent Progress in Surface Science*; Danelli, J. F., Pankhurst, K. G. A., Riddiford, A. C., Ed.; Academic Press: New York, NY, 1964; Vol. 1, pp 379-393.

(9)   Sisido, M. Photoenergy harvesting on two-dimensional vesicular assemblies. In *Vesicles*, First ed.; Rosoff, M., Ed.; Marcel Dekker: New York, NY, 1996; Vol. 62, pp 563-592.

(10)   Tilcock, C. *Liposome Technol. (2nd Ed.)* **1993**, 65-87.

(11)   Chang, T. M. S. *Journal of Internal Medicine* **2003**, *253*, 527-535.

(12)   Gerasimov, O. V.; Rui, Y.; Thompson, D. H. Triggered Release from Liposomes Mediated by Physically and Chemically Induced Phase Transistions. In *Vesicles*, First ed.; Rosoff, M., Ed.; Marcel Dekker: New York, 1996; Vol. 62, pp 679-746.

(13)   Lasic, D. D. Liposomes in Drug Delivery. In *Vesicles*, First ed.; Rosoff, M., Ed.; Marcel Dekker: New York, 1996; Vol. 62, pg 448.

(14)   Dean, J. M.; Lipic, P. M.; Grubbs, R. B.; Cook, R. F.; Bates, F. S. *Journal of Polymer Science, Part B: Polymer Physics* **2001**, *39*, 2996-3010.

(15)   Israelachvili, J. N. *Intermolecular and Surface Forces*, 2nd ed.; Academic Press: San Diego, CA, 1992; pp 16-21.

(16) Clint, J. H. *Surfactant Aggregation*; Chapman & Hall: New York, NY, 1992; pp 1, 2.

(17) Myers, D. *Surface Science and Technology*; VCH Publishers: New York, NY, 1988; pg 106.

(18) Rosen, M. J. *Surfactants and Interfacial Phenomena*, Second ed.; Wiley-Interscience: New York, NY, 1989; pp 120-133.

(19) Clint, J. H. *Surfactant Aggregation*; Chapman & Hall: New York, NY, 1992; pp 100-115.

(20) Myers, D. *Surface Science and Technology*; VCH Publishers: New York, NY, 1988; pg 96.

(21) Molyneux, P.; Rhodes, C. T.; Swarbrick, J. *Transactions of the Faraday Society* **1965**, *61*, 1043-1052.

(22) Birdi, K. S. *ACS Symposium Series* **1975**, *9*, 233-238.

(23) Aranow, R. H.; Witten, L. *Journal of Physical Chemistry* **1960**, *64*, 1643-1648.

(24) Franks, H. S.; Evans, M. W. *Journal of Physical Chemistry* **1945**, *13*, 507.

(25) Shinoda, K. *Journal of Physical Chemistry* **1977**, *81*, 1300-1302.

(26) Evans, D. F. *Langmuir* **1988**, *4*, 3-12.

(27) Beesley, A. H.; Evans, D. F.; Laughlin, R. G. *Journal of Physical Chemistry* **1988**, *92*, 791-793.

(28) Israelachvili, J. N. *Intermolecular and Surface Forces*, 2nd ed.; Academic Press: San Diego, CA, 1992; pp 345-372.

(29) Wall, S. N.; Aniansson, G. E. A. *Journal of Physical Chemistry* **1980**, *84*, 727-736.

(30) Rosen, M. J. *Surfactants and Interfacial Phenomena*, Second ed.; Wiley-Interscience: New York, NY, 1989; pp 112-114.

(31) Fendler, J. H. *Membrane Mimetic Chemistry: Characterizations and Applications of Micelles, Microemulsions, Monolayers, Bilayers, Vesicles, Host-Guest Systems, and Polyions*; John Wiley and Sons: New York, NY, 1982; pp 25, 26.

(32) Shioi, A.; Harada, M.; Adachi, M. *Recent Research Developments in Physical Chemistry* **1999**, *3*, 149-182.

(33) Aniansson, G. E. A. *Progress in Colloid & Polymer Science* **1985**, *70*, 2-5.

(34) Tanford, C. *The Hydrophobic Effect: Formation of Micelles and Biological Membranes*, Second ed.; WIley-Intersciences: New York, NY, 1980; pg 52.

(35) Schick, M. J. *J. Colloid Sci.* **1962**, *17*, 801-813.

(36) Schick, M. J. *J. Am. Oil Chemists' Soc.* **1963**, *40*, 680-687.

(37) Alexandridis, P.; Athanassiou, V.; Fukuda, S.; Hatton, T. A. *Langmuir* **1994**, *10*, 2604-2612.

(38) Betageri, G. V.; Jenkins, S. A.; Parsons, D. L. *Liposome Drug Delivery Systems*; Technomic Publishing Company Inc: Lancaster, PA, 1993; pp 1,2.

(39) Tien, H. T. *Journal of Physical Chemistry* **1967**, *71*, 3395-3401.

(40) Betageri, G. V.; Jenkins, S. A.; Parsons, D. L. *Liposome Drug Delivery Systems*; Technomic Publishing Company Inc: Lancaster, PA, 1993; pp 7-17.

(41) MacDonald, R. C. The Relationship and Interactions Between Lipid Bilayer Vesicles and Lipid Monolayers at the Air/Water Interface. In *Vesicles*, First ed.; Rosoff, M., Ed.; Marcel Dekker: New York, NY, 1996; Vol. 62, pp 3-48.

(42) Gradzielski, M. *Journal of Physics: Condensed Matter* **2003**, *15*, R655-R697.

(43) Fendler, J. H. *Membrane Mimetic Chemistry: Characterizations and Applications of Micelles, Microemulsions, Monolayers, Bilayers, Vesicles, Host-Guest Systems, and Polyions*; John Wiley and Sons: New York, NY, 1982; pp 145-153.

(44) Bangham, A. D.; Standish, M. M.; Watkins, J. C. *Journal of Molecular Biology* **1965**, *13*, 238-252.

(45) Gregoriadis, G. Fate of injected liposomes: Observations on entrapped solute retention, vesicle clearance and tissue distribution in vivo. In *Liposomes as Drug Carriers. Recent Trends and Progress*; Gregoriadis, G., Ed.; Wiley & Sons: New York, NY, 1988; pp 176-188.

(46) Lasic, D. D. Liposomes in Drug Delivery. In *Vesicles*, First ed.; Rosoff, M., Ed.; Marcel Dekker: New York, NY, 1996; Vol. 62, pp 447-476.

(47) Tran, C. D.; Klahn, P. L.; Romero, A.; Fendler, J. H. *Journal of the American Chemical Society* **1978**, *100*, 1622-1624.

(48) Tien, H. T. *Bilayer Lipid Membranes (BLM), Theory and Practice*, 1974; pg 672

(49) Tilcock, C.; Utkhede, D.; Meng, G. Vesicles as imaging agents. In *Vesicles*, First ed.; Rosoff, M., Ed.; Marcel Dekker: New York, NY, 1996; Vol. 62, pp 593-648.

(50) Takeoka, S.; Ohgushi, T.; Sakai, H.; Kose, T.; Nishide, H.; Tsuchida, E. *Artificial Cells, Blood Substitutes, and Immobilization Biotechnology* **1997**, *25*, 31-41.

(51) Graff, A.; Winterhalter, M.; Meier, W. *Langmuir* **2001**, *17*, 919-923.

(52) Gerasimov, O. V.; Rui, Y.; Thompson, D. H. Triggered Release from Liposomes Mediated by Physically and Chemically Induced Phase Transitions. In *Vesicles*, First ed.; Rosoff, M., Ed.; Marcel Dekker: New York, 1996; Vol. 62, pp 679-746.

(53) Hianik, T.; Ottova-Leitmannova, A.; Tien, H. T. *Surfactant Science Series* **1996**, *62*, 49-77.

(54) Sisson, T. M.; Srisiri, W.; O'Brien, D. F. *Journal of the American Chemical Society* **1998**, *120*, 2322-2329.

(55) Sells, T. D.; O'Brien, D. F. *Macromolecules* **1994**, *27*, 226-233.

(56) Laibin, L.; Eisenberg, A. *Journal of the American Chemical Society* **2001**, *123*, 1012-1013.

(57) Alexandridis, P.; Olsson, U.; Lindman, B. *Langmuir* **1998**, *14*, 2627-2638.

(58) Liu, G.; Ding, J. *Journal of Physical Chemistry B* **1998**, *102*, 6107-6113.

(59) Nardin, C.; Hirt, T.; Leukel, J.; Meier, W. *Langmuir* **2000**, *16*, 1035-1041.

(60) Haverstick, K.; Pakalns, T.; Yu, Y.-C.; McCarthy, J. B.; Fields, G. B.; Tirrell, M. *Polymeric Materials Science and Engineering* **1997**, *77*, 584,585.

(61) Rosen, M. J. *Surfactants and Interfacial Phenomena*, Second ed.; Wiley-Interscience: New York, NY, 1989; pp 23-31.

(62) Watson, K. J.; Anderson, D. R.; Nguyen, S. T. *Macromolecules* **2001**, *34*, 3507-3509.

(63) Maskos, M.; Harris, J. R. *Macromolecular Rapid Communications* **2001**, *22*, 271-273.

(64) Discher, B. M.; Won, Y.-Y.; Ege, D. S.; Lee, J. C.-M.; Bates, F. S.; Discher, D. E.; Hammer, D. A. *Science* **1999**, *284*.

(65) Alexandridis, P.; Olsson, U.; Lindman, B. *Langmuir* **1997**, *13*, 23-34.

(66) Kelarakis, A.; Havredaki, V.; Yu, G.-E.; Derici, L.; Booth, C. *Macromolecules* **1998**, *31*, 944-946.

(67) Pople, J. A.; Hamley, I. W.; Fairclough, J. P. A.; Ryan, A. J.; Komanschek, B. U.; Gleeson, A. J.; Yu, G. E.; Booth, C. *Macromolecules* **1997**, *30*, 5721-5728.

(68) Derici, L.; Ledger, S.; Mai, S.-M.; Booth, C.; Hamley, I. W.; Pedersen, J. S. *Phys. Chem. Chem. Phys.* **1999**, *1*, 2773-2785.

(69) Yu, G.-E.; Masters, A. J.; Heatley, F.; Booth, C.; Blease, T. G. *Macromol. Chem. Phys.* **1994**, *195*, 1517-1538.

Chapter 2

Synthesis and Characterization of 1,2-Butylene Oxide/ Ethylene Oxide Diblock Copolymers

2.1 Overview of Synthesis

The 1,2-butylene oxide/ ethylene oxide (BO/EO) diblock copolymers used in this work were prepared by sequential anionic polymerization, which exhibits pseudo-living characteristics for low molecular weight blocks.[1] Synthesis began with dissolution of the alkoxide initiator in toluene, addition of butylene oxide monomer and polymerization of the BO block (Scheme 2.1). The EO monomer was then added and polymerized from the

$$CH_3CH_2O^+K \xrightarrow[\text{Toluene}]{\begin{array}{c} O \\ \wedge \\ CH_3CH_2CHCH_2 \end{array}} \quad \overset{I}{CH_3CH_2O[CH_2CH(CH_2CH_3)O^-]_n \, {}^+K}$$

$$\overset{II}{CH_3CH_2O[CH_2CH(CH_2CH_3)O]_n[CH_2CH_2O^-]_m \, {}^+K} \xleftarrow[\begin{array}{c} O \\ \wedge \\ H_2CH_2C \end{array}]{}$$

$$\overset{III}{CH_3CH_2O[CH_2CH(CH_2CH_3)O]_n[CH_2CH_2O]_m\text{-H}} \quad + \quad KOAc \downarrow \xleftarrow{HOAc}$$
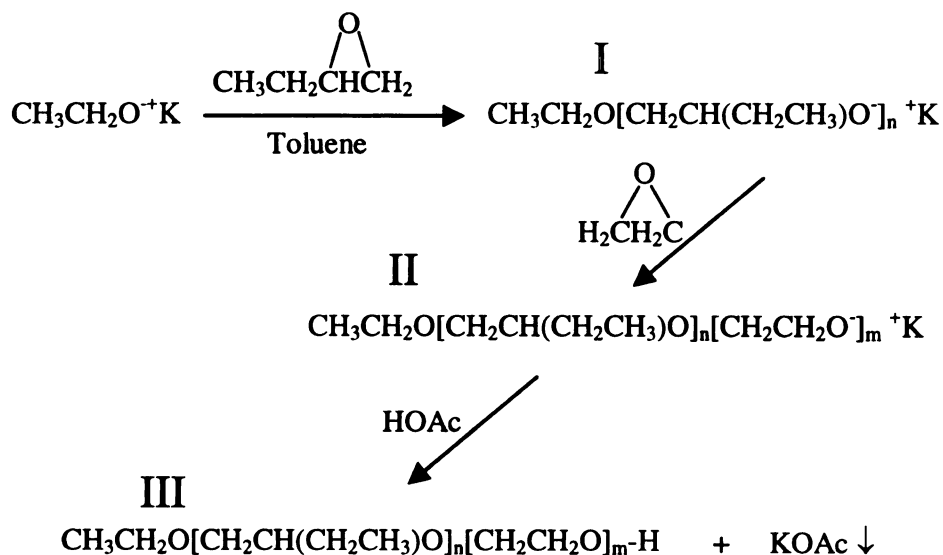
Scheme 2.1. Synthesis of 1,2-butylene oxide/ ethylene oxide copolymers; (I) BO oligomer formation, (II) BO oligomer with active EO site, (III) acid quenching of reaction.

BO oligomer, and the reaction was finally quenched by the addition of a strong acid. This synthesis affords a diblock copolymer with an aliphatic-initiated hydrophobe and a hydroxyl-terminated hydrophile (Figure 2.1). The terminal hydroxyl functionality strongly influences the hydrophilic nature of the head group.[2]

Figure 2.1. Representative BO/EO molecule showing amphiphile shape.
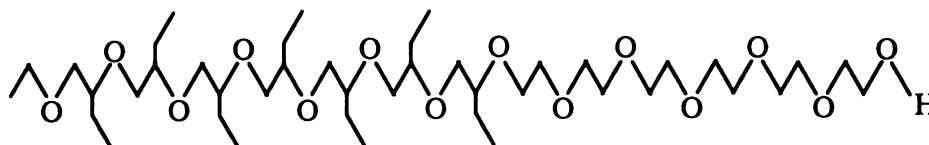
Copolymer composition dramatically affects surfactant performance and is always a concern.[3] While this synthesis produces the desired end groups, inefficient coupling of EO groups to the BO oligomer can lead to uncapped, residual BO oligomer. Additionally, as in all copolymer syntheses, the product is not homogenous, but rather a mixture of copolymers having EO and BO blocks of varying lengths. Since EO length strongly affects structure formation,[4] characterizing the copolymer is critical to understanding and predicting aggregation. Finally, byproducts or contaminants must be identified to ensure the desired copolymer performance.

This chapter will discuss the synthesis of BO/EO oligomers and the subsequent copolymer purification and characterization. I will address specific characterization procedures, highlighting the advantages and drawbacks of each. Finally, I will present profiles of the copolymer compositional distribution and explain why the methodology used to determine the "average composition" was chosen.

2.2 *Parr Reactor Synthesis*

This work began by examining a range of BO/EO copolymers previously prepared by The Dow Chemical Company using a lab-scale reactor. Lab-scale batches are denoted with the prefix "L" and were synthesized using either a 450 or a 600 mL Parr Reactor (Parr Instruments, Moline, IL). The reactors consist of two components: a head unit, which contains the stirrer, thermocouple well, cooling line and assorted ports, and a base, which is the actual reaction vessel. Both reactors use the A1120HC head unit, but the 450 mL reactor uses base unit 452HC2, while the 600 mL reactor uses base unit 452HC3. The polymerizations were performed in batch mode, with all of the monomer added and mixed before heating began. Typical copolymer yields were between 50 and 200 mL per batch or about 90 % of added monomer.

The Parr Reactor is equipped with a temperature controller that continuously adjusts the heating rate, and the temperature is monitored using redundant thermocouples inserted into a well filled with silicone oil. The controller also monitors the reactor pressure and controls a magnetically-coupled, shaft-driven stir rod. A cooling line circulates a refrigerated solution through a coil in the reaction solution for more precise temperature control and acts as a fail-safe device in case of an uncontrolled, exothermic reaction. The reactor also has a sampling port to extract product, a blanketing port for pressurizing the headspace above the solution, and an injection port for introducing materials into the reactor. A 750-psi frangible disk on the head unit prevents over pressurization, and a 0–300 psi pressure gauge serves as back-up to the pressure transducer.

Ethylene oxide (EO, liquefied gas, 99.5+%), 1,2-butylene oxide (BO, liquid, 99+%), toluene (HPLC grade), and potassium ethoxide (powder, 95%), were purchased from Sigma-Aldrich. Dry molecular sieves were added to the toluene upon receipt and to the BO approximately 24 hour before use. Otherwise, materials were used as received. The quality of the EO supply was erratic, and oligomerization in the cylinder was common. To test monomer quality, ~ 0.5 g of the material was injected into a glass bottle and allowed to evaporate. The bottle was inspected for a residue that would indicate oligomerization. Several synthesis runs had to be aborted due to oligomerized EO.

Variations in alkoxyl block lengths, which are unavoidable in this type of polymerization, can be reduced by using low monomer concentrations and only alkoxide salts as chain initiators. Such conditions were used in all of the lab-scale syntheses. (The conjugate alcohol for a given alkoxide is frequently added to the reactor to provide an inexpensive source of additional initiation sites, but these sites are active for only a portion of the total synthesis time and thus, contribute to EO capping inefficiencies.)

An example of the lab-scale synthesis procedure is as follows: the potassium ethoxide initiator (12.63 g), dried toluene (250 g) and 1,2-butylene oxide (110 g) were added to an oven-dried 600 mL Parr reactor in a dry box blanketed with dry N_2, and the reactor was immediately sealed. The reactor was then purged with N_2 for 5 min, blanketed with 30 psi of N_2 and heated to 110 °C with constant stirring. Within 2 to 5 minutes of reaching 110 °C, a controlled, exothermic reaction reaching ~ 115 °C was observed. The reactor was adjusted to maintain 115 °C for about 4 hours, then cooled to 5 °C (6 °C below the boiling point of EO), and approximately 5 mL of the BO oligomer solution was removed. (The N_2 pressure inside the reactor forces the oligomer out the

sampling port so opening the reactor is not necessary to remove this aliquot.) Next, the

N_2 pressure was dropped to ~ 2 psi and liquid EO (75 g) was transferred, using the

internal pressure of the EO cylinder, from the supply cylinder to the reactor via 1/8"

stainless steel tubing. *Caution*: EO is a suspected teratagen and should be handled with

care.[5] The reactor was re-heated to 90 °C, and a second controlled exothermic reaction

reaching about 120 °C was observed and allowed to run to completion, ~ 2 hours, before

cooling the reactor back to room temperature. At this point, the reaction was either

complete, or a portion of the product could be removed via the sampling port and a

second addition of EO to the remaining product could be conducted.

In this example, a second EO addition was performed after half (~ 240 g) of the

initial product was removed. The reaction of the removed material was terminated by

addition of 2 mL of hydrochloric acid (12 N), and the copolymer was set aside. A second

aliquot of EO (18 g) was added to the remaining copolymer, and the reactor was re-

pressurized with N_2 to about 30 psi and re-heated to 90 °C. Another exothermic reaction

reaching 120 °C was observed, and the reaction ran to completion in ~ 2 hours. The

reactor was cooled to room temperature, purged with N_2 and the reaction terminated by

injection of hydrochloric acid. The product was transferred to a glass container to stand

overnight.

The copolymer was extracted using a toluene/ 3 M NaCl aqueous dispersion and

decantation of the organic, upper phase. The solvent was removed by evaporation. If salt

was found in the product, the copolymer was mixed 1:1 with DI water and the resulting

emulsion heated until phase separation occurred (~ 80 °C). The organic phase was

decanted and the residual water removed by evaporation. Synthesis yield was calculated

by dividing the final copolymer mass by the total mass of monomers added and multiplying by 100. This synthesis produced 96 g from the first EO addition (Batch# L1150-51A) and 82 g from the second addition (Batch# L1150-51B) for a combined yield of greater than 85 %.

Aqueous samples of various concentrations were prepared from each copolymer listed in Table 2.1 and allowed to equilibrate for ~ 20 days at room temperature. These samples were then examined using white-light and laser-light scattering and plane-polarized light microscopy (see section 3.3) to ascertain which materials demonstrated micellar structure formation properties. (The strong hydrophobic nature of some copolymers lead to dispersions and emulsion formation rather than micellar structures.) Those that formed structures were examined further.

Table 2.1. BO/EO copolymers screened for evidence of micellar formation.

Sample Name	Theor. BO block length[a]	Actual BO block length[b]	Theor. EO block length[a]	Actual EO block length[c]	Wt % PEO
L1573-9a	6.3	6.2	5.1	5.1	30
L120-15a	9.8	10	10	10.2	35
L1150-51a	9.8	10	11	11.1	40
L1150-51b	9.8	10	18	18.2	51
L1150-55	13.2	14	23	22.7	50
L1573-65b	13.2	14	35	35.0	60
L120-53a	16.7	17	15	14.8	35
L741-45b	16.7	17	44	44.4	61
L120-29b	20.2	21	50	50.0	60
L1150-21a	23.6	24	23	17.0	30
L1150-21b	23.6	24	40	39.7	50
L1150-21c	23.6	24	93	92.6	70
L741-68b	34.0	34	101	101	64

[a] Calculated from ratio of monomer to initiator
[b] Average value determined from NMR spectra. (see Section 2.4 for details)
[c] Based on GPC calculations of total MW using NMR data for BO MW. (see Section 2.6 for details)

2.3 PolyGlycols Mini-Plant Synthesis

To prepare larger quantities of copolymer, and to evaluate the feasibility of large-scale production, several BO/EO batches were prepared at the PolyGlycols Mini-plant Facility of The Dow Chemical Company in Freeport, Texas. The copolymer was prepared using conditions as close as possible to those that could be used in a commercial operation. The mini-plant employed a continuous addition, solvent-free synthesis in contrast to the batch, solution process used in the lab-scale runs. The mini-plant procedure also held the copolymer at high temperatures for longer periods that are frequently more than twice as long as reaction times in the lab-scale synthesis. Polymerizations were performed in an 8-L reactor and typically produced between 2.5 and 3.5 L of copolymer per batch. Using the mini-plant process, multiple additions of EO were conducted to produce copolymers with sequentially longer EO blocks from the same BO oligomers. This resulted in a series of copolymers that differed only in their EO block lengths.

Batches prepared by the mini-plant are denoted by the prefix "M". The recipe and general synthesis procedure were provided to the reactor operator. In a representative procedure, 227 g of 24 wt % potassium ethoxide in ethanol (Sigma-Aldrich, ~ 4.94 mol of initiator sites) was used as the initiator. The reactor was loaded with the initiator solution and 20 g of the BO monomer and heated to 120 °C with constant agitation. Over the next 6 hours, additional monomer was added at a rate of 10 g/ min for a total of 3710 g (51.5 mol) of BO monomer. The material was held at 120 °C for another 3 hours, and the reactor was allowed to cool and stand at room temperature overnight while under N_2. The following day, 2435 g (55.3 mol) of EO monomer was

added over a 4-hour period while the reactor was held at 120 °C. (The rate of addition

automatically varied with the reactor internal pressure, which decreased as monomer was

consumed by the reaction.) The material was held at 120 °C for 4 more hours, and the

reactor was allowed to cool to room temperature. Continuous stirring continued

overnight under flowing N_2. The following morning the product was removed, tested,

labeled and shipped.

Generally, fundamental research was conducted using materials produced from

the Parr reactors, while studies of dispersion properties, such as stability and

encapsulation capacity, were conducted on materials from the mini-plant. Any variation

from this pattern in the following discussions will be noted. In either case, the copolymer

composition was determined using the same characterization processes. Specific

purification procedures are described below.

2.4 *Copolymer Purification*

Copolymer purification was required to remove residual solvent, unreacted

monomer, and contaminants from the synthesis mixture. Due to the slight possibility of

residual ethylene oxide monomer, care was taken to minimize exposure to the copolymer

prior to complete purification. Low EO capping efficiency is the primary source of

contamination in this work, as it yields BO oligomers with no EO head group.[6] Butylene

oxide polymerizes much more slowly than does ethylene oxide, primarily because of

steric hindrance. However, once the BO oligomer reacts with an ethylene oxide unit,

steric hindrance is minimal, and EO-capped oligomers tend to grow at the expense of

uncapped BO oligomers. As a result, the final product contains some fraction of non-

ethoxylated BO oligomers, while capped oligomers have EO blocks that are longer than would be expected from the reactant ratio. Thus the slow initiation rate and low capping efficiency lead to polydispersity in EO block lengths.

Monomer isomerization and product oxidation can also affect the final copolymer composition, but these unwanted reactions can be reduced by minimizing both synthesis temperature and duration. EO does not undergo rearrangement, but BO can form crotyl alcohol when the anionic active site on a growing chain extracts a proton from a BO monomer instead of opening the epoxide ring. This process terminates the growing chain and transfers the anionic site to the monomer, which becomes unstable and rearranges to produce $CH_3CH=CHCH_2O^-$, ionized crotyl alcohol. The anionic crotyl alcohol acts as an initiator and starts a new oligomer chain. Thus, in principle, crotyl alcohol formation can significantly reduce the average BO block length by premature block termination and an increase in the number of oligomeric chains. Nevertheless, rearrangement of BO is a relatively rare process. Crotyl alcohol can be detected by NMR, but was not found in any of the copolymers studied.

Copolymer oxidation cleaves the ether bond and produces peroxides, aldehydes and ketones.[6] This process takes place in the presence of strong base and oxygen at elevated temperatures, so minimizing exposure to these conditions is important. Hence, the reactor was blanketed with N_2 to limit exposure to O_2 and H_2O. As with isomerization, oxidation products can be detected by NMR if they are present at levels high enough to affect surfactant performance. We did not observe any oxidation products using proton NMR, but ^{13}C NMR showed trace levels of aldehyde formation, particularly in the mini-plant materials.

The previously described extraction process used in the lab-scale synthesis (Section 2.2) was not used with the mini-plant batches because of its cost. Instead, mini-plant batches stood undisturbed for at least 48 hours before purification. During this time most copolymers separated into a clear, upper phase and a much smaller opaque, lower phase, although in some cases formation of multiple phases was observed. Phases were isolated by decanting and labeled with a suffix to denote position, "A" being uppermost, i.e. "M1038A". The copolymer was then vacuum filtered to remove any residual salts such as potassium acetate. (Viscous copolymer batches were thinned with hexane to reduce viscosity and make filtration easier.) After paper filtration, the surfactant was vacuum filtered through 40-60 mesh sintered glass filters. Any residual volatiles were removed by rotary evaporation at a minimum of 75 °C for 2 hours. (If hexane had been added to thin the copolymer, it was removed in this step.) NMR was used to confirm solvent removal and estimate product composition.

Samples that displayed discoloration or did not appear homogeneous after solvent removal, were purified by centrifugation. These mixtures were centrifuged (IEC, Centra GP8R, Needham Heights, MA) at 3400 rpm for between 1 and 24 hours to isolate the contaminant or induce phase separation. Salt contamination was apparent as "dust" on the centrifuge tube bottom, while other contaminants were visible as phase-separated components. The clarified material was decanted, and the contaminant was discarded. These same purification procedures were used on copolymers that I later synthesized using the Parr reactor.

The following is a list of the copolymers prepared at the PolyGlycols mini-plant. The number of phases identifies the extent of separation that occurred in the batch over

time. Copolymer phase separation is generally attributed to residual salt which can complex with the EO chain, or to crystallization of the longer (> 25 units) EO blocks. Batches M1190, M2013 and M2075 were a series of copolymers made with sequentially increasing EO block lengths. Many of the compositions with shorter EO blocks in these runs were single phase while those having EO blocks greater than 16 tended to form 2 phases. The average BO block length differed among the three series so that the effect of both BO and EO block lengths on structure formation could be studied.

Table 2.2. Copolymers prepared by the Mini-plant Process.

Batch	Expected Composition	Actual Composition*	Number of phases
M1038	$EO_{12}BO_{12}$	$EO_{12}BO_{11}$	4
M1096	$EO_{12}BO_{12}$	$EO_{11}BO_{11}$	4
M1101	$EO_{12}BO_{12}$	$EO_{11}BO_{10}$	3
M1190 series	$EO_{10\text{-}24}BO_{10}$	$EO_{8\text{-}22}BO_9$	~ 2 ea
M2013 series	$EO_{10\text{-}24}BO_{20}$	$EO_{10\text{-}26}BO_{18}$	~ 2 ea
M2075 series	$EO_{10\text{-}24}BO_{30}$	$EO_{8\text{-}24}BO_{30}$	~ 2 ea

*as determined by proton NMR

Surfactants with short EO blocks (< 20 units) form clear liquids at room temperature, however increasing the EO block length leads to increasing self-association and, consequently, higher viscosity and increased opacity.[7] Due to EO crystallinity, when the average EO block length exceeds ~ 25, the copolymer is a wax-like solid at room temperature. After initially screening numerous BO/EO compositions, this work focused on liquid copolymers with average EO block lengths less than 20. Butylene oxide oligomer is a liquid at block lengths up to at least 30, so increases in BO block length had less effect on the copolymer appearance. The purified products were clear,

48

colorless liquids with moderate viscosity (~ 95 cP). These surfactants had molecular

weights ranging from ~ 500 to 2200 amu and were soluble in a range of organic solvents.

2.5 Copolymer Characterization

Each copolymer batch is a mixture of BO/EO diblock copolymers having various

BO and EO block lengths. Because copolymer composition has a dramatic effect on

micellar structure formation,[8] one must accurately determine the composition of each

copolymer batch to assess the impact of changes in block length on micellar structure

development. Because of EO-capping inefficiencies, the average BO/EO compositions

calculated from reactant concentrations are insufficient to describe batch composition or

predict batch performance. A more extensive examination of the copolymer is required.

Copolymer characterization was performed using three analytical methods: NMR

spectroscopy, gel-permeation chromatography (GPC) and electro-spray ionization mass

spectrometry (ESI-MS). NMR spectroscopy provided a bulk composition,[9] but was used

primarily to detect selected contaminants. GPC was useful in determining the

approximate mass range and polydispersity of the materials,[10] but ESI-MS provided the

most accurate evaluation of the copolymer composition.[3] ESI-MS was also useful in

determining the level of contaminants and byproducts in the batch.

2.6 Analysis by Nuclear Magnetic Resonance Spectroscopy

NMR spectroscopy has been used to study the composition of ethoxylated block

copolymers for many years, and the techniques used here have been partially described

before.[3] Our NMR studies were conducted using FT-NMR on a Varian Mercury Vx 300

instrument (Varian, Palo Alto, CA). The copolymer was dissolved at about 10 wt % in

deuterated chloroform ($CDCl_3$) with 0.1 vol % TMS as a reference. A relaxation rate test was performed, and complete copolymer relaxation was determined to require about 8 seconds, so samples were analyzed with a first delay time $\geq$ 10 seconds. The pulse width was set at 6 or 7 ms with an acquisition time of 3.7 seconds.

The methyl protons on the initiator (λ) produced a unique peak at 1.24 ppm, while the methyl protons of the BO units (α) appeared at 0.92 ppm (Figure 2.2). The ratio of the areas of the BO and initiator methyl peaks (α/λ) gave the average number of BO units per initiator and hence, per chain. A multiplet from the methylene peak (β) of the ethyl substituent of the BO unit is found from 1.4 –1.7 ppm. To confirm the average BO block length value, the β/λ area ratio was also calculated and multiplied by 3/2 to adjust for the difference in the number of protons on the two groups. This value matched the α/λ value within $\pm$ 5 %. NMR analysis of EO blocks in BO/EO copolymers showed only methylene signals that overlap similar peaks from the backbone methylene of the BO oligomer. Therefore, calculation of EO block length required determination of the EO contribution to the total methylene peak area by subtraction of the methylene peak areas generated by the initiator and BO blocks from the total methylene peak area. The contribution of each group to the total number of methylene protons per chain, MP_T, is: 2 from each BO block, 2 from the initiator and 4 from each EO block. If n is the number of BO blocks and m the number of EO blocks, then the total number of methylene protons per chain is:
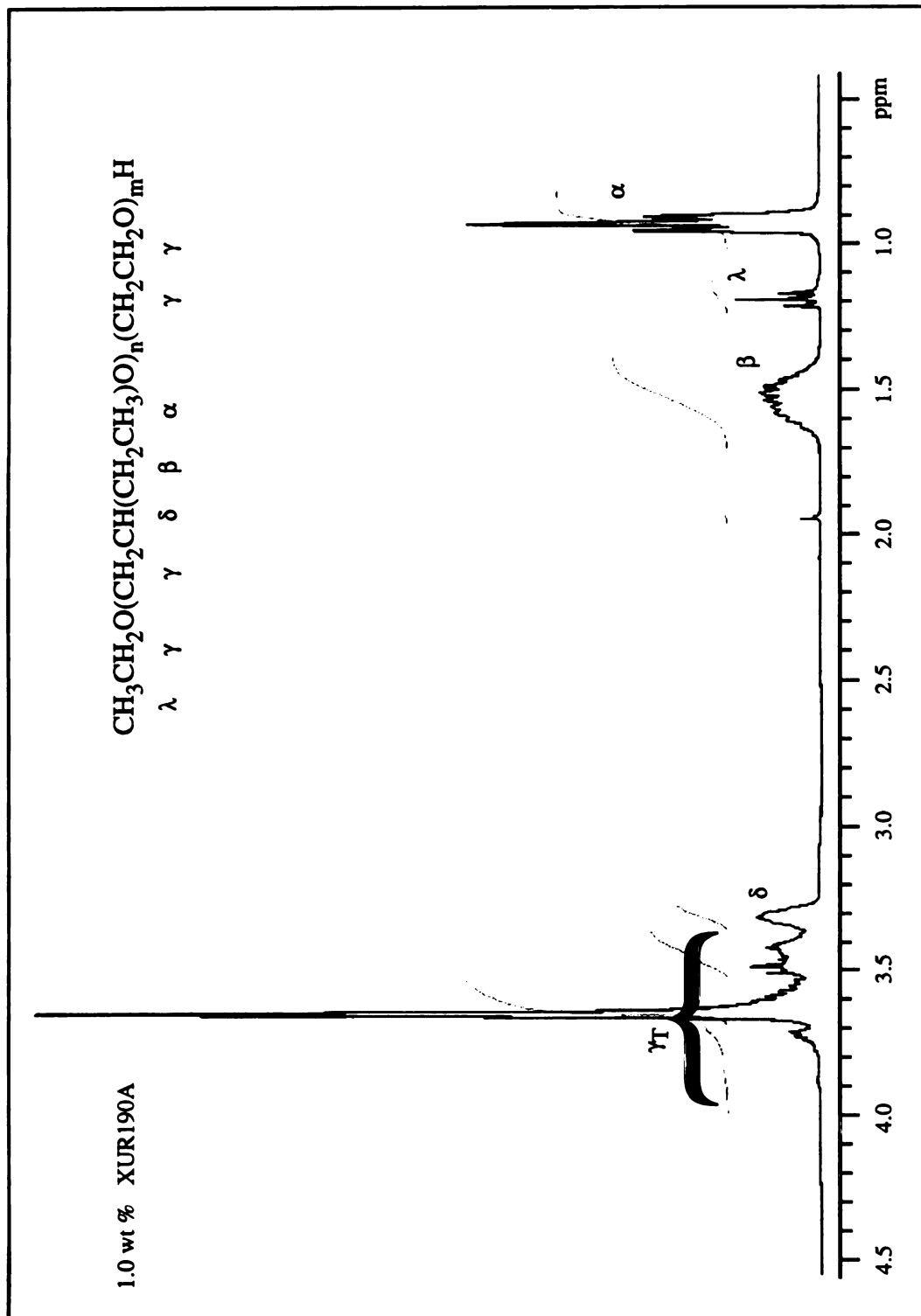
Figure 2.2. NMR spectrum of BO/EO diblock copolymer M1038 ($BO_{11}EO_{12}$). Note lack of unidentified peaks. (Peak at 1.95 ppm is probably water.)

$$MP_T = 2n + 2 + 4m \qquad\qquad \text{eq. 2.1}$$

The number of BO blocks per chain, n, is equal to α/λ. The total number of methylene

protons is represented by the peak area γ_T. To convert the NMR peak areas to number of

protons, we use the conversion factor of $3/\lambda$, so $\gamma_T(3/\lambda) = MP_T$. Substitution of these

values into equation 2.1 produces equation 2.2.

$$\gamma_T (3/\lambda) = 2(\alpha/\lambda) + 2 + 4m \qquad\qquad \text{eq. 2.2}$$

Or, rearranging equation 2.2 to isolate the average number of EO blocks per chain yields

equation 2.3:

$$\left(\frac{3\gamma_T - 2\alpha}{4\lambda}\right) - \frac{1}{2} = m \qquad\qquad \text{eq. 2.3}$$

Compositions calculated from NMR data were considered to be within $\pm$ 10 % of the

actual composition and were used primarily to confirm that the product was similar to

that expected from the formulation. The molecular weights derived from these

calculations represent the number-averaged molecular weight (M_n) of the compositions.

Synthesis of the BO block prior to the EO block allows for selection of both a

strong hydrophobe to initiate BO polymerization and a hydrophilic hydroxyl group to

terminate the EO block. However, because of the low EO capping efficiency inherent in

this method, the expected and actual block lengths of the final product will probably

differ. Unfortunately, these differences are not detectable by NMR analysis. BO/EO

average composition is calculated by determining the molar ratios of total EO units and

total BO units to total ethoxide (initiator) units. Since the *total* number of ethoxide units

is not changed by the inefficiency of the capping process, the average EO length

determined by NMR will be the same regardless of the number of copolymers that

actually contain EO blocks. Thus, several batches of copolymer could have the same calculated average composition, but vary significantly in actual block composition depending on the capping efficiency.

Oxidation of the monomer and copolymer can produce peroxides, aldehydes, ketones, and other byproducts that are readily detectable using NMR. The two most probable contaminants are toluene (residual solvent) and crotyl alcohol from the BO rearrangement (Section 2.4). Toluene, which produces a distinct NMR peak at 2.32 ppm and a pair of triplets between 7.1 and 7.3 ppm, is easily removed by evaporation. Crotyl alcohol produces 3 NMR peaks: a singlet at 2.45, a triplet at 4.05 and a broad multiplet at 5.68 ppm. However neither crotyl alcohol, nor toluene, nor any of the other possible byproducts, were detected in the copolymers used in this study.

For ^{13}C NMR spectra, the integration was considered to be indicative, rather than definitive, of actual copolymer composition, so this technique was used primarily to identify the presence of contaminants. The vinyl group of the crotyl alcohol and the carbonyl of an aldehyde ($CH_3CH_2CH_2C(=O)H$) could be easily identified. Carbon-13 NMR showed that aldehyde formation was ~ 4 times greater in materials synthesized in the mini-plant than in copolymers prepared using the Parr Reactor. However in neither case were contaminants present at high enough concentrations (< 1 mol % of total BO) to interfere with micellar structure formation.

2.7 Gel Permeation Chromatography

The copolymers in this work have a distribution of EO and BO block lengths and therefore a distribution of masses. Gel permeation chromatography (GPC) is frequently

used to separate the components of a polymer mixture according to molecular weight. The GPC employed in this work consisted of a Waters 590 pump (Waters Corp., Milford, MA), a Waters 712 Autosampler, a Waters CHM column heater, a Waters TCM temperature control module and a Waters 410 refractive index detector. The eluent, tetrahydrofuran (THF), was degassed and blanketed with helium throughout the operation. GPC samples were prepared at 1.0 wt % copolymer in THF with 0.1 wt % dodecane added as a flow marker. The system was fitted with two Waters columns, an HR0.5 and HR2 (cat # WAT044231 and WAT044237), that were maintained at 35 °C. The system was controlled using the Polymer Labs Cirrus software that provides both data acquisition and processing capabilities, and calibration was performed using polyethylene glycol (PEG) standards obtained from Polymer Labs (Polymer Laboratories Inc., Amherst. MA).

This technique was used primarily to examine the polydispersity of the oligomers, both prior to EO addition and in the final product. However, GPC alone is not applicable for determining the actual average copolymer composition because only ethylene oxide standards are available for calibrating the instrument; no butylene oxide standards are available. Surprisingly, however, if the value of the BO MW taken from the NMR analysis is substituted into the GPC MW calculations, the value of the EO block determined by the GPC data closely matches the theoretical value. Nonetheless, while an absolute molecular weight could not be determined by the GPC data alone, an overall polydispersity could be measured for the BO oligomer and the final copolymer.

Figure 2.3 contains chromatographs of copolymers L1150-51A and L1150-51B, whose synthesis was described in section 2.2. Since these copolymers are generated from

the same BO oligomer, they should vary only in EO block length. Molecular weight

calculations based on the peak molecular weights (Mp) of EO standards indicate that

batch L1150-51A had an M_p of 1303 amu, and batch L1150-51B had an M_p of 1501

amu. However, molecular weight assignments are dubious because the EO standards are

being applied to BO. (As noted above, BO standards are not available.) The most

important point to note from the chromatograms in Figure 2.3 is that the peak shapes are

relatively narrow and unimodal. However, the small peaks between retention times of 19

and 23 minutes probably represent residual, uncapped BO oligomer. The GPC data
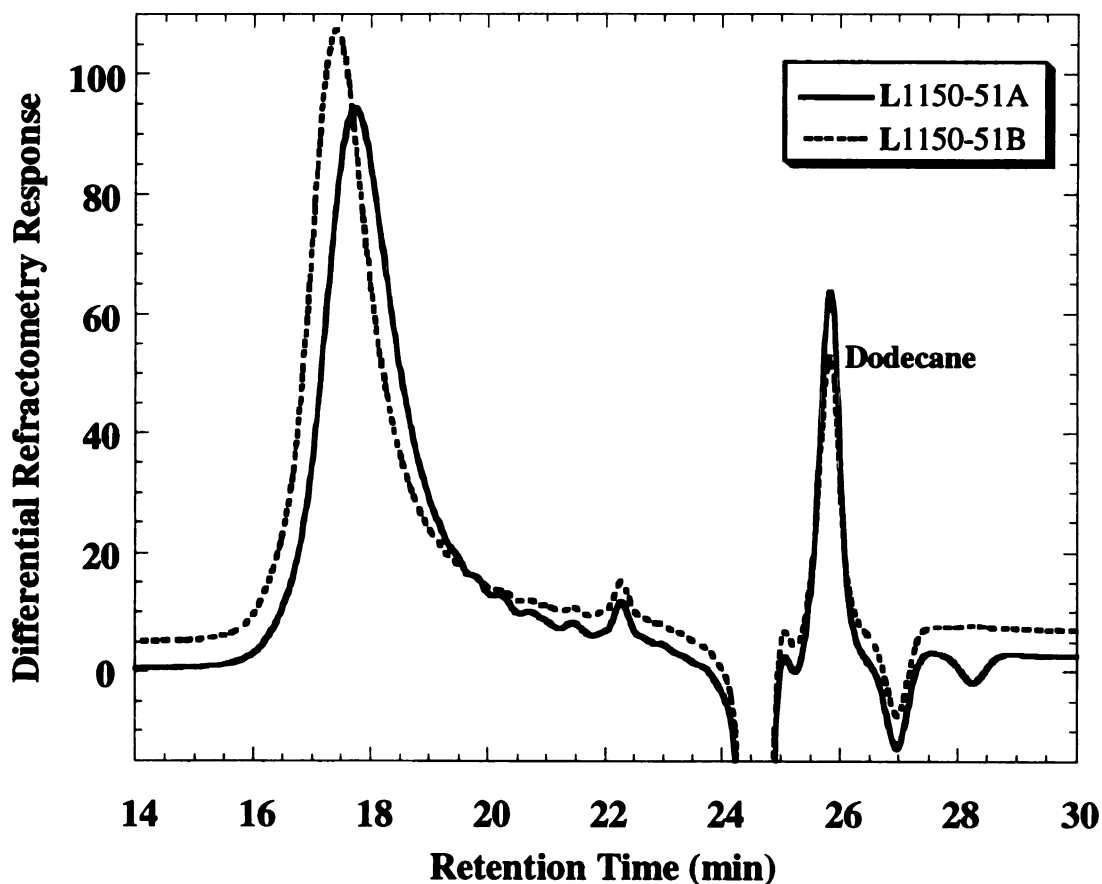
Figure 2.3. GPC chromatographs of the two copolymers whose synthesis was described

in section 2.2.

showed that all of the oligomers and copolymers used in this work had essentially unimodal MW distributions. The BO oligomers typically had a polydispersity index (PDI) between 1.05 and 1.15, while the copolymer PDI was between 1.09 and 1.17. I should note, however, that at low molecular weights, low polydispersities can still occur with a wide range of oligomeric compositions.

2.8 *Copolymer Analysis by Mass Spectrometry*

Mass spectrometry provides the most detailed information about the copolymer composition. Mass spectrometric analysis was performed by Bruce Bell of the Analytical Laboratories at The Dow Chemical Company using a liquid chromatography/ electro-spray ionization time of flight mass spectrometer. To prepare testing solutions, the copolymers were dissolved in methanol at a concentration of 0.5 mg/ mL. The samples were injected into a Waters Alliance 2690 ternary gradient liquid chromatograph coupled to a Micromass QTOF2 quadrupole/ time of flight MS/MS system via a Micromass Z-spray electrospray ionization (ESI) interface operating in the positive ion (PI) mode. No column was used in the liquid chromatograph. The mobile phase was 0.01 M ammonium acetate in 50/50 water/ methanol flowing at a rate of 1.0 mL/ min with a 2:1 split away from the electrospray interface. The system used a diode array with a range of 200 to 400 nm as the UV detector. In the ESI, the source block was held at 120 °C and desolvation occurred at 250 °C. The capillary was held at 2.5 kV and the cone was set at −15 V. The mass spectrometer was operated at a multi-channel plate (MCP) setting of − 2550V in the +TOFMS mode as a continuum. The resolution, which is the ratio of the mass over the delta mass, where delta mass is the peak width at half height, was set at 10000 (+).

(This is the same as saying that the instrument sensitivity was 1 part in 10000.) The scan range was set from 50 to 3100 m/z (+) with a scan rate of 1.0 sec/ scan. The raw data were collected and transformed using MaxEnt3 software to remove multiply charged ions. The transformed data were imported into an Excel spreadsheet, and calculations using the entire data set were made to determine M_W, M_N, M_P, M_W/M_N, and PDI. These values, and the raw data, were then forwarded to me for additional processing.

Using masses of 46.0419 amu for the ethoxide initiator, 44.0262 amu for the ethylene oxide unit and 72.0575 amu for the butylene oxide unit, the molecular weight of each possible combination of EO and BO block lengths, from BO_3 oligomer to $EO_{30}BO_{25}$, was calculated and arranged in a spreadsheet. (The initiator mass includes the proton of the terminal hydroxyl group.) The values are unique (differences between neighboring values are > 4 amu) in the compositional range defined by an array bounded by BO_3EO_0, BO_3EO_{17}, $BO_{13}EO_0$ and $BO_{13}EO_{17}$. However, once the BO length exceeds 13, or the EO length exceeds 17, duplication of masses begins. The BO oligomer was analyzed first to determine the minimum and maximum values of the BO block length, thus limiting the range of possible BO/EO compositions and making mass-to-composition matching easier and more accurate.

To determine the copolymer composition, the transformed mass spectrometry data were arranged by decreasing intensity to ensure that those components most prominent in the copolymer were included in the calculations. The corresponding mass (actual mass detected minus 18 for the NH_4^+ ion) was then matched to a composition. The difference between the theoretical mass and that recorded by the instrument generally fell into one of two groups: less than 0.09 amu, which was viewed as instrumental noise, and between

0.95 and 1.15 amu, which was attributed to slight variations in isotropic distribution. More than 98 % of the recorded values were in these categories. If the mass could be assigned to more than one composition, it was awarded to the composition with the theoretical mass most closely matching the measured mass.

The intensity value from the actual mass measurement was then entered into a second spreadsheet under the corresponding composition. Due to instrument sensitivity, minute variations in mass (0.0001 amu) were recorded as separate moieties. Therefore, multiple entries could be recorded for the same composition. When this occurred, each intensity value was recorded for the composition and the intensities were summed to determine the final total intensity per composition. This process was repeated until more than 70 % of the total intensity produced by the analysis had been matched to an BO/EO composition. The composition spreadsheet was then converted into a 3-dimensional surface plot showing EO length versus BO length versus signal intensity (See Figure 2.4 below). This generated a visual image of copolymer polydispersity, dominant compositions and the range of compositions.

The intensity "cut-off point" of ~ 70 % of the total intensity was chosen for three reasons. First, the values were arranged by decreasing intensity so values at the cut-off were typically less than 5 % of the largest intensity values. Therefore, each subsequent entry was a small fraction of the total by this point and had little impact on the population distribution. Second, there was generally little change in the calculated average composition when using 25 % of the intensity data versus 50 % versus 70 %, so further sorting would most likely not prove to be illuminating with respect to compositional distribution. Third, about this level, unassignable peaks began to appear, so to make

comparisons between batches more credible, I stopped including data below this level. Overall, the 70 % cut-off usually involved the first ⅓ to ½ of all of the peaks, when arranged by decreasing intensity.

The average copolymer composition was calculated using a mean-intensity procedure. The compositional spreadsheet was arranged with increasing rows for increasing EO block length and increasing columns for increasing BO length. The intensity values for a given row in the two-dimensional array were summed, and then multiplied by the EO block length of that row to produce the total number of EO units represented by that row. This was repeated for each row, and the products were summed to give the total number of EO units represented in the spreadsheet. This sum was divided by the total intensity recorded on the spreadsheet to produce an intensity-averaged EO block length. This same procedure was repeated for the BO blocks and the two average values were combined to give a composite, intensity-averaged copolymer structure. This value should correspond to a number average molecular weight if sensitivities for ions of differing masses are the same. A more detailed description of the procedure and additional data are provided in Appendix B.

2.9 Mass Spectrometry Results

In using this procedure, I make four assumptions. The first is that the copolymer polydispersity is low, and therefore, the range of compositions within a given batch is manageable. This is generally true for polyethers prepared by anionic polymerization and is confirmed by the GPC data. The second assumption is that the amount of molecular fragmentation during mass spectrometry analysis is low, and thus the vast

majority of mass spectrometry peaks represent complete copolymers and not fragments or rearrangement products. This is likely true given the gentle conditions of electro-spray ionization. I also assumed that the instrument sensitivity is independent of copolymer molecular weight, probably valid given the molecular weight range I examined. The final assumption is that the monomers undergo little rearrangement or produce few byproducts during synthesis so that the product is relatively pure. This is generally true for the lab-scale synthesis, with the only common, possible rearrangement product being crotyl alcohol. Replacing the ethoxide initiator with crotyl alcohol (CA) increases the oligomer molecular weight by 26.0156 amu.[6] For example, an $EtO(BO)_8H$ oligomer weighs 622.502 amu while a $CA(BO)_8H$ weighs 648.518 amu. Such a mass difference (+ 26.02 or − 46.04 amu) would be unmatchable to an ethoxide-initiated BO/EO composition and is rarely found in the mass spectrometry data prior to the "70 %" cut-off. (The vinyl group of the crotyl alcohol is also detectable by NMR when present at sufficient levels to affect copolymer performance (sec 2.5), and none was found.) Oxidation of the monomer and polymer can produce peroxides, aldehydes and ketones, many of which would be detectable by mass spectrometry as unmatchable masses. In fact, several batches produced by the mini-plant showed higher levels of materials that could not be matched to an BO/EO composition than did the lab scale batches of similar compositions. Nonetheless, even these levels are low (< 2 mol %) and considered to be insignificant factors in structure formation.

Figure 2.4 is a 3-dimensional surface plot of the composition of copolymer L1150-51A (section 2.2, first EO addition). The aliquot of BO oligomer removed prior to EO addition was lost, so BO block analysis could not be performed for these batches.

The plot shows that a substantial fraction of the BO present (~ 4.0 mole %) is uncapped oligomer. The molecular weight distribution of uncapped butylene oxide oligomer is fairly symmetric around BO_{11}, and no BO_3, BO_4 or BO_5 oligomers were detected. The maximum peak for copolymer **L**1150-51A occurs at a composition of BO_9EO_8, however the intensity-averaged composition is $BO_{10}EO_{10}$, close to the composition expected from

Copolymer Batch L1150-51A
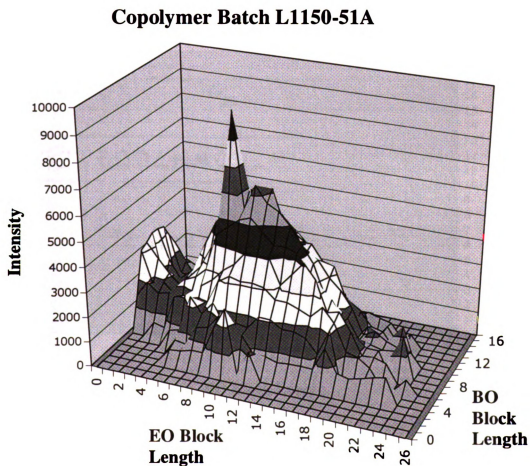
Figure 2.4. Compositional profile of copolymer **L**1150-51A (angled view) determined from ESI Mass spectrometry.

the formulation, $BO_{10}EO_{11}$. This is also similar to the ratio-averaged structure determined by NMR, $BO_{11}EO_{11}$.

Figure 2.5 shows an overhead view of the same distribution. Here the dozen or so highest peaks are represented by the dark, center region, which is approximately bounded by the compositions BO_8EO_7, BO_8EO_{12}, $BO_{11}EO_7$, and $BO_{11}EO_{12}$. This area represents about 27 % of the total intensity plotted, and the copolymer distribution is

Copolymer Batch L1150-51A
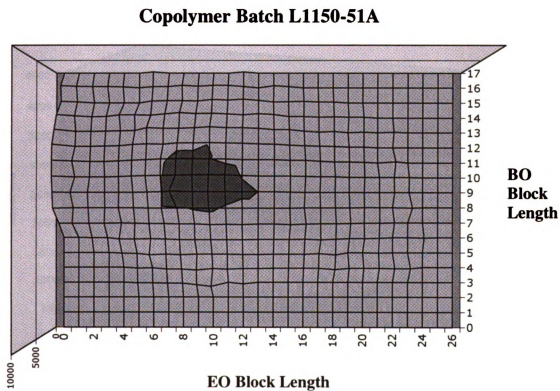
Figure 2.5. Compositional profile of copolymer L1150-51A (overhead view) as determined from ESI Mass spectrometry.

fairly symmetrical about this region. The average composition of this region, the "peak-averaged composition", has a formula of ~ $BO_{10}EO_{10}$, while the highest peak is found at BO_9EO_8. The "kinks" in the grid represent smaller peaks.

Figure 2.6 shows the compositional distribution of the copolymer batch prepared by the second addition of EO monomer (section 2.2). Note that the average peak intensity is about 50 % of that found in Figure 2.4. The overall range of EO block

Copolymer Batch L1150-51B
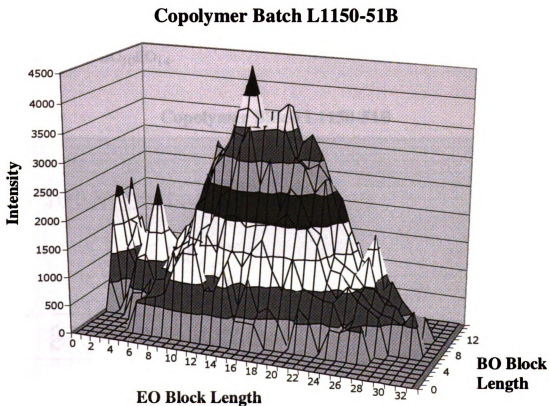
Figure 2.6. Compositional profile of copolymer L1150-51B (angled view) as determined by ESI-mass spectrometry.

lengths has increased by about 50 % as would be expected from the additional EO. The level of BO oligomer has dropped to ~ 2.6 mole %. The intensity-averaged composition for this batch is $BO_{10}EO_{15}$. This formula is slightly lower in EO block length than the $BO_{10}EO_{19}$ composition determined by NMR.

Figure 2.7 shows the overhead view of the same distribution. The largest two dozen peaks are represented by the dark, center region. This region is approximately the center of a rectangle whose corners are the compositions BO_6EO_{12}, BO_6EO_{21}, $BO_{13}EO_{12}$, and $BO_{13}EO_{21}$. The average structure defined by this region is $BO_{9.5}EO_{16.5}$, and the highest peak is found at $BO_{10}EO_{14}$.

Copolymer Batch L1150-51B
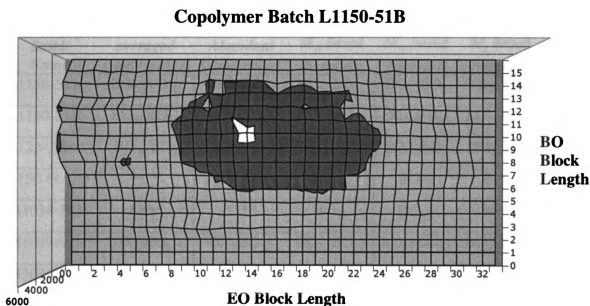
Figure 2.7. Compositional profile of copolymer L1150-51B (overhead view) determined by mass spectrometry.

Based on these results, we find several designations for the composition of copolymers as shown in Table 2.3. The number-averaged (M_n), weight-averaged (M_w), and peak molecular weights (M_z), as well as PDI, are based on the entire data set for a given sample as opposed to the intensity-averaged composition, which is calculated using only data with the highest intensity (70% of the total). M_n, M_w, and M_z were converted to compositions using the BO block length found in the intensity-averaged composition. Table 2.3 compares ESI-MS values for copolymers synthesized in both lab-scale and mini-plant methods.

Table 2.3. Copolymer compositions derived from mass spectrometry data.

Batch Name	Intensity-averaged Composition	Most Abundant Composition	M_n based Formula	M_w based Formula	M_z based Formula	PDI
L1150-51A	$BO_{10}EO_{10}$	BO_9EO_8	$BO_{10}EO_{11}$	$BO_{10}EO_8$	$BO_{10}EO_{14}$	1.12
L1150-51B	$BO_{10}EO_{15}$	$BO_{10}EO_{17}$	$BO_{10}EO_{15}$	$BO_{10}EO_{11}$	$BO_{10}EO_{18}$	1.14
L120-15A	$BO_{10}EO_6$	$BO_{10}EO_6$	$BO_{10}EO_4$	$BO_{10}EO_6$	$BO_{10}EO_9$	1.13
L150-66 BO	****	****	BO_{10}	BO_{11}	BO_{12}	1.10
M1038-BO	****	****	BO_{11}	BO_{12}	BO_{13}	1.06
M1038A	$BO_{12}EO_{9.5}$	BO_8EO_{17}	$BO_{12}EO_{14}$	$BO_{11}EO_{12}$	$BO_{13}EO_{15}$	1.11
M1038D	$BO_{12}EO_{14}$	$BO_{10}EO_{15}$	$BO_{12}EO_{15}$	$BO_{11}EO_{13}$	$BO_{13}EO_{17}$	1.13
M1096-BO	****	****	BO_{10}	BO_{11}	BO_{12}	1.06

The data in Table 2.3 can be compared to the molecular weights and probable compositions obtained from NMR and GPC. Table 2.4 is a list of the copolymers produced and their compositions calculated using different methods. As mentioned previously, the GPC measured mass for BO oligomers is generally higher than the actual

mass because the calculation is based EO standards. (BO is more soluble in the mobile phase and therefore is a fully elongated, "larger" molecule than EO. Thus it moves through the column more rapidly than its actual molecular weight would suggest that it should.) NMR results are quite consistent with mass spectrometry data for the BO oligomer. The results from the various methods are especially comparable when the BO block length obtained from NMR is substituted for the BO value determined by GPC in the EO block length calculation from the GPC data. GPC shows that the copolymer polydispersities are generally low, though the polydispersity index (PDI) is included primarily for comparison, because at low molecular weights such as these, it provides little useful information. Other copolymer batches that were synthesized are not included in this discussion for the sake of brevity.

Table 2.4. Comparison of compositions based on analytical method.

Batch Name	NMR Composition	GPC Composition	GPC PDI	MS Composition[b]	MS PDI
L1150-51A	$BO_{11}EO_{12}$	$BO_{11}EO_{11}{}^a$	1.21	$BO_{10}EO_{10}$	1.12
L1150-51B	$BO_{11}EO_{19}$	$BO_{11}EO_{15}{}^a$	1.25	$BO_{10}EO_{15}$	1.14
L120-15A	BO_6EO_4	$BO_6EO_5{}^a$	1.34	$BO_{10}EO_6$	1.13
L1150-66 BO	BO_{10}	BO_{14}	1.13	BO_{10}	1.10
M1038-BO	BO_{11}	BO_{16}	1.04	BO_{11}	1.06
M1038A	$BO_{11}EO_{12}$	$BO_{16}EO_{10}$	1.04	$BO_{12}EO_{10}$	1.14
M1038D	$BO_{12}EO_{18}$	$BO_{16}EO_{12}$	1.04	$BO_{12}EO_{14}$	1.13
M1096-BO	BO_{10}	BO_{12}	1.07	BO_{10}	1.06
M1096B	BO_9EO_{11}	$BO_{12}EO_{15}$	1.08	-----	---

[a] No BO oligomer was available for measurement so NMR values for BO were substituted
[b] Intensity-averaged molecular weight.

66

2.10 Conclusions

Analysis of the copolymers is important for discerning the effects that changes in block length have on structure formation. Analysis by NMR quickly indicates the presence and level of contaminants in the material and provides an M_n value, but it cannot distinguish provide information on copolymer homogeneity. GPC provides a polydispersity and an M_p value that can be converted into a composition, but due to differences in solubility between the EO and BO blocks, GPC overestimates the length of BO blocks. Mass spectrometry requires the most data manipulation, but also provides the greatest detail about copolymer composition, polydispersity and the extent of EO capping. While data provided by mass spectrometry are probably the most accurate in describing average copolymer composition, the real advantage of this method is the compositional profile, which provides the best illustration of the distribution of copolymer compositions. However, given the relative speed and accuracy of NMR, it was selected as the initial method for copolymer analysis.

2.11 References

(1)   Inoue, S.; Aida, T. Living polymer systems, epoxides and lactones. In *Encycl. Polym. Sci. Eng.*, 1990; Vol. Supplemental, pp 412-420.

(2)   Shinoda, K.; Carlsson, A.; Lindman, B. *Advances in Colloid and Interface Science* **1996**, *64*, 253-271.

(3)   Kalinoski, H. T. Chemical analysis of polyoxyalkylene block copolymers. In *Nonionic Surfactants: Polyoxyalkylene Block Copolymers*; Nace, V. M., Ed.; Marcel Dekker: New York, NY, 1996; Vol. 60, pp 31-66.

(4)   Harris, J. K.; Rose, G. D.; Bruening, M. L. *Langmuir* **2002**, *18*, 5337-5342.

(5)   Thier, R.; Bolt, H. M. *Critical Reviews in Toxicology* **2000**, *30*, 595-608.

(6)   Whitmarsh, R. H. Synthesis and chemical modification of polyoxyalkylene block copolymers. In *Nonionic Surfactants: Polyoxyalkylene Block Copolymers*; Nace, V. M., Ed.; Marcel Dekker: New York, NY, 1996; Vol. 60, pp 1-30.

(7)   Nace, V. M. Properties of polyoxyalkylene block copolymers. In *Nonionic Surfactants: Polyoxyalkylene Block Copolymers*; Nace, V. M., Ed.; Marcel Dekker: New York, NY, 1996; Vol. 60, pp 145-183.

(8)   Dan, N.; Safran, S. A. *Europhysics Letters* **1993**, *21*, 975-980.

(9)   Ribeiro, A. A.; Dennis, E. A. Structure and Dynamics by NMR and Other Methods. In *Nonionic Surfactants: Physical Chemistry*; Schick, M. J., Ed.; Marcel Dekker: New York, NY, 1996; Vol. 23, pp 971-1009.

(10)   Provder, T., Ed. *Chromatography of Polymers: Characterization by SEC and FFF.*; American Chemical Society, 1993; Vol. 521.

Chapter 3

Effect of Butylene Oxide and Ethylene Oxide Block Length on Structure Formation

3.1 *Introduction*

BO/EO diblock copolymers offer special opportunities in the study of vesicle formation because the surfactant head group properties change with increasing EO block length as well as solution conditions. The EO block forms hydrogen bonds with water; therefore larger EO blocks increase amphiphile hydrophilicity and hence, the critical micelle concentration (CMC), which is the surfactant concentration required to initiate structure formation. However, increasing either EO block length or surfactant concentration can lead to pronounced interaction of aggregates and loss of discrete structures.[1] Longer EO blocks also change the head group diameter, altering the critical packing factor and potentially the type of micellar structures that form.[2]

Solvation of EO is enthalpically driven, so the hydrophile has decreasing solubility with increasing temperature.[3] Like many ethoxylated surfactants, BO/EO copolymers can form liquid crystalline structures that are temperature sensitive and have an obvious phase-transition point.[4,5] Above this temperature, loss of EO hydrophilicity eventually leads to structure degradation. As with most surfactants, high concentrations of selected salts or organic solvents also alter aggregate formation.[6] Thus, variation of block length, temperature, solvent, or ionic strength should allow for manipulation of ethoxylated structures.

As discussed in section 1.6, Israelachvili *et al.* described micellar structure formation in terms of a critical packing factor (CPF), Φ, which is defined in equation 3.1.

In this equation, V is the hydrophobe volume in the micelle core, a_o is the cross-sectional area of the head group, and l_c is the hydrophobic chain length.[2]

$$\Phi = V/(l_c\, a_o) \qquad\qquad\qquad \text{eq. 3.1}$$

Israelachvili's model hypothesizes that changes in V, l_c, or a_o affect micelle formation by altering the amphiphile shape and hence, the geometry of structures it can form. These changes include modifications of the surfactant composition or changes in the local environment that lead to alternate amphiphile geometries. Here I focus on surfactant composition changes and their effects on micelle formation particularly the impact of EO block length.

Once formed, the micelles themselves can organize into structures called meso-phases. The top row of Figure 3.1 shows the most common micellar structures as they exist under dilute conditions. Rows 2 and 3 indicate the types of micellar aggregates that can form as surfactant concentration increases. Several of these meso-phases, such as hexagonal, tetragonal and lamellar, are optically anisotropic and produce a birefringence pattern when viewed under plane-polarized light. Examination of such meso-phases reveals the type of micelle involved and provides insight into the effects of EO and BO block length on micelle formation.

Thus two factors dominate meso-phase formation; the critical packing factor because it determines micellar shape and the amphiphile concentration. However with ethoxylated surfactants these two factors are not necessarily independent. Amphiphile concentration changes may lead to changes in head group area, a_o, which can alter the micelle shape and therefore change the meso-phase.[6]
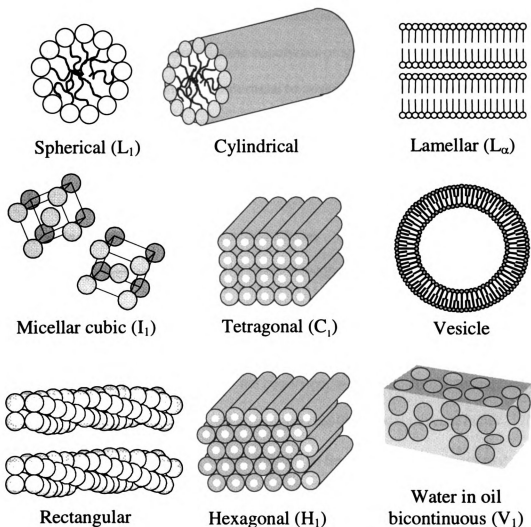
Figure 3.1. Micellar aggregate structures and the resulting meso-phases. (Meso-phase designation in parentheses.)

This chapter will discuss the process for selecting BO/EO compositions that demonstrate the potential for vesicle formation and evaluation of the structures that these materials form. I begin by examining the meso-phases formed by numerous compositions as a function of concentration in water, searching for the birefringent patterns indicative of liquid-crystalline, meso-phase formation. I then identify vesicle-

forming copolymers and discuss the physical characteristics of vesicles produced by these amphiphiles. Finally, I describe the copolymer properties, e.g., average EO block length and polydispersity, that are most critical to vesicle formation and how those properties can be manipulated to alter the amphiphile packing geometry and influence structure formation.

3.2 *Screening Tests for Liquid Crystalline Phases*

It has been previously shown that planar lamellae can be converted to vesicles using shearing techniques.[7-10] Therefore my initial work focused on identifying BO/EO copolymers with block lengths appropriate for lamellae formation. If either the EO or BO block is too short (less than 4 units) the copolymer will not demonstrate amphiphilic properties. While BO block length has little impact on the critical packing factor (V/l_c is almost independent of BO length), it does impact the free energy requirement to disperse the molecules in water, a critical step in surfactant self-assembly. Thus the upper limit of BO block length is set by the dispersibility of the surfactant. Once a BO block length is selected, V and l_c are essentially constant.

Conversely, if the EO block is too long, the copolymer will show increased solubility in water and structures will form only at high concentrations. Therefore a copolymer which forms vesicles must have not only a BO block length suitable for forming micelles in water, it must have a corresponding EO length sufficient to produce the proper a_o. Although previous studies showed that the head group area at the air/ water interface changes with EO block length,[11] no accurate means of predicting head group size in solution is currently available. Because *a priori* prediction of structure

geometry is not currently possible, I used a screening method for determining the structure-formation capabilities of BO/EO copolymers with various block lengths.

Clint describes a screening test that quickly indicates the types of meso-phases a given surfactant will form with increasing levels of hydration.[12] The surfactant is placed on a glass microscope slide adjacent a drop of water. A slide cover is then placed over both drops, forcing them into contact. The sample is allowed to equilibrate for ~ 20 minutes before examination during which time a concentration gradient arises from the surfactant/ water interface into the surfactant rich area. Structures develop along this gradient as a function of hydration level. Meso-phase formation is monitored using plane-polarized light microscopy (PLM). Meso-phase type is indicative of micelle type and reveals how a_o is changing with hydration. The primary goal of this test was to identify compositions that produced lamellae, although all meso-phase structure formation was recorded. Planar lamellar structures can be precursors to vesicle formation, so identification of such structures suggests that a particular composition may form vesicles under selected conditions.

Crystalline structures are often optically anisotropic and are common among inorganic materials occurring whenever molecules become organized in a periodic fashion.[13] Liquid crystalline structures also display this property,[12] but the molecules are not held in as rigid an array as in crystalline solids, and thus the structures are frequently temperature and shear sensitive.[13,14] I examined BO/EO dispersions using plane-polarized light to determine if liquid crystal formation had occurred.

Six crystalline structures were identifiable by birefringence patterns observed using PLM (Olympus Vanox Transmission microscope, Olympus Optics, Tokyo):

73

tetragonal (C_1), hexagonal (H_1), reverse tetragonal (C_2), reverse hexagonal (H_2), planar lamellar (L_α) and spherical lamellar phases. (I follow the phase designations proposed by Gray and Windsor.[15]) Domain sizes of 500 nm or greater were necessary to produce a recognizable pattern, but for the majority of samples, this was not an issue.

Figure 3.2 shows an example of the tetragonal phase. It has been proposed that these patterns arise from the two-dimensional square tetragonal array of micellar rods, or worms, as shown schematically in Figure 3.1.[15] A "bundle" of rods associate to form a thick filament which weaves throughout the structure, but can remain fairly linear. Figure 3.2a shows the thicker, larger, more visible "fibers" produced by this meso-phase whereas Figure 3.2b shows a finer version of the same structure. The resulting optical pattern appears fuzzy and indistinct because of the weak impact each filament has on light transmission. The extent of optical rotation, and hence regional brightness, is largely a function of the tetragonal meso-phase thickness. This meso-phase is a highly viscous gel due to the extensive entanglement of these structures.
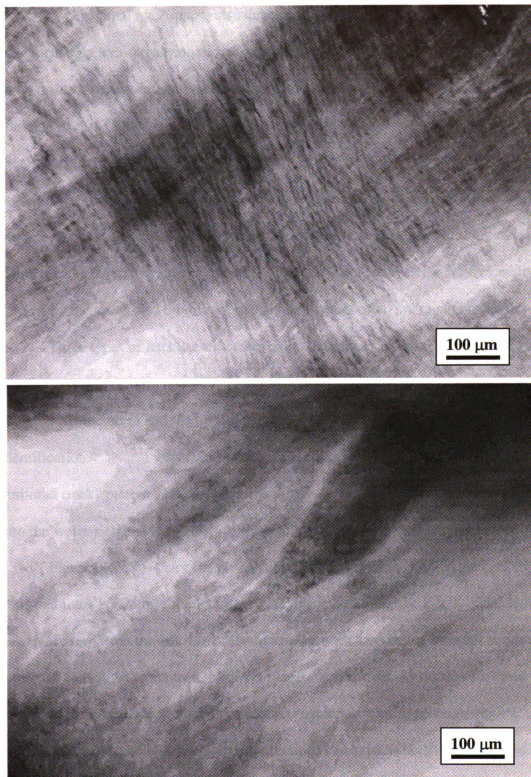
Figure 3.2. Tetragonal meso-phase produced by $BO_{11}EO_{12}$ in water (70 wt %).

The hexagonal meso-phase also develops from the packing of micellar rods, in this case forming a two-dimensional hexagonal array (Figure 3.1). The hexagonal packing of the rods leads to less entanglement and produces a more defined shear-face when shearing occurs. Thus, in contrast to the tetragonal phase, this meso-phase has prominent facets, well-defined repeat units and sharp edges (Figure 3.3). The only difference between the normal and reverse phases of the tetragonal and hexagonal phases is the volume fractions of the "oil" and water; structural organization is essentially the same. However, the reverse hexagonal phase is of interest because vesicles are frequently formed by the controlled dilution of this phase in water often under slight shearing.[16]

Three types of lamellar structures exist: flat planar as discs and sheets, tubular as myelin, and spherical as vesicles. (Numerous micrographs of these structures can be found in the literature and the optical patterns are sufficiently distinct as to allow facile identification.[12-14,17-22]) Planar lamellae are described as having a "streaky-oil" or "railroad track" pattern. Myelin appear as fingers of copolymer which extent outward into the water-rich phase and display this same pattern along the structure edges.

Figure 3.4 shows an example of planar lamellae sheets. Notice the broken "railroad track" pattern prominent in Figure 3.4a and running the length of the lamellae band. Moving from the left side of the image, between two strong lamellar bands is a region of hexagonal structures. Multiple phase states commonly occur with these materials because the high viscosity makes formation of a homogenous sample a slow process. Note also how planar lamellar structures can exist as both straight strands or produce tight bends and twists (Figure 3.4b). These shape differences are explained by the CPF model (equation 3.1).
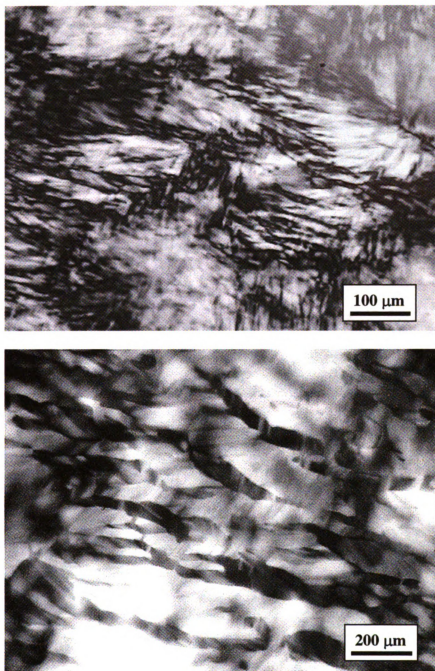
Figure 3.3. Hexagonal meso-phases produced by $BO_{11}EO_{19}$. (Copolymer/ water/ dodecane at 71/ 9.5/ 19.5 wt %.)
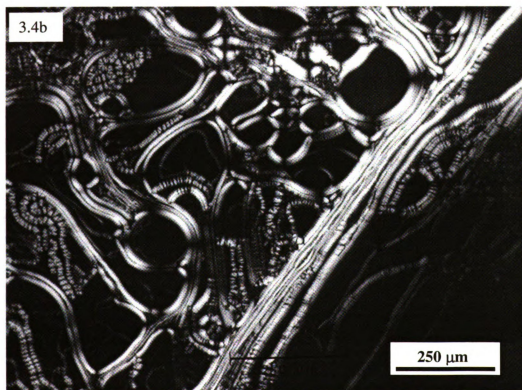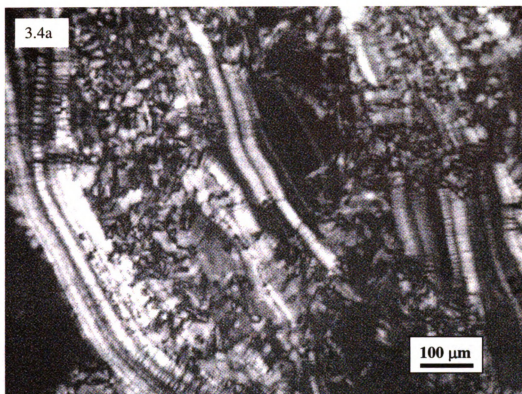
Figure 3.4. Planar lamellar formed by $BO_{11}EO_{12}$ in water (30 wt %).

A typical screening test result is shown in Figure 3.5. The pure water region is at the top of the figure with the copolymer concentration increasing from top to bottom. Three meso-phases can be identified when moving from low to high copolymer concentration. The first is the lamellar phase which consists of both myelin extending into the water region and of planar lamellar sheets. Next is the bicontiuous phase (V_1) which is not anisotropic and appears as a black band. The final phase, reverse hexagonal (H_2), is apparent by the sharp edges and numerous facets of the structure. The dark region following the hexagonal phase is the copolymer.

100 μm
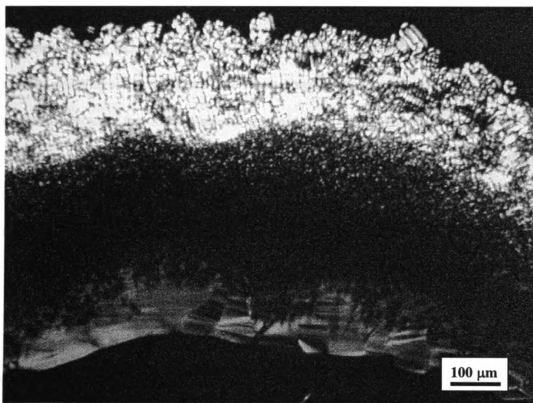
Figure 3.5. Example of screening test results of $BO_{11}EO_{12}$ copolymer.

It is important to note that the first structures encountered at the copolymer/ water interface are myelin, which are curved lamellar structures. This indicates that under dilute conditions the copolymer will probably form lamellar structures, possibly vesicles. It should also be noted that the myelin have a fairly large diameters (greater than 25 μm) which suggests a moderate value of a that would almost certainly increase when fully hydrated. An increase in a leads to greater curvature in the lamellar structure resulting in either vesicle or bicontinuous meso-phase formation.

I examined more than 30 BO/EO diblock copolymers using this screening technique. Copolymers with BO block lengths greater than 20 units did not readily produce liquid crystalline structures and, in fact, did not absorb the water droplet at all. Copolymers having BO lengths of ~ 10 units and EO block lengths of greater than 30 units were solubilized by the water until meso-phase formation began. (Liquid crystal formation occurred if the copolymer concentration was typically greater than about 40 wt %.) Compositions with BO blocks of approximately 10 units and EO blocks less than 25 units were most likely to form lamellae, and the tendency improved with decreasing EO block lengths.

3.3 *Spherical Lamellar Structures*

As with the other lamellar structures, vesicles are optically anisotropic and produce a visually unique birefringence pattern called the Maltese Extinction Cross. The Maltese cross results from the uni-axial nature of the structures[14] and is visible in structures with diameters greater than ~ 500 nm. Light passing through the polarizing filter interacts weakly with the liquid crystalline structures oriented parallel to the light

path and is therefore easily blocked by the analyzing filter. This produces a horizontal black band (Figure 3.6). Light passing through liquid crystals which are not oriented parallel to the filter is rotated slightly by the structures and passes through the analyzing filter. Light perpendicular to the analyzer is blocked, however, and the result is a pattern of two dark lines crossed at right angles to one another. Figure 3.7 shows a typical sample containing vesicles in both a PLM image and a white-light image. PLM reveals the Maltese cross patterns indicative of spherical lamellae, while the white-light image confirms the spherical nature of the structures.

Crystal orientation   Optical pattern
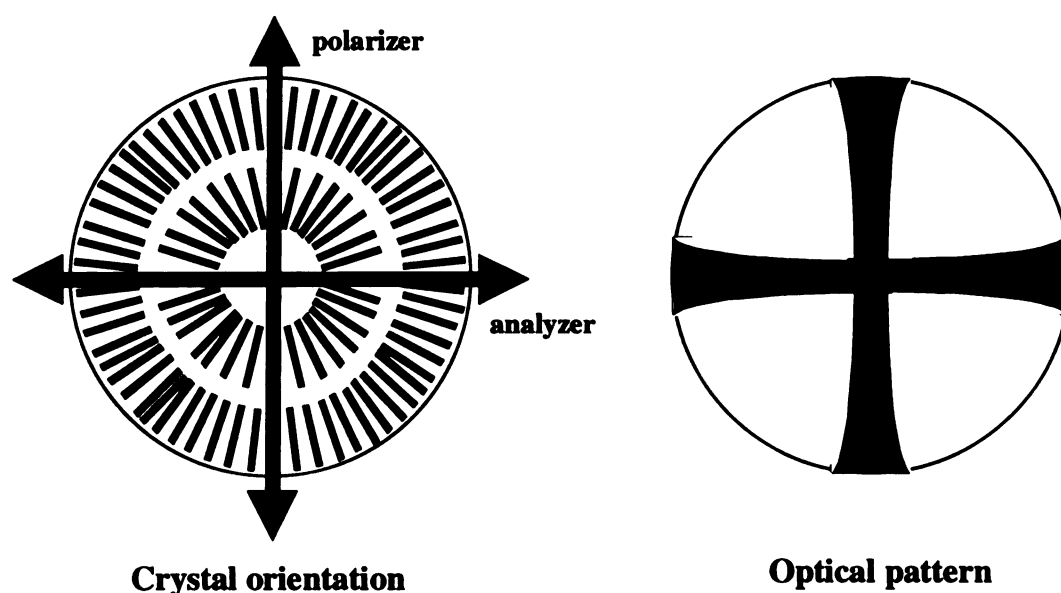
Figure 3.6. Maltese Cross formation occurs in plane-polarized light because of the uniaxial liquid crystalline structure of spherical lamellae. *Adapted from Collings.*[14]
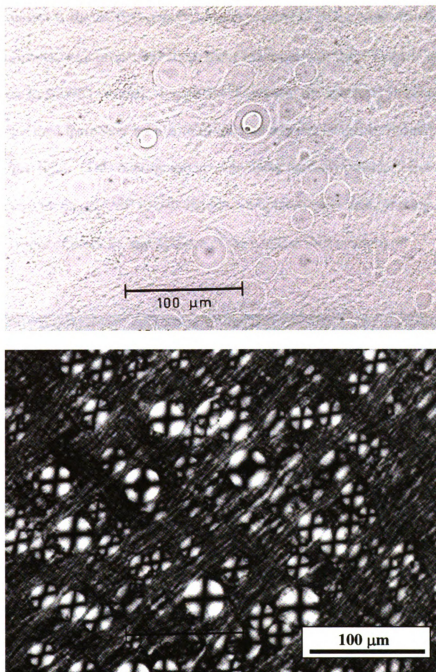
Figure 3.7. Vesicles of $BO_{11}EO_{12}$ (20 wt %) viewed through white light (above) and plane-polarized light (below). Note that vesicles are intermixed with planar lamellae. (Micrograph by Deborah Rothe, The Dow Chemical Company.)

In contrast to the BO/EO copolymer, dispersions of BO_{12} oligomers do not form vesicles. However, with proper agitation, these materials will form droplets that are similar in size to BO/EO vesicles. Figure 3.8 shows that the spherical BO droplets are easily distinguished from vesicles due to the lack of any birefringence properties under plane-polarized light. (This micrograph is taken using partially polarized light because when the filters are aligned 90° to one another, completely polarized, nothing is visible.) Note the grayness of particles and absence of the Maltese cross pattern.

50 μm
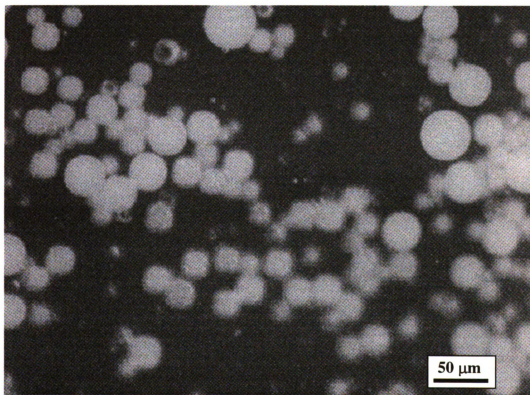
Figure 3.8. Butylene oxide oligomer, BO_{12}, (2 wt %) dispersion viewed under partially plane-polarized light microscopy.

Figure 3.9 shows an interesting phenomenon observed during screening tests of several BO/EO compositions. Here lamellae tubes, myelin, reach from the interface into the aqueous phase. Myelin lengthen as water at the interface diffuses up the tube to the end.[23] At the top-center of the micrograph, a vesicle can be seen forming at the end of the myelin as the copolymer becomes water saturated. The vesicle expands until it detaches from the myelin, and floats away to be replaced by another growing vesicle. This cycle can be repeated several times and these "budding" myelin are quite common.
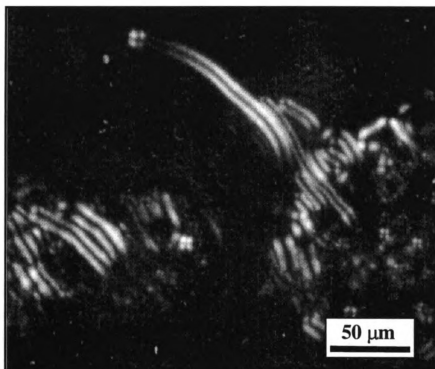
Figure 3.9. Vesicle of $BO_{11}EO_{12}$ "budding" from myelin tip formed at copolymer/ water interface.

Of the copolymers tested, those having BO lengths between 8 and 12 and having EO
lengths between 10 and 14 most commonly displayed this pattern. Based on these
observations, we refer to BO/EO vesicle formation as "spontaneous".

3.4   Vesicle Structures

Having identified several BO/EO copolymers that spontaneously produce vesicles
on contact with water, I began to study the vesicular structures themselves. The
following micrographs provide some indication of the size and types of vesicles that
could be formed using only the surfactant and water. The dispersions shown in Figures
3.10 and 3.11 were prepared by placing a drop of copolymer in a vial, adding about 0.5
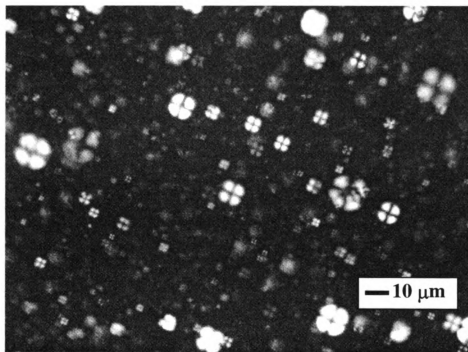
Figure 3.10. Plane-polarized light micrograph of $BO_{11}EO_{12}$ (1 wt %) without slide
cover.

85

mL of deionized water and agitating the sample by hand. Dispersions were examined within 2 hours of preparation. Figure 3.10 shows the range of vesicle diameters formed when the vials experience minimal agitation during vesicle formation. In this figure, the slide is not covered therefore the sample thickness is much greater than in Figure 3.11. The dispersion shown in Figure 3.11 was vigorously agitated for about 1 minute immediately upon addition of water. Note the improved uniformity in structure size as compared to Figure 3.10. Given the size range of all of these spontaneously-formed structures, they are probably multi-lamellar vesicles (MLV, Figure 1.7).
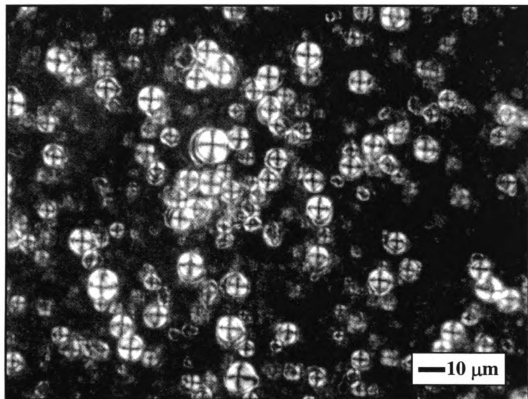
Figure 3.11. Plane-polarized light micrograph of vesicles from $BO_{11}EO_{12}$ dispersion (1 wt %).

3.5   Cryo-SEM

Because the Maltese cross patterns may result from either uni-lamellar or multi-lamellar vesicles, we examined dispersions using cryo-SEM (JEOL JSM-6320FV) to differentiate between these two possibilities. The dispersions were flash frozen in liquid propane and stored in liquid nitrogen. They were then transferred to a cryo preparation chamber at -90 °C, fractured with a cooled scalpel, held at -90 °C for 2 min in vacuum to sublime the surface ice, and sputter coated with conductive chromium. Samples were examined at -125 °C using a 3 keV electron beam. Figure 3.12 shows that the larger
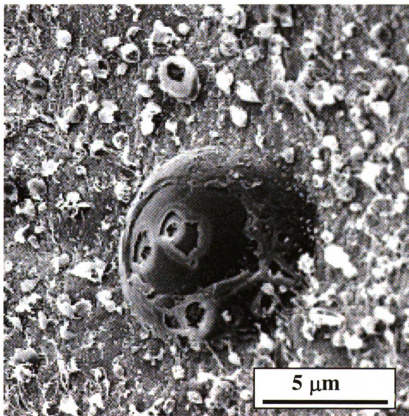
Figure 3.12. Cryo-SEM micrograph of $BO_{11}EO_{12}$ vesicle (1.0 wt %) taken 10 weeks after formation.   (Micrograph by David Williams, The Dow Chemical Company.)

structures formed from $BO_{11}EO_{12}$ are multi-lamellar vesicles (MLV). The concentric layers are apparent from spots where the structure was punctured during freeze fracture. Figure 3.13 also shows that the structures are composed of numerous layers, although in this micrograph the layers appear less uniform and spherical.
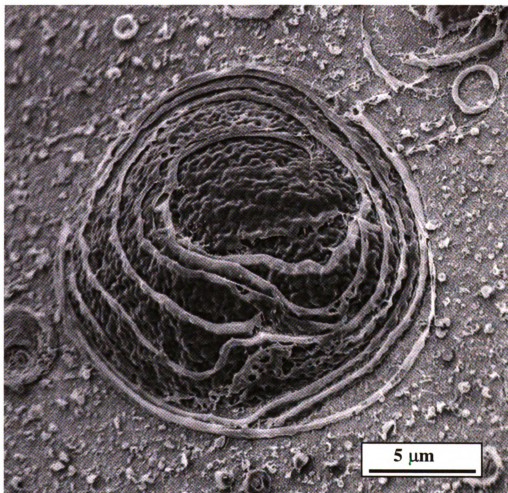
Figure 3.13. Cryo-SEM of vesicle from $BO_{11}EO_{12}$ (1 wt %) showing numerous layers of MLV structure. (Micrograph by David Williams, The Dow Chemical Company.)

3.6 Effect of EO Length on Vesicle Formation

The critical packing factor (equation 3.1) can be re-written as $\Phi = (V/l_c)(1/a_o)$.

For a given hydrophobe, e.g. BO_{11}, V/l_c is constant and independent of the head group.

Vesicle formation then requires finding a hydrophile with the appropriate value of a_o to

yield $0.5 < \Phi < 1$. For an ionic surfactant, where the hydrophile is generally short and

composed of a few atoms, the head group is envisioned as a sphere whose diameter

determines the head group area. For nonionic hydrophiles, which may be 20 times longer

and consist of dozens of atoms, the head group "shape" is not as obvious, and

determination of head group area is more complicated.

The relationship between EO block length and head group area for micellar

structures is not first order as it is at the air-water interface.[24] Instead, as the EO block is

hydrated, it forms an expanding coil whose diameter is dependent on EO length.[25] The

most pronounced changes in coil size, and hence head group area, occur with increases to

shorter EO blocks. Alexandridis et al. showed that the head group area for EO_2 to EO_{10}

varies with the square root of the number of EO units.[11] Thus, using an EO block as the

hydrophile, one can generate various values of a_o simply by changing the block length

during synthesis. Note that a_o is inversely proportional to Φ, so increasing the head

group area is expected to produce smaller structures.

Evaluation of numerous copolymers shows that surfactants with a BO block

length of ~ 10 and an EO block length of between 6 and 12 will spontaneously produce

vesicles even under dilute conditions. As the EO length increases the concentration for

vesicle formation also increases. Table 3.1 shows that increasing EO length produces

slightly smaller structures, consistent with an increase in a_o. Continued increases in EO

block length should eventually lead to a copolymer with a_O too large to produce vesicles. Consistent with this pattern, $BO_{10}EO_{24}$ did not form vesicles at any concentration, and dynamic light scattering showed the mean particle diameter in a 5 wt % $BO_{10}EO_{24}$ dispersion to be 14 nm, a value appropriate for micelles formed from a copolymer of this size.[26] Others have found that $BO_{10}EO_{40}$ produces only micelles.[27]

Table 3.1. Composition, molecular weight, density and concentration range for PLM-detectable vesicle formation for BO/EO diblock copolymers.

Copolymer[a]	M_n[b]	Density (g/mL)	Concentrations for MLV Formation	Ave. Diameter
$BO_{11}EO_6$	1154	1.00	0.05 – 20 wt %	5 μm [c]
$BO_{10}EO_{14}$	1322	1.01	0.05 - 20 wt %	5 μm [c]
$BO_{10}EO_{14}$	1384	1.02	0.5 – 20 wt %	3 μm [c]
$BO_{11}EO_{19}$	1661	1.03	2.0 – 20 wt %	1 μm [d]
$BO_{10}EO_{24}$	1824	---	none	----

a) H^1 NMR, b) mass spectrometry, c) 1 wt % dispersions, d) 5 wt % dispersions

To confirm that head group size is the primary reason for the structure-forming differences between copolymers, we attempted to induce micron-sized vesicle formation from a dilute $BO_{11}EO_{19}$ dispersion through chemical changes that affect head group diameter. One method for doing this is the addition of selected salts that compete with the hydrophile for free water.[6,28] Thus, a saline solution should "dehydrate" the EO group, decrease the head group size and make large MLV formation more favorable.[2] A 1.3 wt % sample of $BO_{11}EO_{19}$ was prepared using 12.5 wt % NaCl with gentle agitation.

After 24 h the sample contained an abundance of multi-lamellar structures with diameters of ~ 1.0 μm. No MLVs were observed at the same concentration without salt.

Alternately, the head group size may be reduced using thermal dehydration of the EO block. A 1.0 wt % dispersion of $BO_{11}EO_{19}$ was heated to 85 °C for 3 h, agitated while cooling and then examined using PLM. Figure 3.14 shows the changes in the dispersion due to heating. The large MLVs (> 3 μm dia.) were visible for up to 24 h after heating. (This provides some information as to the time required for complete rehydration of the EO block after thermal dehydration.) Based on these results, we conclude that the differences in structure formation between $EO_{12}BO_{11}$ and $EO_{19}BO_{11}$ are based primarily on head group size.

We also explored the effect of EO length on structure formation using a series of copolymers prepared by a sequential addition process. An $BO_{10}EO_{10}$ copolymer was prepared using a standard procedure. After copolymer formation, however, instead of quenching the entire reaction, only an aliquot was removed and quenched. A second reaction was performed to add another ~2 EO units to the remaining copolymer. An aliquot of this material was also removed and quenched, followed by another addition of EO_2 to the remaining copolymer. This procedure was repeated until a series of copolymers having the same BO block length and EO block lengths ranging from 10 to 24 was prepared.

Dispersions of 1 wt % surfactant were prepared from these copolymers. For copolymers with EO < 18, phase separation occurred after 5 days, forming a sediment of large structures and leaving a dilute, opaque, upper phase of structures less that 1 μm in diameter. After allowing the two phases to equilibrate for 3 weeks at room temperature,

an aliquot of the upper phase was removed and ultra-sonicated. Ultra-sonication should

yield smaller structures which should have a head group area, a, closer to the optimal

area, a_O and reduce structure polydispersity. The structures were then evaluated using

dynamic light scattering (Brookhaven 90Plus, Brookhaven Instruments, USA).
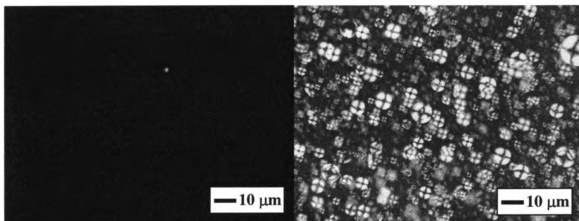
Figure 3.14. Plane-polarized light micrographs of an $BO_{11}EO_{19}$ aqueous dispersion (1 wt %) before and after heating. No vesicles are visible prior to heating (left), but numerous structures are visible after heating at 85° C for 3 hours (right).

Figure 3.15 shows structure diameter as a function of the EO block length. These data clearly show that sonicated structures produced from copolymers with shorter EO blocks are much larger than those produced from copolymers with EO lengths greater than 16 units, which is in general agreement with the geometric model (eq. 3.1). Structures produced by $EO_{10}BO_{10}$ to $EO_{14}BO_{10}$ are too large to be spherical micelles and are probably uni-lamellar vesicles. Conversely, the structures produced by EO_{20} to EO_{24} have diameters appropriate for spherical micelles formed from surfactants of this

size. Particles produced from EO_{16} may represent transitional aggregate structures, such as rods or worms, and EO_{18} structures are likely swollen micelles.
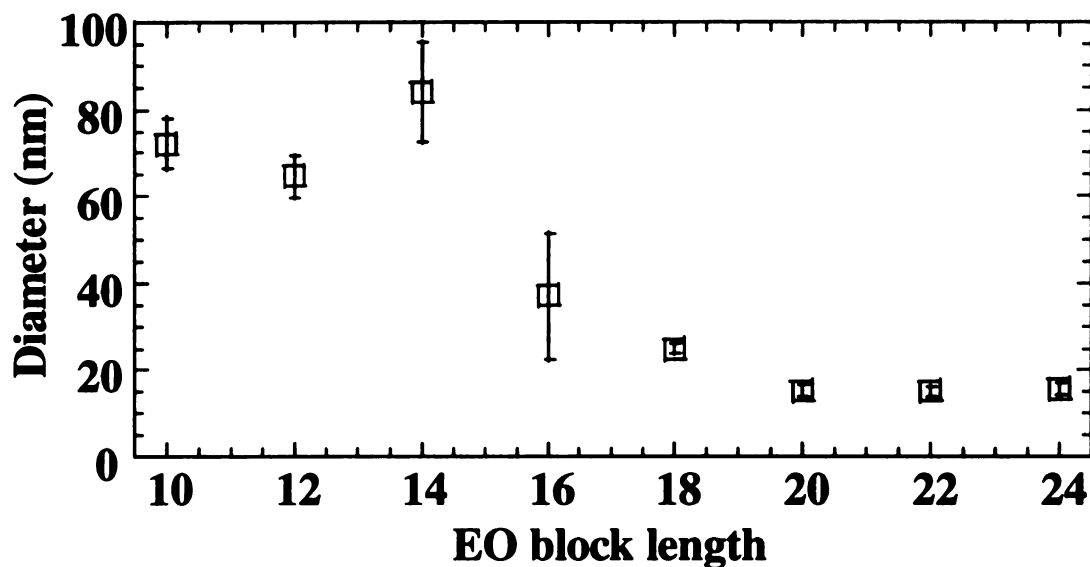
Figure 3.15. Mean structure diameters as a function of EO block length for $BO_{11}EO_x$ copolymers. (Error bars represent standard deviations of 5 consecutive measurements.)

3.7 *Effect of Concentration on Vesicle Formation*

The head group diameter for an ethoxylate group is concentration dependent, so I also studied the effect of copolymer concentration on vesicle formation. In a typical procedure, one drop of a particular copolymer was added to a tared 5-dram vial and the amount of water required for the desired concentration was added. The vial was moderately agitated by hand (~ 1 shake sec^{-1}) for 30 seconds and allowed to stand for a minimum of 24 h before examination. Aqueous dispersions of each copolymer were prepared in concentrations ranging from 0.005 to 20 wt %, but the majority of work focused on 0.5, 1.0, 2.0, 5.0 and 10.0 wt % samples. This concentration range was

selected to ensure that the EO head groups were fully solvated, and to minimize the effects of micelle-micelle interactions. (Samples greater than 40 wt % copolymer were known to produce gels.) Samples were visually inspected for clarity, relative viscosity, and examined using plane-polarized light microscopy (PLM) to determine the number and type of any meso-phases present.

Copolymers with the shorter EO blocks ($< EO_{12}$) make PLM-detectable MLVs at all concentrations studied (Table 3.1). PLM images also showed that $BO_{11}EO_{12}$ formed the highest density of large, stable MLVs. At 0.5 wt %, $BO_{11}EO_{12}$ formed abundant structures with diameters ranging from 3 to 30 μm as determined by light scattering. As the copolymer concentration increased, so did the apparent vesicle concentration as viewed by PLM. At copolymer concentrations of 1.0 and 2.0 wt %, a sediment of MLVs formed after a few days, and no gel fragments or other liquid crystal structures could be observed in the sediment. In contrast, at 5.0 wt % the copolymer formed a stable dispersion with no indications of phase separation or sediment formation for at least 2 months. MLVs were visible in samples with concentrations greater than 5.0 wt % for at least 2 months when stored at room temperature. From 10 to 40 wt % $BO_{11}EO_{12}$, PLM revealed planar lamellae with MLVs (Figure 3.16), with the level of planar structures increasing until samples of 50 wt % $BO_{11}EO_{12}$ were exclusively planar lamellar.

For $BO_{11}EO_{19}$, vesicle formation depended on copolymer concentration, with identifiable vesicles only visible at concentrations of 2.0, 5.0 and 10 wt %. At 0.1 wt %, the sample formed a single, translucent phase with no crystalline structures observable by PLM. Sample opacity increased without PLM-detectable vesicle formation until the copolymer concentration reached 2.0 wt %. At concentrations less than 2 wt %,
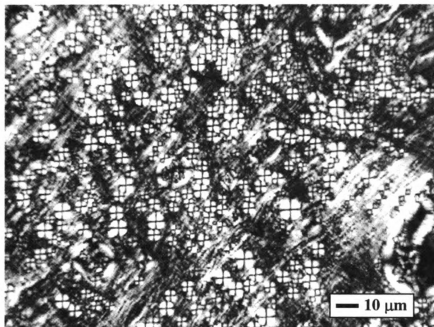
Figure 3.16. $BO_{11}EO_{12}$ dispersion (15 wt %) showing vesicles with planar lamellae.

$BO_{11}EO_{19}$ may form vesicles that are too small to be detected with PLM. (Smaller vesicles would be consistent with an increased a_o, and light scattering data (Brookhaven 90Plus, Brookhaven Instruments, USA) for a 0.1 wt % aqueous dispersion showed particles with diameters of ~ 60 nm.) Within a few days of preparation, the 2.0 wt % dispersions formed a sediment consisting of MLVs having a mean diameter of 1 μm. No other liquid crystal phases were visible in either the sediment or the continuous phase, although the continuous phase was not clear. The composition of the sediment did not change after standing for 1 month at room temperature. Sediment formation, if it occurred, was less apparent in 5.0 and 10.0 wt % dispersions due to increased opacity. Planar lamellar structures first appear at a concentration of about 35 wt % and aggregates were exclusively planar lamellar at 70 wt %.

These results are consistent with the current understanding of ethoxylate head group changes as a function of block length and copolymer concentration. Increasing the block length increases a_o and shifts micelle formation from vesicles to spherical micelles. Increases in copolymer concentration have two effects; reduced hydration of the EO block and increases block interactions both leading to a decrease in the head group size. This is evidenced by the formation of vesicles as the copolymer concentration increases.

3.8 *Effects of Polydispersity on Vesicle Formation*

As discussed in chapter 2, the BO/EO copolymers synthesized for this work are not monodisperse, and copolymer polydispersity may impact structure formation.[29] In a preliminary investigation of the effects of polydispersity, we examined BL50-1500, a commercial surfactant (The Dow Chemical Company, USA) described as having an average composition of $BO_{10}EO_{17}$. Based on the results described above, $BO_{10}EO_{17}$ should spontaneously produce MLVs at elevated concentrations. However for 5 wt % dispersions of this copolymer, dynamic light scattering (Brookhaven) showed only micelles with diameters of ~ 18 nm. The bulk copolymer was a waxy solid, suggesting that a significant portion of the surfactant had an EO length greater than 25, so I decided to fractionate the material. The copolymer was suspended in hexane and then centrifuged at room temperature for up to 16 hours to produce a two-phase sample.[30] The clear, upper phase was decanted while the solid, lower phase, which contained the longer, insoluble EO chains, was removed after melting. The upper phase was re-centrifuged at - 5 °C. The newly formed clear, upper phase was also decanted while the white solid was

melted and removed. Finally, the hexane was removed from the upper phase to produce a clear liquid.

This clear liquid, which had an average composition of $BO_{11}EO_8$ as shown by H^1 NMR, spontaneously produced $1 - 5$ μm-diameter MLVs just as our $BO_{11}EO_{11}$ had, even at concentrations well below 1 wt %. This fraction accounted for ~ 30 wt % of the BL50-1500 copolymer, while the remaining material had an average EO length greater than 25. This result confirms that determination of the mean composition alone is not sufficient to indicate whether a given copolymer will form vesicles.

A screening test (section 3.2) of the $BO_{11}EO_8$ copolymer also produced an unexpected structure. Upon hydration the copolymer produced myelin, as frequently occurs with the other BO/EO surfactants we studied. However, many of these structures were twisted into helical shapes that persisted for hours (Figure 3.17). This may be an indication that a substantial fraction of these molecules have an average head group size at this level of hydration that is close to that required for planar lamellae structures, however further investigation is necessary. It should be noted that no vesicles were observed "budding" from the helical structures.
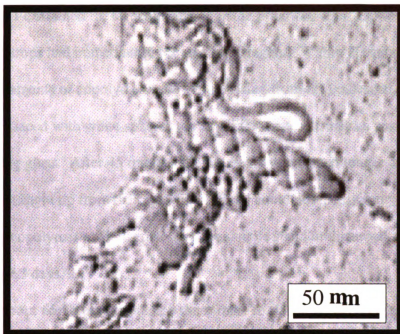
Figure 3.17. Plane-polarized light micrograph of $BO_{11}EO_8$ (BL50-1500A) shows helical myelin at water/ surfactant interface upon hydration.

3.9 *Giant Vesicles*

Based on my observations of MLV formation and the effects of EO block length on structure size, I proposed that if the proper copolymer were allowed to hydrate slowly and without agitation, it might produce much larger structures than those produced by agitation after a short hydration period. Thus I chose copolymer M1038, which mass spectrometry indicated has a mean composition of $BO_{12}EO_{9.5}$, because the shorter EO block length, even when fully hydrated, will produce a small head group and yield a large radius of curvature, therefore larger, more easily detected structures.

As a "proof-of-concept" test I deposited 4 drops (~ 0.11 g) of copolymer dropwise into a glass bottle containing 10 g of DI water. The droplets flattened and fell to the

bottle bottom. I examined the structures using plane-polarized light and found that the surface of the drops had immediately become birefringent. Within 20 minutes birefringent filaments of copolymer were visible rising from the coalesced droplets. The filaments were laced with white spheres too small for me to identify as vesicles using a 15X magnifying glass. After 45 minutes the filaments were much longer and in several cases moving straight up from the copolymer. I still could not identify any Maltese cross patterns in the copolymer or filaments. I let the sample stand undisturbed at room temperature for 3 days.

After about 65 hours, I examined the sample to find several changes. The copolymer was now a swollen white gel about 4 mm thick above which was an opaque liquid layer also 4 mm thick. Approximately 10 mm above the copolymer surface the solution was completely clear. When viewed through the crossed polarizing filters, the copolymer surface appeared covered with numerous bright spots that appeared to be Maltese crosses. Several vesicular structures were obvious close to the bottle wall however I could not confirm structure formation within the copolymer.

As the filaments passed through the opaque layer, they became chains of vesicles (up to 10) that were about 0.5 mm in diameter. The structures were faint suggesting that they were composed of few lamellar layers. Concentric layers (3 to 5) were visible inside the structures. Above the opaque layer the filaments did not produce vesicles.

I re-examined the sample 138 hours after the copolymer addition. The copolymer surface now displayed considerably more Maltese crosses than previously. In addition to the large structures (~ 1 mm in dia.) there were hundreds of structures with diameters of 0.1 mm. The large structures did not appear any more intense than they had previously.

The opaque layer above the copolymer was now filled with smaller, shorter strands of copolymer creating a "fuzzy" surface appearance. The opaque layer volume had doubled and the remaining liquid above it was no longer clear. The extent of vesicle formation by the filaments had increased; they now contained twice as many vesicles as they had at 65 hours. The vesicles were also larger, averaging almost 1 mm in diameter although they were no brighter suggesting that the number of lamellar layers that each contained was unchanged.

The expansion of the "fuzz" and opaque layers continued until I ceased observations after about 520 hours. At this point the "fuzz" layer was 12 mm above the copolymer surface and the opaque layer reached the top of the bottle. The number of vesicles had increased by 5X, with diameters ranging from 0.01 to 1 mm. The filaments were covered with vesicles (they appeared to be "budding" from the filament surface) however the structures were no brighter than when originally observed.

To repeat this experiment under conditions more amenable to recording my observations, I prepared a rectangular, glass cell as the sample holder and capped it with cork (Figure 3.18). To minimize vibration, I glued the cell to a wooden dowel that I inserted into a clamp holder and mounted it to a lattice. I also attached a plastic ruler to the cell face as a reference scale. I then positioned 150 W spotlight, a glass bottle (5" x5" x8") of water to act as an IR filter and polarizing filter mounted on a quartz plate sequentially behind the sample and a camera (Minolta X700) equipped with a second polarizing filter in front of a macro zoom lens at a 4:1 setting. I used 400 ASA TMax black and white film (Kodak Co., Rochester, NY) for increased clarity. This way, I could easily record the any large structure formation using plane-polarized light.
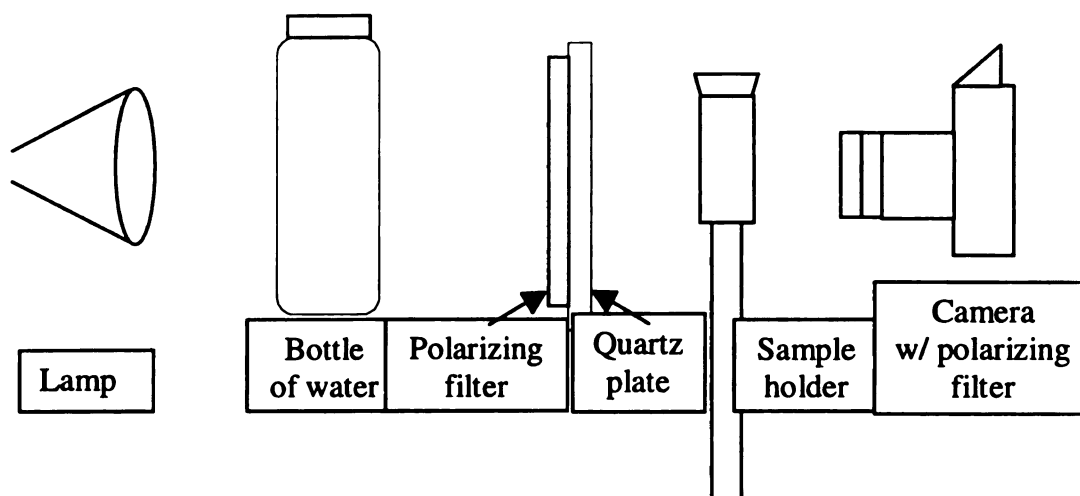
Figure 3.18. Experimental set-up for photographing giant vesicle formation.

I added about 4 drops (~ 0.12 g) of copolymer to about 15 g of DI water

depositing the drops on the cell bottom. Within minutes the copolymer surface was

birefringent and in less than an hour spherical structures were apparent. They followed

the same developmental sequence as structures in the first experiment. However

overnight the temperature in the lab rose to more than 32 °C and I realized that

temperature increases each evening were probably common place. Because of the

sensitivity of the EO block to temperature changes, I transferred the entire apparatus to a

constant temperature lab (22 °C), switched the light source to a 120 W lamp (less IR) and

let the experiment continue.

After a total of four days numerous large vesicles were visible on the bottom of

the cell. Figure 3.19 shows the abundance and size of these structures. Most have

diameters in excess of 0.1 mm with many exceeding 0.5 mm. This is a smaller average

diameter than for structures in the original experiment, but clearly shows the proliferation

of these structures. Note that few of the vesicles are suspended in the aqueous phase.

Most remain on the copolymer surface or along the bottom of the cell.
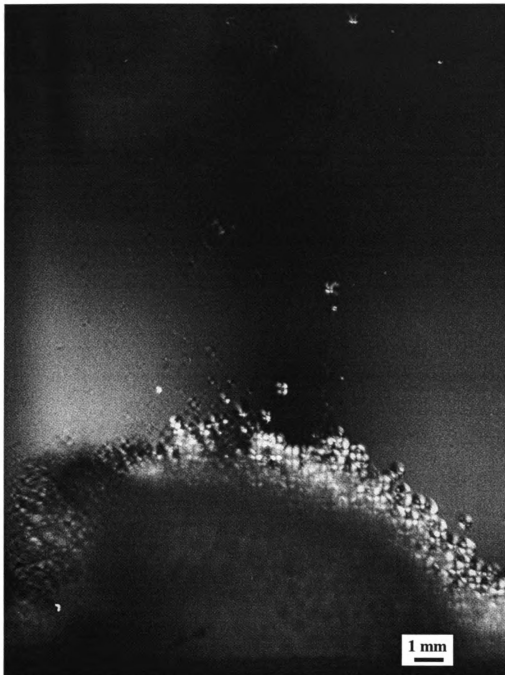
Figure 3.19. Giant vesicles from copolymer $BO_{12}EO_{9.5}$ in glass cell.

There are also several larger structures which have a much less distinct Maltese cross pattern. These may contain fewer lamellae or they may not be vesicles at all.

To evaluate the number and fragility of the structures I gently tilted the cell about 45° and held it in that manner for ~ 15 seconds. The vesicles were quickly and thoroughly dispersed through out the aqueous phase and remained so for several hours. Figure 3.20 shows the dispersion 22 minutes after tilting.
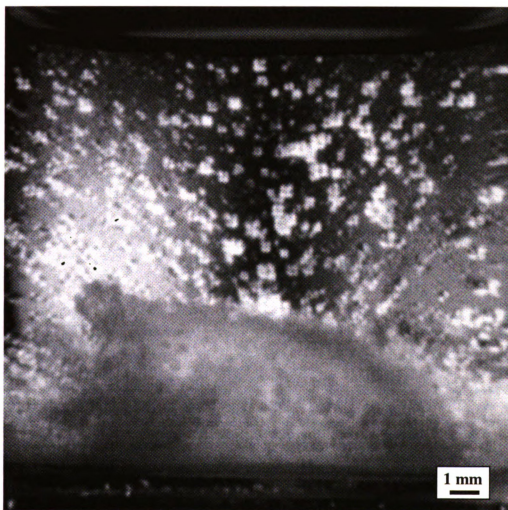
Figure 3.20. Giant vesicles dispersed after slight agitation.

I extracted several vesicles and aqueous phase using a pipette, placed them into a vial and set them aside. After 3 days I transferred several structures to a deep-well slide and obtained micrographs using PLM. In Figure 3.21 the multi-lamellar composition of these structures is quite apparent. In spite of rough handling, these structures appeared to be relatively unaffected. They easily rolled along the bottom of the vial for weeks. They could be damaged, but it required considerably more effort than expected.
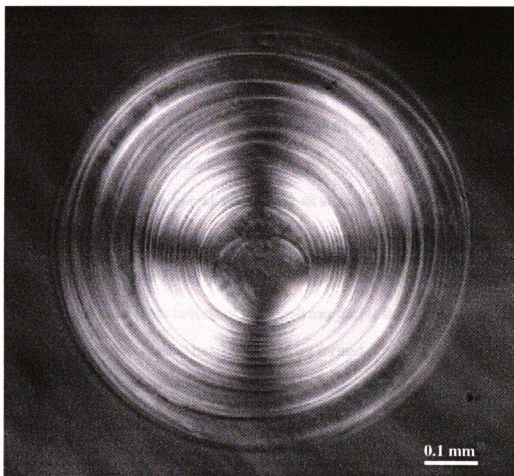
Figure 3.21. Plane-polarized light micrograph of giant vesicle isolated from copolymer of second experiment.

I repeated the experiment a third time using the same apparatus, but having the entire experiment take place in the constant temperature lab. The drops were placed on the cell bottom and the structural development sequence was similar to the first and second attempts. However, the filaments did not produce structures in the same manner as the first two experiments. Only the filament tips showed the spherical structure formation and while they were as large as the previous vesicles they were not as bright and appeared to be composed of few layers. Instead of development via filaments, it appeared that the copolymer itself slowly expanded to produce the structures, eventually becoming saturated with vesicles after about 3 weeks, much longer than required by the first two runs. A fourth attempt under exactly the same conditions as the third produced essentially the same results; no vesicle growth from the filaments and the structures which did develop were much fainter.

I decided to see if post-heating would have an affect on the structures. I transferred the entire cell and holding apparatus into an oven to stand at 30 °C for 90 hours. Upon re-examination I could see no change in the nature or quantity of structures. It appears then that even slight heating of the copolymer during the first 48 of hydration has an effect on both the type and number of vesicles formed.

The most probable cause of these differences concerns changes in the head group as a function of temperature which directly affect the amphiphile packing and nature of the resulting structure. If the copolymer hydrates at a temperature which yields an equilibrium head group diameter consistent with planar lamellar structures, then the copolymer simply swells with time eventually reaching an equilibrium state. However if the temperature drops so that the head group diameter increases the new packing factor

indicates a curved structure will result. The strain of the larger head groups could cause large sections of lamellae to delaminate from the copolymer and form curved structures, the giant vesicles observed.

Conversely, if the head group diameter is also large enough to produce a strain in the copolymer, then as soon as a few layers become hydrated they may delaminate from the bulk copolymer and form structures. These would have a similar diameter to those formed in the two-temperature process because the final head group diameter is the same. However they would not contain as many lamellae because the strain initiated curvature before the copolymer microns below the surface was hydrated enough to curve as well. Further study on this process is warranted.

3.10 *Conclusions*

The use of BO in amphiphilic BO/EO diblock copolymers results in large hydrophobe volumes. This leads to surfactants with compositions that spontaneously produce vesicular structures in water at room temperature. However for spontaneous vesicle formation, the BO block must be less than 20 units long, otherwise the copolymer is not dispersible in water. Differences in structure formation between the various BO/EO compositions follow the general trend put forth by Israelachvili's geometric model. For a given BO length, shorter EO chains favor the formation of vesicles by decreasing the area of the head group. The tendency for vesicle formation can be manipulated with concentration, thermal cycling or ionic strength.

Cryo-SEM micrographs indicate that the structures formed are multi-lamellar spheres, and this is not unexpected given the particle diameters of > 1 μm. MLVs

spontaneously form in concentration ranges from 0.05 to 20 wt % for the copolymers

with EO < 15 and in concentrations of 2.0 to 20 wt % for $BO_{11}EO_{19}$. If the block length

is short (< 10), slow copolymer hydration will produce giant MLVs having diameters in

the 0.5 mm range. However, vesicles do not form for EO > 23. Also the mean EO block

length is not sufficient alone to predict vesicle formation. The polydispersity of the EO

block length must be narrow enough that the actual head group size is similar to that

predicted by the mean.

3.11 References

(1)   Derici, L.; Ledger, S.; Mai, S.-M.; Booth, C.; Hamley, I. W.; Pedersen, J. S. *Phys. Chem. Chem. Phys.* **1999**, *1*, 2773-2785.

(2)   Israelachvilli, J. N.; Mitchell, D. J.; Ninham, B. W. *J. Chem. Soc., Faraday Trans. 2* **1976**, *72*, 1525-1568.

(3)   Bailey, F. E., Jr.; Koleske, J. V. Configuration and hydrodynamic properties of the polyoxyethylene chain in solution. In *Nonionic Surfactants: Physical Chemistry*; Schick, M. J., Ed.; Marcel Dekker: New York, NY, 1987; Vol. 23, pp 927-969.

(4)   Hamley, I. W.; Pople, J. A.; Booth, C.; Yang, Y. W.; King, S. M. *Langmuir* **1998**, *14*, 3182-3186.

(5)   Bedells, A. D.; Arafeh, R. M.; Yang, Z.; Attwood, D.; Padget, J. C.; Price, C.; Booth, C. *J. Chem. Soc., Faraday Trans.* **1993**, *89*, 1243-1247.

(6)   Rosen, M. J. *Surfactants and Interfacial Phenomena*, Second ed.; Wiley-Interscience: New York, 1989; p 194.

(7)   Mueller, S.; Boerschig, C.; Gronski, W.; Schmidt, C.; Roux, D. *Langmuir* **1999**, *15*, 7558-7564.

(8)   Diat, O.; Roux, D. *Journal de Physique II* **1993**, *3*, 9-14.

(9)   Escalante, J. I.; Hoffmann, H. *J. Phys.: Condens. Matter* **2000**, *12*, A483-A489.

(10)   Panizza, P.; Colin, A.; Coulon, C.; Roux, D. *European Physical Journal B: Condensed Matter Physics* **1998**, *4*, 65-74.

(11)   Alexandridis, P.; Athanassiou, V.; Fukuda, S.; Hatton, T. A. *Langmuir* **1994**, *10*, 2604-2612.

(12)   Clint, J. H. *Surfactant Aggregation*; Chapman & Hall: New York, NY, 1992; pp 158-171.

(13)   Gray, G. W.; Windsor, P. A. *Liquid Crystals & Plastic Crystals; Physico-Chemical Properties and Methods of Investigation*; John Wiley and Sons: New York, NY, 1974; Vol. 1; p 223.

(14)   Collings, P. J. *Liquid Crystals: Nature's delicate phase of matter*; Princeton University Press: Princton, NJ, 1990; p 90.

(15)   Gray, G. W.; Windsor, P. A. *Liquid Crystals & Plastic Crystals; Physico-Chemical Properties and Methods of Investigation*; John Wiley and Sons: New York, NY, 1974; Vol. 1; p 280.

(16)   Marsh, D. *Handbook of Lipid Bilayers*; CRC Press: Boca Raton, FL, 1990; p 387.

(17)   Wanka, G.; Hoffmann, H.; Ulbricht, W. *Macromolecules* **1994**, *27*, 4145-4149.

(18)   Yu, G.-E.; Li, H.; Fairclough, J. P. A.; Ryan, A. J.; McKeown, N.; Ali-Adib, Z.; Price, C.; Booth, C. *Langmuir* **1998**, *14*, 5782-5789.

(19)   Kunieda, H.; Nakamura, K.; Davis, H. T.; Evans, D. F. *Langmuir* **1991**, *7*, 1915-1919.

(20) Gradzielski, M.; Mueller, M.; Bergmeier, M.; Hoffmann, H.; Hoinkis, E. *Journal of Physical Chemistry B* **1999**, *103*, 1416-1424.

(21) Dorfler, H. D.; Knape, M. *Tenside, Surfactants, Deterg.* **1993**, *30*, 196-203.

(22) Franses, E. I.; Hart, T. J. *J. Colloid Interface Sci.* **1983**, *94*, 1-13.

(23) Buchanan, M.; Egelhaaf, S. U.; Cates, M. E. *Langmuir* **2000**, *16*, 3718-3726.

(24) Schick, M. J. *J. Colloid Sci.* **1962**, *17*, 801-813.

(25) Schick, M. J. *J. Am. Oil Chemists' Soc.* **1963**, *40*, 680-687.

(26) Harris, J. K.; Rose, G. D.; Bruening, M. L. *Langmuir* **2002**, *18*, 5337-5342.

(27) Yu, G.-E.; Yang, Y.-W.; Yang, Z.; Attwood, D.; Booth, C.; Nace, V. M. *Langmuir* **1996**, *12*, 3404-3412.

(28) Lange, H.; Jeschke, P. Surface monolayers. In *Nonionic Surfactants: Physical Chemistry*; Schick, M. J., Ed.; Marcel Dekker: New York, NY, 1987; Vol. 23, pp 1-44.

(29) Dan, N.; Safran, S. A. *Europhysics Letters* **1993**, *21*, 975-980.

(30) Yang, Y.-W.; Brine, G.; Yu, G.-E.; Heatley, F.; Attwood, D.; Booth, C.; Malmsten, M. *Polymer* **1997**, *38*, 1659-1668.

Chapter 4

Vesicle Characterization and Stability

4.1 *Introduction to Vesicle Stability*

This chapter examines several properties of BO/EO vesicles that may affect their

potential utility in encapsulation applications. Specifically, I discuss the fraction of

BO/EO that forms vesicle structures, the stability of the structures under a variety of

conditions, and the ability of these vesicles to encapsulate hydrophilic and hydrophobic

materials. Vesicles are attractive encapsulation materials because their bilayer structure

consists of both hydrophobic and hydrophilic portions that can house selected materials.

Encapsulated hydrophilic materials may have little association with the amphiphile head

group, and therefore the volume of solution encapsulated by the vesicle generally limits

the loading of these materials. Limits on loading of hydrophobic guests depend on how

significantly the incorporation of these molecules alters the packing geometry of the

amphiphile. MLVs are especially attractive because their large hydrophobic volume

should permit encapsulation of relatively large numbers of hydrophobic molecules.

Vesicles stability is an issue in encapsulation applications because there is a

constant exchange of surfactant between structures and the bulk aqueous phase.

Although the surfactant exchange rate for vesicles is similar to that of spherical micelles,[1]

the larger size of even small uni-lamellar vesicles (ULVs) yields lifetimes thousands of

times longer than those of micelles. Additionally, the exchange rate between the inner

and outer layer of the curved bilayer (the flip rate) is generally low.[2] The combination of

these effects can result in MLV lifetimes of weeks, months or even years.

Below, I first discuss the fraction of surfactant that is incorporated into vesicles. Subsequently, I examine structure stability, both thermal and mechanical, by monitoring the particle size distribution in vesicle dispersions after various post-formation treatments. Finally, I investigate the structural effects of introducing model hydrophobes or hydrophiles into BO/EO vesicles and monitor the release rate of a model compound.

4.2 *Yield of Structures*

The first question addressed was the fraction of copolymer contained in the vesicles at equilibrium. I had previously prepared numerous aqueous copolymers samples at various concentrations. Based on these samples I decided to initially focus on low concentration dispersions that were much less likely to produce gels or meso-phases. Samples of $BO_{11}EO_{12}$ and $BO_{11}EO_{19}$ had formed structures that settled out of the bulk phase. Vesicle sedimentation is consistent with MLV formation because a multi-layered structure should have a density slightly higher than water. Given copolymer densities of 1.00 to 1.03 g/mL (increasing with increasing BO block length, Table 3.1) and assuming that the copolymer occupies 50 % of the sphere volume, an MLV would have a density about 0.5 % greater than water. This density difference, in addition to the large particle size, explains why MLV sedimentation occurs and makes centrifugation a plausible means of isolating large structures.[3]

To estimate the fraction of copolymers included in MLVs, I centrifuged 1.0 wt % samples of $BO_{11}EO_{12}$ at 3000 rpm for 24 h. Examination of the resulting sediment by plane-polarized light microscopy (PLM) revealed only vesicular structures. I removed the supernatant and dried the precipitate to determine the mass of the MLVs and found

that > 65 wt % of the copolymer was in these structures. In contrast, the yield of MLVs from a 2.0 wt % $BO_{11}EO_{19}$ dispersion, which preferentially forms spherical micelles, or small vesicles, was less than 10 %, again showing the greater propensity for vesicle formation by $BO_{11}EO_{12}$.

4.3 *Thermal Stability of Liquid Crystalline Structures.*

BO/EO structures are liquid crystalline and as such undergo a phase transition with increasing temperature. I examined structures from a 5.0 wt % dispersion of $BO_{11}EO_{12}$ as a function of temperature using plane-polarized light microscopy (PLM) with a microscope hot stage. The temperature was controlled using a Linkam THS600 hot stage and a Linkam PR600 Controller (Linkam Scientific Instruments Ltd, UK). The sample holder consisted of a stainless steel washer glued to a glass slide with epoxy resin. After the dispersion was deposited into the washer center, a glass slide cover was glued to the washer to seal the holder. The samples were heated at 1 °C per min with a 10 min pause every 5 °C to allow for equilibration.

Room temperature liquid crystalline structures were identified by the presence of the Maltese cross pattern. However, upon heating, the EO group undergoes dehydration and becomes increasingly hydrophobic.[4,5] Thus, these crystalline structures persisted only until the sample reached 38 °C. At that point the Maltese crosses disappeared, but non-polarized light microscopy showed that the structures maintained their spherical shape. No liquid crystalline structures were evident between 38 and 65 °C, the maximum temperature examined, and no coalescence or change in structure shape was observed. Upon cooling from 45 to 35 °C the Maltese cross patterns reappeared within 5 minutes.

The same procedure was followed for structures formed from a 5.0 wt % $BO_{11}EO_{19}$ dispersion with similar results (phase transition ~ 42 °C). (This transition temperature is greater than that of many phospholipids.[2]) Results with both $BO_{11}EO_{12}$ and $BO_{11}EO_{19}$ show that there is no obvious redistribution of the block copolymers that make up the vesicles during this thermal cycling and that the formation of liquid crystalline structures in the vesicles is thermally reversible. When dispersions were heated overnight to temperatures above 75 °C, complete phase separation of the block copolymers from water is observed. Reformation of liquid crystalline structures is achieved by gentle agitation of the two-phase system at room temperature, producing a similar particle size distribution (PSD) to that formed upon initial agitation.

4.4 *Thermal Stability of Vesicle Dispersions.*

Light scattering measurements are the most suitable technique for the study of vesicle stabilities. Particle size distributions were obtained using a Coulter LS230 Particle Size Analyzer (Beckman Coulter, Miami, FL) that can detect particles with diameters from 40 nm to 2000 μm. The instrument was fitted with the Small Volume Module and all analyses were carried out using the 'pslref' (*poly*styrene *l*atex *ref*erence) model. Instrument performance was confirmed using 0.357 and 1.0 μm polystyrene latex standards. Screening experiments showed that the dilution process used by this instrument did not alter the particle size distribution of the sample over the time involved. Particle sizes obtained in light-scattering experiments were consistent with MLV sizes viewed in PLM of undiluted samples. For particles smaller than 50 nm, a Brookhaven 90Plus (Brookhaven Instruments Corp., Holtsville, NY) particle size analyzer was used.

113

Dispersions of $BO_{11}EO_{12}$ were thermally cycled to evaluate the effects of heating on PSD. Samples were heated to 85 °C for periods of 15 to 60 min, vigorously agitated by hand and returned to the oven. This procedure was repeated until the samples had been heated for a total of 3 h. After thermal cycling, the samples were gently agitated and set aside to stand undisturbed for 24 h at room temperature. Light scattering data showed no significant difference between the PSD of a $BO_{11}EO_{12}$ dispersion before and after thermal cycling. In contrast, thermal cycling of $BO_{11}EO_{19}$ dispersions that did not spontaneously produce MLVs at room temperature showed MLV formation (as determined by PLM) after heating. Dispersions of 0.5 and 1.0 wt % $BO_{11}EO_{19}$ that were thermally cycled showed vesicle formation with a PLM-determined size distribution similar to that for $BO_{11}EO_{12}$ samples. A 10.0 wt % $BO_{11}EO_{19}$ dispersion appeared unchanged by thermal cycling, showing the same PLM size distribution and apparent abundance of vesicles before and after heating. Thus, although BO/EO vesicle size distributions are stable to thermal cycling, MLVs may undergo phase or shape changes at high temperatures before cooling and returning to MLV structures.

4.5 Structural Stability

Because $BO_{11}EO_{12}$ readily formed MLVs over a wide range of concentrations, we conducted extended structural studies using this copolymer. To test the mechanical stability of these structures, I first prepared 25 g of a 5 wt % dispersion of $BO_{11}EO_{12}$ by the standard hand-shaking method. Light scattering data from this dispersion (Figure 4.1) showed that structure diameters ranged from 3.0 to 30 μm with a mean of 5.1 μm. (Similar distributions occurred with 0.5, 1.0 and 2.0 wt % dispersions.) Interestingly, we

observed no particles with diameters between 0.04 and 2.0 μm. (Based on copolymer

length, spherical micelles would be expected to have diameters less than 0.02 μm and

would be undetectable in these measurements using the Coulter LS230.) The dispersion

was then separated into 5 g aliquots and each was exposed to post-formation treatments.

One aliquot was exposed to moderate speed magnetic stirring overnight, and a

second for 2 minutes to high speed vortex mixing (Thermolyne Vibrational Mixer, model

37615). A third was mildly sonicated in a sonication bath (Branson Sonic Bath, model
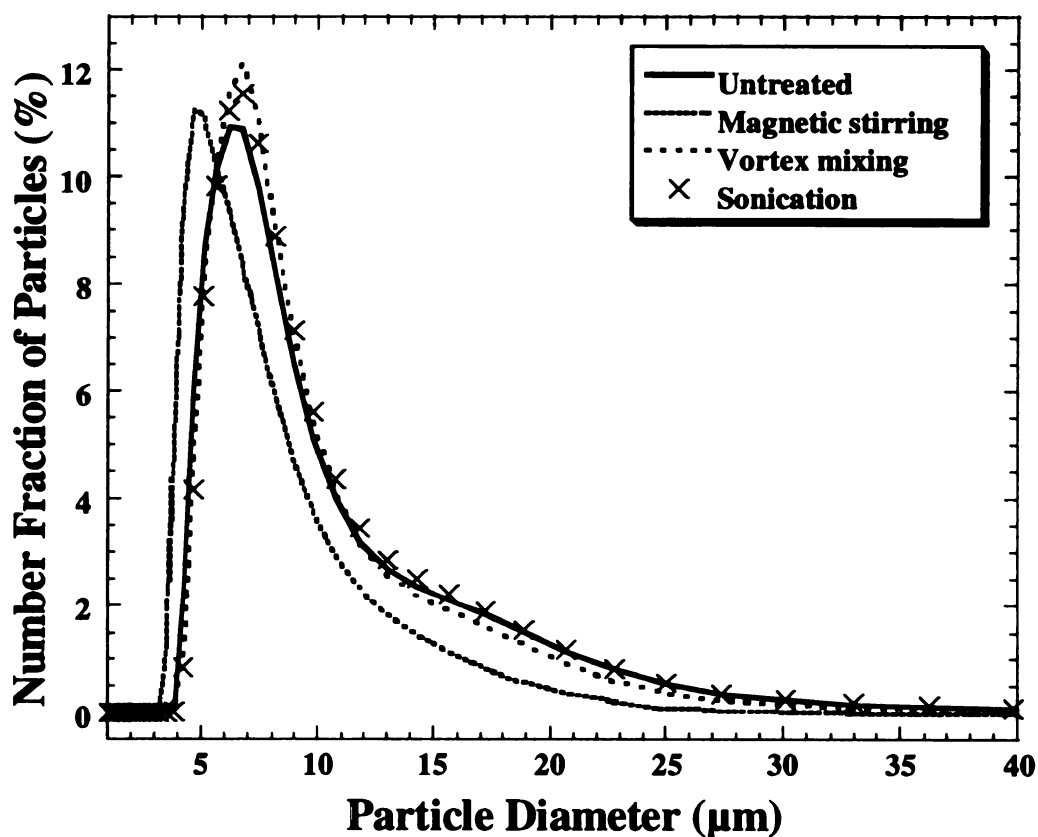
Figure 4.1. Particle size distribution of MLVs in a 5.0 wt % aqueous dispersion of

$BO_{11}EO_{12}$ before and after various post-formation treatments.

2200) for 2 min. The particle size distribution (PSD) was relatively unaffected by these treatments. These techniques are routinely used to generate or alter the size of phospholipid MLVs, so we would not expect them to destroy the vesicle structures.[6] However, we were surprised that these treatments had so little effect on particle size.

The MLV structures are stable in the presence of sonication, moderate and high shear mixing, as well as other post-formation treatments. We think that the stability of these MLVs results from contributions by both the BO and EO blocks. Hydration of an EO block which is in a constrained, close-packed orientation leads to a liquid crystal structure.[7] This crystalline "shell" can be robust and presents an additional energy barrier to vesicle disintegration. Collisions between vesicles are unlikely to penetrate this "shell" or have any impact on structural stability.

The BO block contributes to the vesicle stability because of its length and branching. The free energy of micellization for a CH_2 group is about the same as for a BO unit.[8] Therefore, for an BO/EO copolymer to posses the same hydrophobic character as a phospholipid, the BO length would be twice that of the di-lipid tails. The additional BO length (and ethyl branches) allow for greater hydrophobe entanglement, again slowing the process of disintegration.

4.6 Extrusion of Vesicles

Extrusion is frequently used to reduce MLV sizes or convert MLVs to uni-lamellar vesicles.[4] To evaluate the effect of extrusion, a 5.0 wt % dispersion of $BO_{11}EO_{12}$ was forced through a 5 μm Nylon® filter repeatedly (7 times) using a syringe pump. Figure 4.2 shows the change in structure size due to extrusion and indicates that

116

the mean particle diameter decreased from 5 μm to 70 nm. Greater than 95 wt % of the copolymer was recoverable after extrusion. The same initial dispersion (5.0 wt % $BO_{11}EO_{12}$) was also extruded through a 0.45 μm nylon filter with essentially the same results as with the 5.0 μm filter. This PSD after extrusion was stable for at least 2 months with no reversion to larger structures. As tortuosity may have some effect on extrusion, a 5.0 wt % dispersion of $BO_{11}EO_{12}$ was also extruded through a 0.4 μm track-etched polycarbonate membrane. This resulted in the same particle sizes as found with extrusion through the nylon membranes.

In contrast to the shearing results in section 4.4, extrusion reduced particle size from an initial mean diameter of 5 μm to 70 nm (Figure 4.2). The differences between stability to extrusion and stability to sonication or mixing can be explained by examining the different methods of shear application. In the extrusion experiment, the MLV size or shape must change to pass through the membrane pores, physically altering the liquid crystal structure. Upon entering and exiting the pores, the MLVs experience elongational forces and during the passage through the pores they experience a steady, laminar flow field. This may allow for "delamination" of the lamellae from the vesicles without breaking the liquid crystal structure. These layers quickly close to form spherical lamellae. Steady laminar flow was previously used to transform planar, lamellar liquid crystal structures into MLVs.[9-11] These transformations depended on a critical rheological property such as a critical shear rate, shear stress or strain. Consistent with those results, the shear field presented by extrusion through 0.45 μm pores is evidently more effective at separating the lamellae than sonication or high shear mixing. Furthermore, the particle sizes after extrusion through pores of this diameter suggests that

70 nm is the minimum stable size for vesicles formed from this copolymer. This may represent the lower diameter limit of uni-lamellar vesicles.
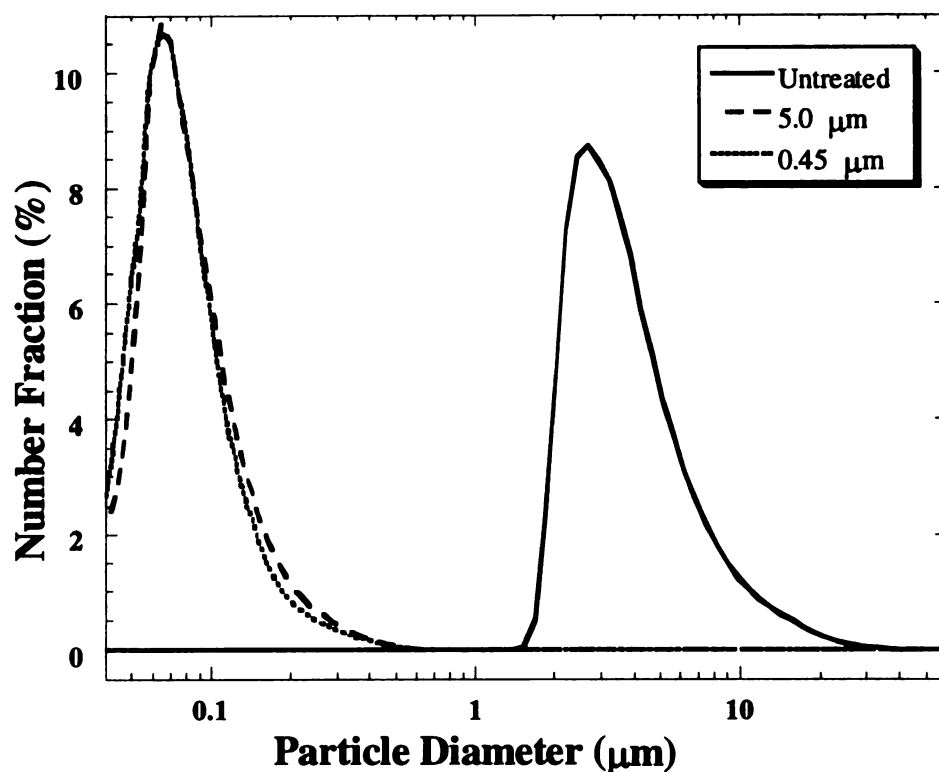
Figure 4.2. Particle size distribution before and after extruding a 5.0 wt % dispersion of $BO_{11}EO_{12}$ through a 5.0 μm or 0.45 μm filter.

4.7 Ultra-sonication of Vesicles

Although a sonication bath had no discernible impact on vesicle size distribution, I decided to evaluate the effects of ultra-sonication because it is a more focused and more powerful application of ultra-sonic energy. I prepared a standard 1 wt % dispersion of $BO_{11}EO_{12}$ using the hand-shaking method. The structures had a mean particle diameter

of about 3 μm. I transferred about 5 mL of the dispersion into a vial that I placed into an ice-water bath. Finally, I inserted the 3 mm diameter horn of the ultra-sonicator (Cole-Parmer Ultrasonic Processor, model CP 130) into the dispersion and used a typical sonication procedure of a "4 sec on/ 1 sec off" cycle at 10 watts, for 2 minutes. This procedure reduced the mean particle diameter to about 70 nm, similar to the size produced by extrusion.

I then decided to test the concentration limits of this process. I prepared 20.0 wt % $BO_{11}EO_{12}$ in water and then agitated the mixture by hand for about 30 seconds and placed it on the vibrational mixer for 30 seconds. The result was a thick, white fluid saturated with bubbles. I placed the dispersion onto the mechanical shaker table for 2 minutes, but saw no change in the sample.

I ultra-sonicated the same dispersion using the standard "4 sec on/ 1 sec off" cycle at 10 watts. After 13 minutes the dispersion appeared considerably clearer and its viscosity was much lower. However, there were several gel fragments visible, so I returned it to the sonicator. After 35 minutes, the dispersion was much clearer with only a few gels attached to the bottle wall. I removed the dispersion from the ice-water bath and placed it onto the vibrational mixer for 2 minutes. I then refilled the water bath with ice and returned the dispersion to the ultra-sonicator. After a total of 70 minutes of ultra-sonication, the dispersion was very clear, only slightly opaque, and only slightly more viscous than water.

I re-examined the dispersion after it stood at room temperature for 3 months. The sample was still a slightly opaque liquid, but there was evidence of particulate settling. A thin (0.1 mm) white coating was visible on the bottom of the vial. By rotating the vial it

was apparent that this was a low viscosity fluid. The volume of material seemed far too low to have been a significant portion of the copolymer. Otherwise the dispersion seemed quite typical; water-like viscosity and uniform opacity. I ran PSD tests on the dispersion using the Brookhaven 90Plus and found an average particle diameter of 99 nm. I returned the sample to the hood, and after 7 months, it was unchanged. It remained a clear liquid with a viscosity slightly above that of water and no indications of precipitation. Based on these observations, I would speculate that the upper limit of concentration for this process is greater than 25 wt % (250 mM) copolymer. This is comparable with the "high loading level" of phospholipids which is typically about 30 wt % or 200 mM.[6]

4.8 *Examination of The Effect of Added Hydrophobe on Structure Formation*

The screening test (section 3.7) showed that selected copolymers produced lamellar structures, however it was important to determine the effect of a hydrophobe (dodecane) on structure formation for two reasons. First, the mass spectrometry data showed that uncapped BO oligomer was present in many copolymers, and understanding its impact on structure formation is critical for establishing a maximum acceptable level of BO. Second, one possible application of BO/EO vesicles is the encapsulation and delivery of hydrophobic materials. Understanding the impact of increasing hydrophobe concentrations on structure formation as a function of BO/EO composition will determine which copolymers might prove useful for these types of encapsulation applications.

After identifying compositions that produced lamellar structures, I began developing phase diagrams for selected compositions. For such studies, the ratios of

copolymer, water and dodecane, the model hydrophobe selected for these studies, were varied at a constant temperature. Samples were prepared by placing the copolymer into a vial, adding dodecane and agitating the clear mixture on a vibrational mixer (Fisher Scientific Instruments, Chicago, IL) until the liquid was homogeneous, typically ~ 15 seconds. Water was then added to give a total mass of ~ 2 g, and the vial was returned to the mixer for about 2 minutes. The sealed dispersions were heated at 80° C, with intermittent mixing, for up to 20 hours, or until the dispersions were uniform. They were then agitated vigorously after cooling (~ 2 minutes) and were stored undisturbed at room temperature for a minimum of 40 days before examination. Samples were visually inspected for clarity, relative viscosity, and number and type of any mesophases present.

Sample examination was conducted using three optical probes: random white light, HeNe laser light, and plane-polarized light. The surfactant/ dodecane mixtures were transparent with neither white- nor laser-light scattering nor any visible features under plane-polarized light. Addition of water, however, generally produced a dispersion with several notable optical characteristics. White-light scattering was indicative of large domain sizes (diameters >100 nm) and phase separation such as occurs in colloidal dispersions, emulsions, and suspensions. (These materials differ primarily in size and nature of the continuous and dispersed phases.) However, random white light is ineffective in identifying small domains (diameter < 50 nm), particularly under dilute conditions, so laser light was used to search for the Tyndall Effect and smaller domains.[12] For example, spherical micelles are too small to produce noticeable scattering from white light, and micellar solutions of greater than 30 wt % surfactant can be optically transparent. The same material illuminated with a HeNe laser will typically display a

faint shaft of red light indicating the presence of some type of structures. (The intensity of the light shaft increases with particle size and concentration.) Conversely, vesicles are generally large enough to brightly scatter laser light, even when present in such low concentrations that they do not produce a detectable opacity. Therefore, examination of a dilute, clear sample using both laser light and white light can discriminate between homogeneous solutions and those having micellar structures. It should be noted, however, that there is no obvious method of distinguishing between a small vesicle (diameter < 40 nm) and a swollen micelle using these techniques. For identification of those types of structures, dynamic light scattering must be employed.

Samples were also examined for the previously described liquid crystalline states (sec. 3.2). Vials were initially placed between two sheets of polarizing material (90° difference between polarizations) and visually examined. Those showing liquid crystalline regions were set aside to be examined using plane-polarized light microscopy (PLM). Three other states, spherical micelle, rod-shaped micelle and the bicontinuous phase, were implied by a combination of properties such as duration of birefringence (none, temporary or permanent), sample viscosity and phase separation.

4.9   BO/EO Copolymer Phase Diagrams

Once equilibrated, dispersions were characterized using the methods described above to prepare phase diagrams. Only single-phase samples were evaluated, since the composition of the different phases in a multi-phase sample was unknown. Thus, not every possible mixture of components was examined. Detailed sample analysis by PLM

occurred whenever the dispersion showed a viscosity increase (compared to the neat

copolymer viscosity) or a birefringence pattern.

Figure 4.3 is the phase diagram for BO_6EO_4. At high dodecane concentrations (>

40 wt %) the mixture formed stable emulsions (a liquid in liquid dispersion), and the

majority of the samples were multi-phase. Only three liquid crystalline phases were

detected: H_1, L_α, and C_2. The L_α phase contained both planar lamellae and vesicle

structures, but I found no region containing only vesicles.
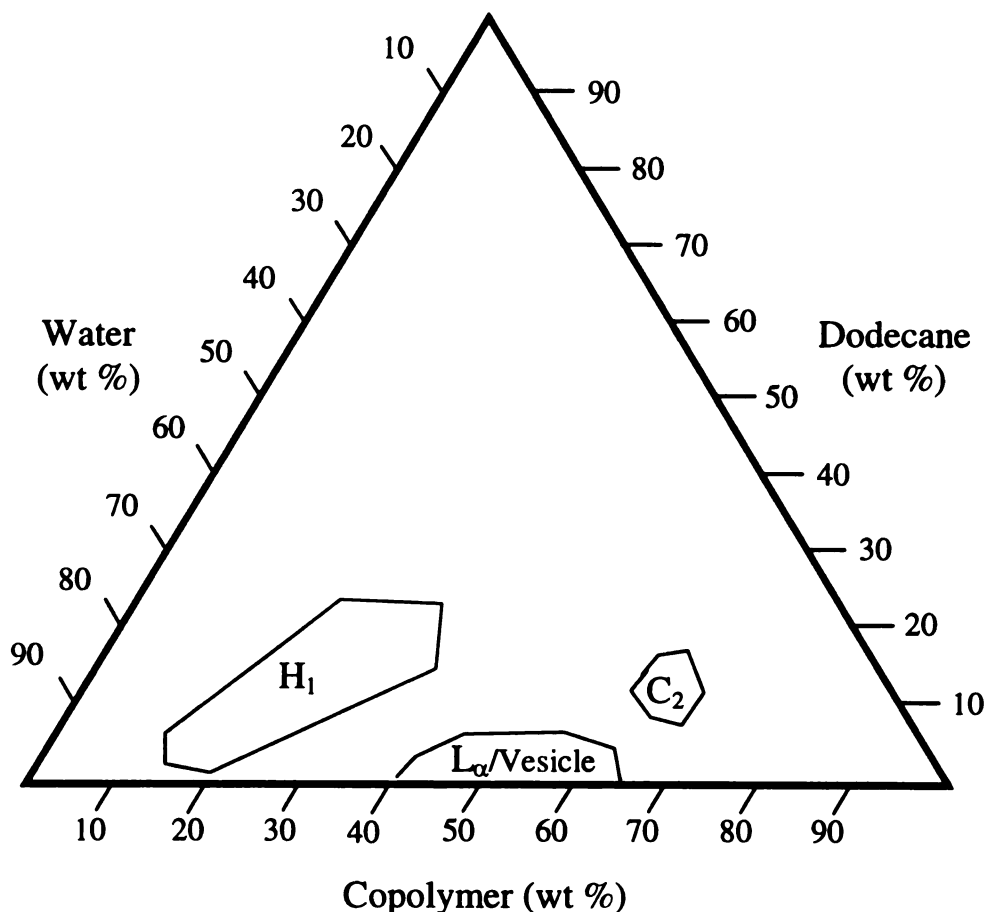
Figure 4.3. Phase behavior of BO_6EO_4 with dodecane and water at room temperature.

A comparison of the phase behavior of BO_6EO_4 (Figure 4.3) and $BO_{11}EO_{12}$

(Figure 4.4) shows some interesting differences. While both copolymers formed

emulsions at elevated levels of dodecane, emulsion formation was significantly reduced

for $BO_{11}EO_{12}$. The copolymer concentrations that produced H_1 phases were similar in

both diagrams, but required much higher levels of dodecane for $BO_{11}EO_{12}$. $BO_{11}EO_{12}$

also showed a larger compositional range for the L_α phase and a region that produced

only vesicles. Additionally, the $BO_{11}EO_{12}$ showed an H_2, C_2, and V_2 regions.
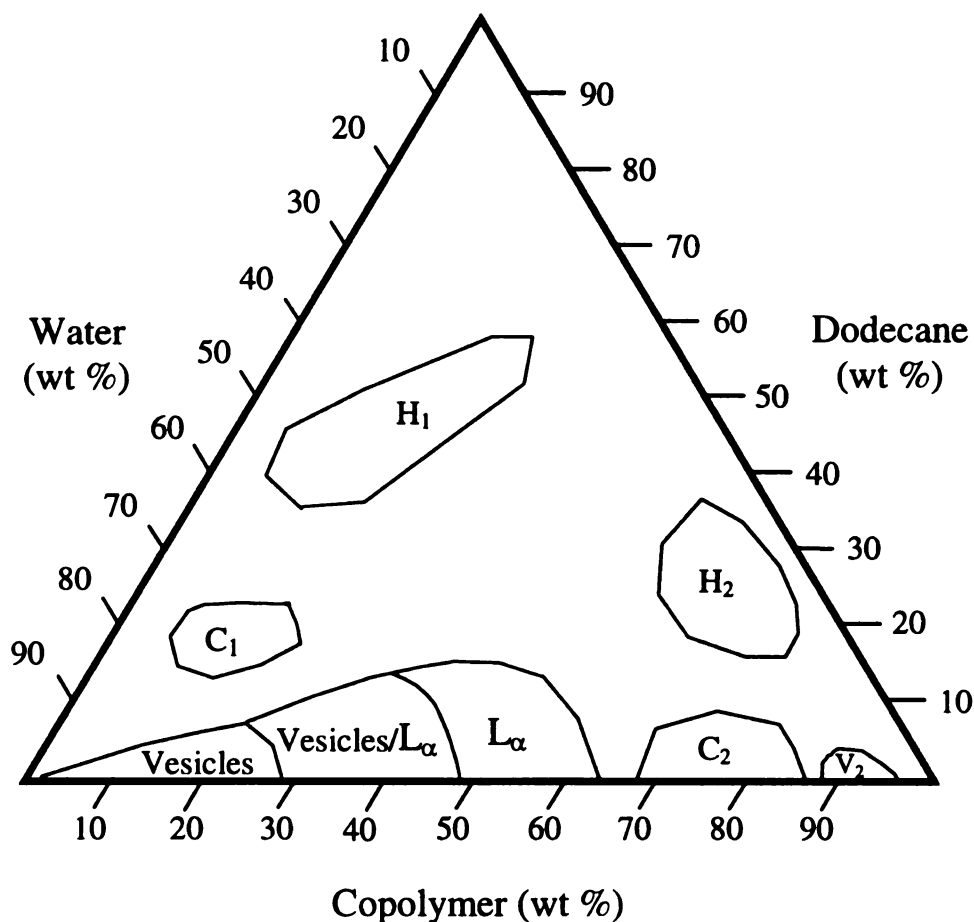
Figure 4.4. Phase behavior of $BO_{11}EO_{12}$ with dodecane and water at room temperature.

Comparison of the phase diagrams for $BO_{11}EO_{19}$ (Figure 4.5) and $BO_{11}EO_{12}$

shows the effects of increased EO block length on vesicle formation. The longer EO

chains make formation of reverse micelles (L_2) easier and more likely. The expanded

region for reverse tetragonal formation (C_2) is also likely due to the increased interaction

of the larger EO blocks. The L_α phase region is reduced because the larger head group

size favors formation of spherical micelles rather than bilayers.

Compared to $BO_{11}EO_{19}$ and $BO_{11}EO_{12}$, we would expect $BO_{12}EO_{10}$ (*MS*

composition used for clarity) also to contain a large region of vesicles or lamellae

because of its shorter EO block. However, Figure 4.6 shows that this is not the case.

Again, the mass spectrometry profile helps explain why. $BO_{12}EO_{10}$ contains about 2.5

times as much BO oligomer as $BO_{11}EO_{19}$ or $BO_{11}EO_{12}$ and, as with BO_6EO_4, the

concentration of this hydrophobe has a strong influence on structure formation. (Table

4.1 shows the relative molar levels of BO oligomer found, as determined by mass

spectrometry, in each of the copolymers listed.) The presence of BO oligomer has the

same effect on copolymer structure formation as the presence of dodecane. Both

hydrophobes associate with the BO block of the copolymer and changes the average

hydrophobe volume. Thus the *V* in the critical packing factor increases, which in turn

makes the formation of planar lamellae more probable. However if the hydrophobe

concentration becomes too large, the copolymer forms a stable dispersion like that shown

in Figure 3.8.

Table 4.1. BO oligomer concentrations in BO/EO copolymers.

Batch Name	NMR Composition	MS Composition	BO Oligomer Conc. (mol %)
L1150-51A	$BO_{11}EO_{12}$	$BO_{10}EO_{10}$	4.0
L1150-51B	$BO_{11}EO_{19}$	$BO_{10}EO_{15}$	2.6
L120-15A	BO_6EO_4	$BO_{10}EO_6$	8.0
M1038A	$BO_{11}EO_{12}$	$BO_{12}EO_{10}$	10.3
M1038D	$BO_{11}EO_{18}$	$BO_{12}EO_{10}$	10.7
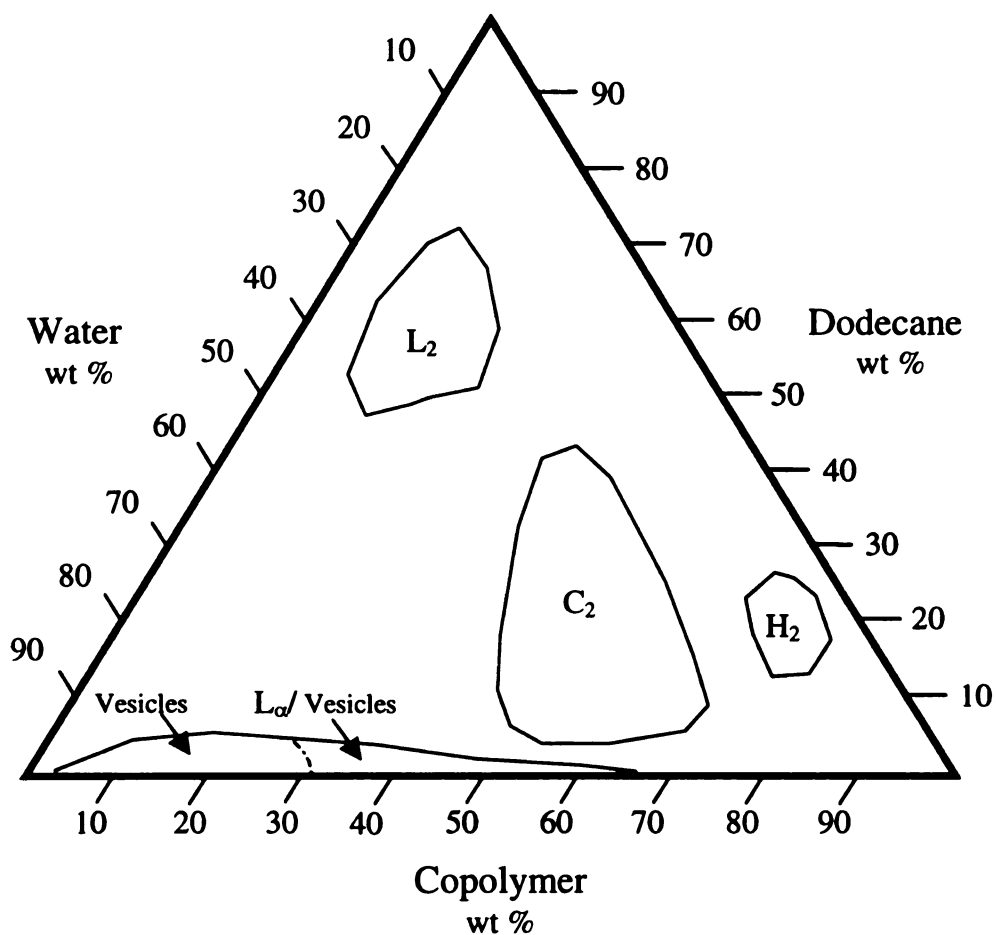
Figure 4.5. Phase behavior of $BO_{11}EO_{19}$ with dodecane and water at room temperature.

Additionally, although the intensity–averaged composition is $BO_{12}EO_{10}$, the compositional profile shows that much of the copolymer has an EO block length of greater than 16, the length at which spherical micelle formation begins to predominate. Mass spectrometry data also indicate that the copolymer has a broad compositional distribution. This may account for the larger number of structures observed in this diagram.
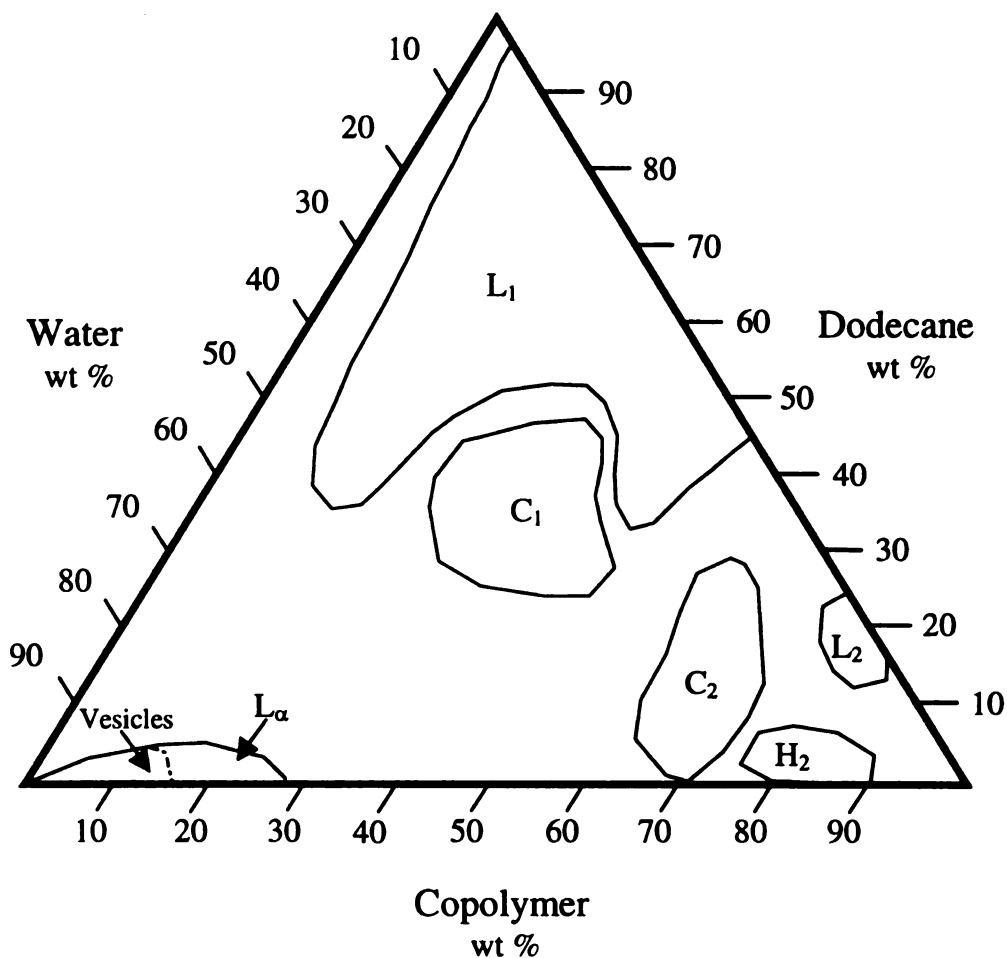
Figure 4.6. Phase behavior of $BO_{12}EO_{10}$ (*mass spectral composition*) with dodecane and water at room temperature.

In addition to showing which compositions of copolymer, dodecane and water will produce vesicles, the phase diagrams indicate a maximum loading level of hydrophobe for encapsulation. If we assume that the hydrophobe is restricted to the region of the vesicle occupied by the BO block, that it is not associated with the head group nor in the water phase, we can see that dodecane can be added to about a 1:1 mole concentration with the copolymer and still produce vesicles. As expected however, the BO oligomer has a detrimental impact on hydrophobe loading by competing for those sites. For those copolymers with high BO oligomer levels, less dodecane was required for vesicle formation to be halted.

4.10 *Hydrophile Loading - Experimental Procedure*

Hydrophiles are generally water-soluble and therefore may be found in the aqueous continuous phase, in the aqueous region between bilayers or in the hydrophilic region of the bilayer, adjacent to the head groups. Any study of hydrophilic loading capacity must first remove the hydrophile from the aqueous continuous phase. This is generally accomplished using gel permeation separation. Then a means of accurately determining the level of the hydrophile encapsulated in the vesicles must be identified.

I chose the sodium salt of fluorescein, which has been used in numerous encapsulation studies,[6,13,14] as a model hydrophile. Though it is a large hydrophile (376 dal), it has good water solubility (> 2 g dye/ g water) and is easily detected at concentrations less than 0.05 ppm using UV or fluorescence spectroscopy (absorbance max at ~ 493.5 nm).[15]

To prepare the gel column I weighed out 1 g of the dry Sephadex G-50 polydextran resin (Sigma-Aldrich, Milwaukee, WI) and added 40 g of deionized (DI) water. The mixture stood overnight so that the resin could swell with water. I selected a glass column that was 22 mm in diameter, 200 mm long and fitted with a sintered-glass frit at the bottom. I chose a large diameter column to accommodate between 8 and 10 mL of dispersion per pass while still providing a clean separation of vesicles from dye. After hydration, I carefully poured the resin into the glass column, making sure that no bubbles were entrained in the gel. Using a rubber tube, I connected the stopcock to a syringe and gently drew water through the column. This was done to compact the resin and minimize the column porosity. However, it is critical that the resin NEVER be allowed to dry, therefore the headspace above the resin was always filled with DI water. (To reduce damage to the vesicles, the aqueous continuous phase in the gel column should have contained a solution with the same ionic strength as the dispersion, however the salt concentration was low enough that I ignored this effect.) I then placed a plug of a hydrophobic, open-cell foam (polypropylene, I believe) onto the top of the gel to act as a baffle and minimize the disturbance of the resin while adding the dispersion. After copolymer addition, a second glass column was attached above the first and filled with deionized water to replace the permeate flow.

I prepared several test dispersions of $BO_{12}EO_{11}$ vesicles prepared using a 300 ppm fluorescein dye solution. The dispersions were ultra-sonicated to produce structures with diameters less than 100 nm, which were probably uni-lamellar vesicles. I passed the dispersions through the gel column to evaluate the column's separation efficacy and found that it could easily separate about 4 mL of a 15 wt % copolymer dispersion in a

single pass. Once I confirmed the utility of the gel column, I turned my efforts a method of dye detection.

Use of ion exchange resin to isolate and pre-concentrate ionic analytes is well known,[16,17] but the process has been generally used to collect ions from solution not extract them from vesicles. To determine the efficacy of such a procedure, I passed a test dispersion of vesicles loaded with 300 ppm fluorescein dye through the gel column and collected the permeate. I then exposed half of the permeate dispersion to Dowex MSA ion exchange resin (The Dow Chemical Company, Midland, MI) to extract the dye from the structures. After allowing the resin/ vesicle mixture to agitate for several hours, I removed the resin, which was now green, by filtration and saved the white dispersion. I added enough methanol to both dispersions to produce a clear solution. (An aqueous solution of greater than 40 wt % MeOH is sufficient to dissolve the copolymer and destroy the vesicle structures.) The sample that had contacted the ion exchange resin produced a clear solution without a hint of color, indicating that there was no residual dye in the vesicles. The second sample, which had not seen the ion exchange resin, produced a green-yellow solution. To evaluate the sensitivity of the coloration to dye concentration, I added a single drop of 1500 ppm fluorescein dye solution to about 300 mL of a 1:1 MeOH:water solution. The resulting liquid had a faint, but distinct green hue at a concentration of about 0.2 ppm. The dispersion which had contacted the resin had no color and must have had a dye concentration lower than 0.2 ppm. Thus, contacting the vesicles with the ion exchange resin alone is sufficient to extract the dye from the structures.

The reason behind the fluorescein extraction may be the high charge density of the resin, given as 1.51 eq/L of resin. The dye dissolves to produce 3 ions (two Na^+ and divalent fluorescein) per molecule and, at a concentration of 300 ppm, yields a mean charge concentration of 2.4×10^{-3} eq/L or about 0.2 % that of the resin. The resin's high surface-charge density may produce an osmotic pressure gradient that bursts the vesicles, causing them to release the dye. (The bursting of liposomes under osmotic pressure gradients is a common problem for controlled delivery.[13]) The structures quickly reform once the pressure has equilibrated, typically with a much lower concentration of encapsulated materials.

Fluorescence spectroscopy can be used to determine the dye concentration on the resin, however, I did not have easy access to an instrument, so I decided to circumvent this problem by using UV/Vis spectroscopy for dye analysis. To do so, I needed to extract the dye from the ion exchange resin which I did using a 30.0 wt % $NaNO_3$ solution. The resin has a high affinity for the NO_3^- ion, which over time displaces the dye. Once the dye was in solution, the ion exchange resin could be removed by filtration. Several dye extractions were necessary to completely remove the dye from the resin. (The resin visibly changes from green to golden as the dye is released.) When complete, the extraction solutions were combined, and UV absorbance was used to determine the dye concentration. From the concentration of fluorescein in the extraction solution, I then calculated the dye level in the structures.

I evaluated the potential of this method by mixing the resin with solutions having a known dye concentration and used the data generated to produce a calibration curve. I prepared 5 solutions of fluorescein dye with concentrations of 500, 300, 150, 50 and 10

ppm, and mixed each solution with 1.5 g of ion exchange resin and let the mixtures agitate overnight. The following day each solution was clear with no hint of color. I isolated the resin by filtration and extracted the dye using 5 mL of a 30.0 wt % $NaNO_3$ solution. To be consistent, each sample was extracted 5 times with $NaNO_3$ solutions regardless of whether or not the extraction solution was colorless prior to the fifth rinse. (Most were colorless after just three extractions.) These extractions were collected and evaluated. Because of the large concentration range, I monitored 5 different wavelength; 450, 463, 473, 484 and 485 nm and produced a calibration curve for each wavelength. Based on the color of the resin, I believe I recovered more than 95 % of the dye from each sample.

4.11 *Hydrophilic Loading and Release*

My first attempted at studying the hydrophile release rate of the $BO_{12}EO_{10}$ copolymer involved a high hydrophile concentration and a high copolymer concentration. I prepared a 15 wt % dispersion of copolymer using a 1500 ppm fluorescein dye solution. The initial product was a thick gel, however after 45 minutes of ultra-sonication (using the standard procedure), the resulting sample was a clear, orange-yellow liquid with water-like viscosity. Structures in the dispersion were probably uni-lamellar vesicles as suggested above.

After allowing the samples to stand overnight, I separated them into 4 aliquots of about 4 g each. Aliquot A was a practice run. I could easily identify the location of the dye by a color band that moved slowly through the gel column. I detected the presence of vesicles by using the hand-held HeNe laser to look for a scattering pattern in the liquid

exiting the column. Vesicles, even small ones, produce a distinct, bright shaft of light if present in the liquid. I observed that between the end of vesicle elution and the beginning of dye elution, there was a gap of about 60 seconds; more than enough time to remove the collection bottle without fear of dye contamination. The vesicle dispersion had a slight greenish hue, but otherwise looked the same as an ordinary vesicle dispersion.

To accurately determine the dye level, I prepared a standard means of testing the dispersions. After the initial gel separation, a release period, and a second gel separation, I added 0.5 g of the resin to each of the vesicle dispersions and placed them onto the shaker table overnight. The following morning the dispersions were white and the ion exchange resin was colored bright green, yellow, orange or red depending on the dye concentration on the resin surface. I isolated the resin by filtration and transferred the beads into a 20 mL vial. I then added 5 mL of the 30 wt % $NaNO_3$ solution to the vials and placed them on the shaker table overnight. The following day, I removed the saline solution from the resin, replaced it with fresh saline and returned the sample to the shaker table. I repeated this procedure five times, and then measured the dye concentration in the saline solution. I calculated the amount of dye extracted by the resin and compared this to the amount of dye in a dispersion that did not undergo a release period.

I ran aliquots B, C and D through the gel column and collected the permeate of each. (The volume of the vesicle dispersion increased ~ 9-fold as it passed through the column.) Upon collecting the last of aliquot B, I immediately added ion exchange resin to the permeate. The dye concentration found in dispersion B became my reference value for fluorescein loading. The other dispersions, C and D were allowed to stand at room temperature for several hours before being passed through the gel column a second time

to separate the released dye from the vesicles. The dye remaining in the vesicles was then extracted using ion-exchange resin, and the amount of dye on the resin was compared to that in dispersion B.

Dispersion C, which had not produced as clean a separation in the gel column as dispersion B (the reference dispersion), showed about 64 % retention of dye in the vesicles over a 5 hour period. Dispersion D, which when passing through the column had a greater separation between the aqueous dye and the vesicles, showed a retention level of 81 % after 24 hours. Because of the high dye concentrations, I used the calibration curve generated by absorbances at 485 nm wavelength.

I decided to repeat the experiment using a lower dye concentration and allowing the structures to stand for a longer interval before measuring the release rate. The reduced concentration was intended to minimize the osmotic pressure gradient across the bilayer and limit rupture of the vesicles primarily to that which occurred in the presence of ion-exchange resin. I also used a BO/EO copolymer with a longer BO block that I believed would increase the vesicle stability and reduce the release rate. I prepared a 13.25 wt % dispersion using a $BO_{20}EO_{12}$ copolymer and a 100 ppm fluorescein dye solution. The dispersion was ultra-sonicated to produce an opaque, pale-yellow liquid with water-like viscosity.

I passed the dispersions through the gel column in the manner described above and combined aliquot A with ion-exchange resin immediately after elution. Thus, aliquot A served as my reference material. I allowed the other aliquots to stand for a period of time before a second gel separation and subsequent extraction of dye from the vesicles.

The amount of dye extracted by the ion exchange resin was measured and compared to the dye level of dispersion A. The results are plotted below.

Figure 4.7 shows the fraction of fluorescein dye released as a function of time. The dye concentration in batch A was the reference concentration and is shown as the 100% value at "0" hours. The graph shows that the release rate is quite low for these uni-lamellar vesicles; they retain almost 60 % of the encapsulated dye for more than 3 weeks. This is significantly better than typical phospholipid structures, which can lose from 15 % of encapsulated fluorescein in 300 minutes to 80 % in 200 hours.[6,18]
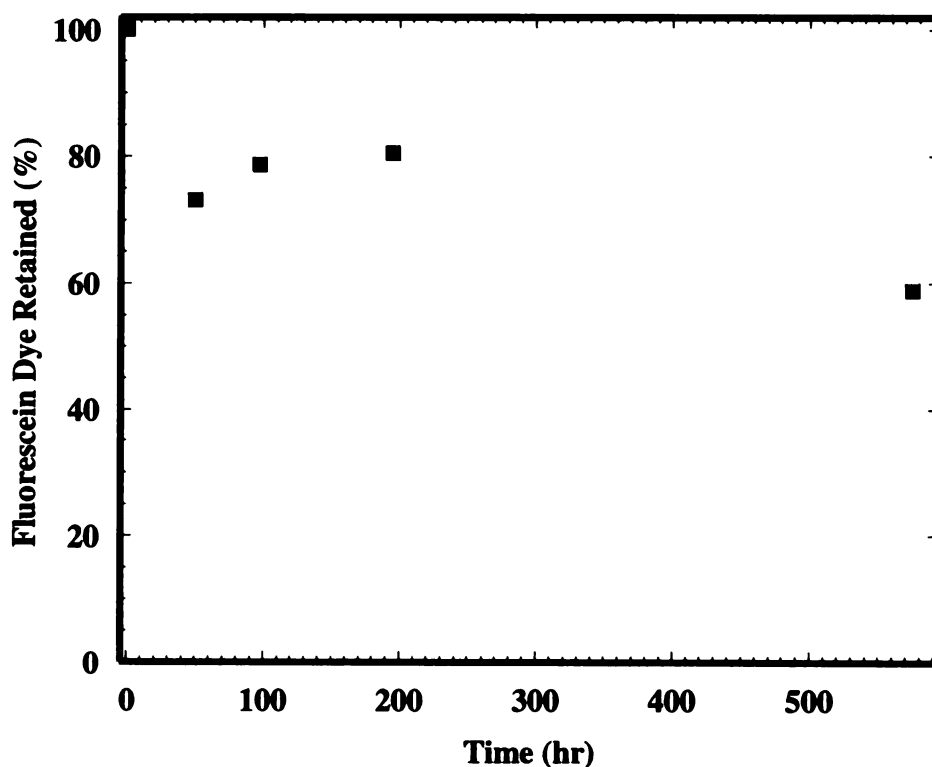
Figure 4.7. Fraction of fluorescein dye retained by $BO_{20}EO_{12}$ uni-lamellar vesicles as a function of time.

(NOTE: Gel filtration results are somewhat dependent on technique, and the initial small rise in retention may be due to improvements in my ability to isolate the vesicles from the released dye.)

It should also be noted that the resin release period was as long as several weeks, and no precautions were taken to retard photo-oxidation of the dye. To determine if this was a significant concern, I re-tested the 50 ppm standard used to prepare the calibration curve after 140 days, about 20 % longer than the samples had been extracted. I found an ~ 10 % decline in the sample absorbance, and would conclude that a 3 to 5 % decrease in fluorescein dye concentration would be reasonable for the dye samples shown here.

During the second gel separation, I collected both phases: vesicles and released dye. In this way I could do a fluorescein dye mass-balance calculation. Figure 4.9 plots the interval between the first and second gel separations versus the total dye concentration (dye in vesicles plus dye released) for each sample. The shaded area at the top of the graph represents a ± 10 % variation in the dye mass measured in batch A, the standard. Ten percent seems to be a reasonable level of error given the technique. Clearly the first three batches produce sums that are within the range of errors allowed and thus account for all of the dye. However, the final run is outside this range, indicating that some of dye is unaccounted for. A problem arose during this run that may explain this deviation. As the dispersion passes through the column the vesicles separate from the dye, which is slowed by the gel. Therefore the vesicles exit first. Following the vesicle collection for the final run, I inadvertently allowed the column to dry out. I do not believe that this affected the separation of vesicles from dye, but I may not have

collected all of the released dye. If so, then the retention value of ~ 60 % is valid, but the sum is short of the actual value.
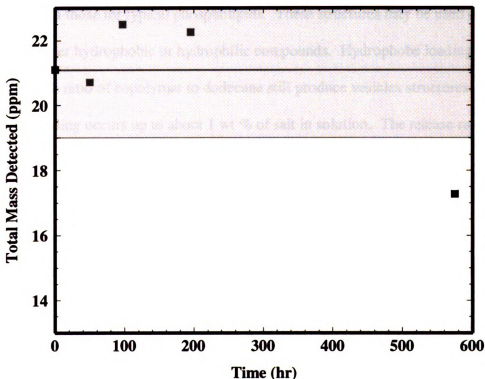
Figure 4.8. Sum of retained and released fluorescein dye for each batch of vesicles.

4.12 *Conclusions*

The use of BO in amphiphilic BO/EO di-block copolymers results in large hydrophobe volumes that lead to surfactants with compositions that spontaneously produce vesicular structures in water at room temperature. Mean particle diameter is about 3 μm for hand-shaken dispersions, and typical structure yields are approximately 65 % of the total amount of copolymer. The vesicular structures are mechanically stable and resistant to a variety of post-formation treatments, but they can be extruded or ultra-sonicated to form structures of ~ 70 nm diameter. Additionally, both $BO_{11}EO_{12}$ and

$BO_{11}EO_{19}$ vesicles are thermally stable to ~ 40 °C, at which point they undergo a transition to a non-crystalline phase.

Ultra-sonication allows for the formation of vesicles at copolymer levels similar to or higher than those for typical phospholipids. These structures may be used to encapsulate either hydrophobic or hydrophilic compounds. Hydrophobe loading levels of up to a 1:1 mole ratio of copolymer to dodecane still produce vesicles structures. The hydrophilic loading occurs up to about 1 wt % of salt in solution. The release rate for hydrophiles is equal to or slower than that for conventional phospholipids.

4.13 *References*

(1)   Aniansson, G. E. A. *Progress in Colloid & Polymer Science* **1985**, *70*, 2-5.

(2)   Marsh, D. *Handbook of Lipid Bilayers*; CRC Press: Boca Raton, FL, 1990; pp 353-355.

(3)   Giddings, J. C. *Unified Separation Science*; Wiley-Interscience: New York, NY, 1991; p 173.

(4)   Bailey, F. E., Jr.; Koleske, J. V. Configuration and hydrodynamic properties of the polyoxyethylene chain in solution. In *Nonionic Surfactants: Physical Chemistry*; Schick, M. J., Ed.; Marcel Dekker: New York, NY, 1987; Vol. 23, pp 927-969.

(5)   Rosen, M. J. *Surfactants and Interfacial Phenomena*, Second ed.; Wiley-Interscience: New York, 1989; p 21.

(6)   Lasic, D. D. Liposomes in Drug Delivery. In *Vesicles*, First ed.; Rosoff, M., Ed.; Marcel Dekker: New York, NY, 1996; Vol. 62, pp 447-476.

(7)   Gray, G. W.; Windsor, P. A. *Liquid Crystals & Plastic Crystals; Physico-Chemical Properties and Methods of Investigation*; John Wiley and Sons: New York, NY, 1974; Vol. 1; p 4.

(8)   Bedells, A. D.; Arafeh, R. M.; Yang, Z.; Attwood, D.; Padget, J. C.; Price, C.; Booth, C. *J. Chem. Soc., Faraday Trans.* **1993**, *89*, 1243-1247.

(9)   Bergmeier, M.; Gradzielski, M.; Hoffmann, H.; Mortensen, K. *Journal of Physical Chemistry B* **1998**, *102*, 2837-2840.

(10)   Zipfel, J.; Lindner, P.; Tsianou, M.; Alexandridis, P.; Richtering, W. *Langmuir* **1999**, *15*, 2599-2602.

(11)   Mueller, S.; Boerschig, C.; Gronski, W.; Schmidt, C.; Roux, D. *Langmuir* **1999**, *15*, 7558-7564.

(12)   Ingle, J. D. C., Stanley, R. *Spectrochemical Analysis*; Prentice-Hall: Englewood Cliffs, NJ, 1988; pp 513-515.

(13)   Gregoriadis, G. Fate of injected liposomes: Observations on entrapped solute retention, vesicle clearance and tissue distribution in vivo. In *Liposomes as Drug Carriers. Recent Trends and Progress*; Gregoriadis, G., Ed.; Wiley & Sons: New York, NY, 1988; pp 176-188.

(14)   Betageri, G. V.; Jenkins, S. A.; Parsons, D. L. *Liposome Drug Delivery Systems*; Technomic Publishing Company Inc: Lancaster, PA, 1993; pp 17,18.

(15)   Budavari, S., Ed. *The Merck Index*, Twelfth ed.; Merck Research Laboratories: Whitehouse Station, NJ, 1996.

(16)   Ellis, D. W. *Flame Emiss. At. Absorption Spectrom.* **1971**, *2*, 263-287.

(17)   Schwartz, M. K. *Analytical Chemistry* **1972**, *44*, 9R-33R.

(18)   Gerasimov, O. V.; Rui, Y.; Thompson, D. H. Triggered Release from Liposomes Mediated by Physically and Chemically Induced Phase Transistions. In *Vesicles*, First ed.; Rosoff, M., Ed.; Marcel Dekker: New York, 1996; Vol. 62, pp 679-746.

Spontaneous Vesicle Formation from Poly(1,2-Butylene Oxide) Sulfate Oligomers

5.1 Introduction

Chapter 3 showed that poly (1,2-butylene oxide/ ethylene oxide) (BO/EO) diblock copolymers spontaneously form multi-lamellar vesicles (MLVs) upon addition of water if the average EO block length is between 5 and 18 units. If the EO block is larger than 18 units, spherical micelles result; if smaller than 5 units, an emulsion forms. This behavior is consistent with a geometric packing model (section 1.6) that suggests that micellar structure is determined by surfactant geometric properties such as head group area and hydrophobe length and volume.[1]

Interestingly, while numerous ethoxylated surfactants exist, few demonstrate spontaneous vesicle formation. The propensity of certain BO/EO copolymers to form MLVs is thus most likely due to the large volume-to-length ratio of the BO hydrophobe. If this is the case, BO surfactants with other head groups (anionic, cationic or nonionic) should also form vesicles as long as the head group has the appropriate size. Based on the similarity in head group areas calculated for an EO_{11} block and measured for $-OSO_3^-$, we thought that sulfonated BO surfactants would also form vesicles.[2,3] In this chapter we show that sulfonated BO is indeed capable of forming vesicles, thus expanding the versatility of BO surfactants.

An ionic surfactant that spontaneously produces vesicles offers several options as a dispersant that ethoxylated materials do not. Due to charge repulsion, vesicles prepared from ionic surfactants are less likely than ethoxylated structures to form gels at elevated

concentrations.[4] Anionic vesicles should also be stable at higher temperatures than structures formed from nonionic surfactants. Finally, strongly ionic head groups, such as sulfate, are relatively unaffected by changes in pH, although hydrolysis of the $-OSO_3^-$ group could be problematic.[5]

5.2 Oligomer Synthesis and Characterization

BO oligomers (Scheme 5.1a) were prepared following the procedure we previously used to make EO/BO diblock copolymers, except that the butylene oxide polymerization was terminated with acetic acid instead of continuing with the addition of the EO block. The hydroxyl terminated BO was then sulfonated using a DMF*SO_3 complex.[6] In a typical procedure, I transferred 10.00 g (0.0287 mol) of the BO_4 oligomer to a bottle and added about 45 mL of anhydrous methylene chloride ($MeCl_2$) to form a clear solution. Next, about 100 mL of anhydrous $MeCl_2$ was placed into a reaction flask, which was cooled in an ice-bath and stirred under dry N_2. To this was added 4.8 g of the sulfur trioxide/ DMF complex (Sigma-Aldrich, cat # 37,368-0). The complex was not completely soluble in the $MeCl_2$, so a white solid was visible. The solution containing BO oligomer was then added dropwise (over a 1 h period) to the cooled solution using an addition funnel. The ice completely melted about 90 minutes after BO addition began, and the flask was allowed to warm to room temperature with constant stirring. The mixture, now a clear solution, was allowed to stir overnight under N_2 at room temperature.

The following morning I added another 90 mL of $MeCl_2$ to dilute the solution and decrease its viscosity. The sample was evaporated to produce a golden, viscous liquid.

Deionized water (~ 50 mL) was added to the flask to produce a yellow liquid, and then 4.6 mL of a 5 N NaOH was added dropwise to the sample over 2 minutes while stirring. (This is about 80% of the calculated amount of NaOH required to neutralize the sample.) The pH of the solution was still quite acidic. Another ~ 0.7 mL of the 5 N NaOH was added dropwise over 10 minutes, and the pH of the solution was examined after every four drops. After the pH reached 7, I stirred the sample for 1 h and found the pH unchanged.

After evaporation of the water at 75 °C for 2 hours, the resulting product (Scheme 5.1b) was a grainy yellow solid at room temperature. (The grains may have been residual Na_2SO_4; BO_{12} and BO_{17} produced clear, yellow oils after drying.) The SO_3 group insertion was confirmed by FT-IR (Figure 5.1), where new peaks at 1270, 750 and ~ 600 cm^{-1} indicate the formation R-O-SO_2-$O^{-+}Na$.[7] Average BO lengths were determined by ^1H NMR in $CDCl_3$.

$$\textit{1a} \quad CH_3\text{–}CH_2\text{–}(O\text{–}CH_2\text{–}\underset{\underset{\underset{CH_3}{|}}{\overset{|}{CH_2}}}{CH})_n\text{–}O\text{–}H \quad \xrightarrow[DMF]{SO_3} \quad \textit{1b} \quad CH_3\text{–}CH_2\text{–}(O\text{–}CH_2\text{–}\underset{\underset{\underset{CH_3}{|}}{\overset{|}{CH_2}}}{CH})_n\text{–}O\text{–}\underset{\underset{O}{||}}{\overset{\overset{O}{||}}{S}}\text{–}O^{-+}Na$$
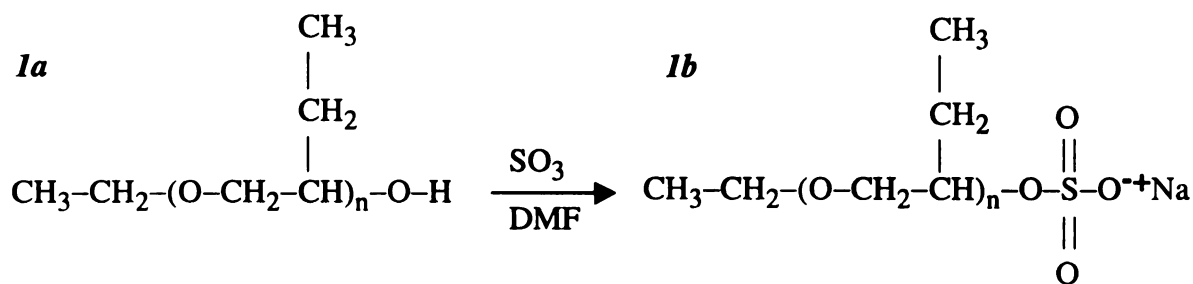
Scheme 5.1. Poly(1,2-butylene oxide) oligomer structure before (1a) and after (1b) sulfonation.

After the material cooled, I weighed out 0.0395 g into a vial and added 3.243 g of DI water to create a 1.20 wt % dispersion. I agitated the vial vigorously and set it aside. Light scattering data suggested a particle diameter of between 170 and 190 nm.

Interestingly, after a few months, the $EtBO_4SO_4Na$ and $EtBO_{11}SO_4Na$ underwent phase separation. The oligomers formed a clear, upper phase and a viscous, opaque, lower phase that contained a white precipitate. Dispersions prepared from the upper phase did not form vesicles, but phase separated from water after mixing. All of the vesicle data presented here were obtained from samples prior to any phase separation.
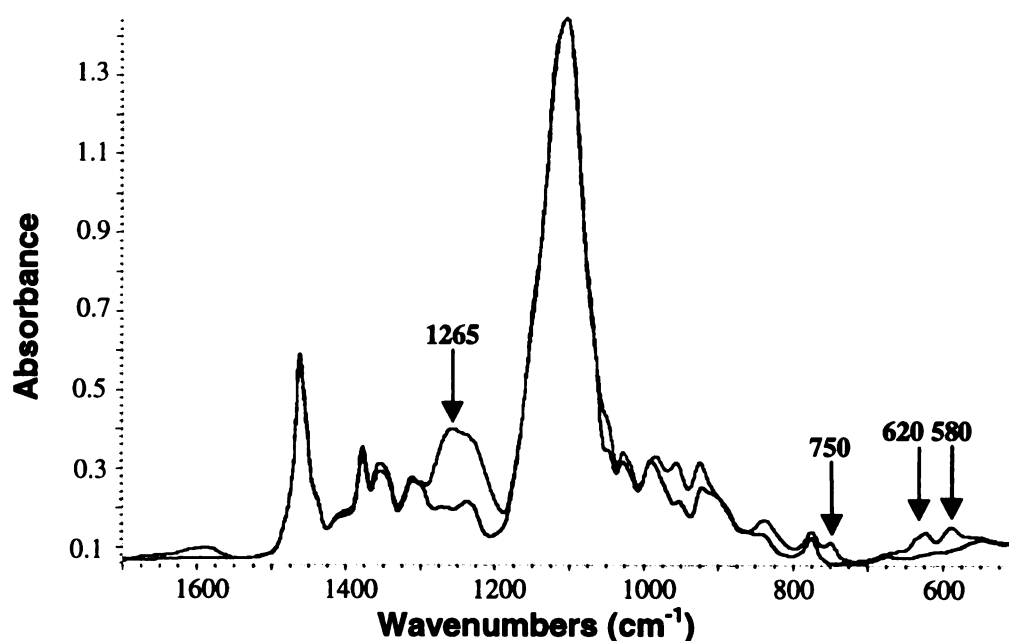
Figure 5.1. FT-IR spectra of the BO_{17} oligomer before and after sulfonation.

Vesicles were formed by placing 1 drop (~ 0.03 g) of the surfactant into a 5 dram vial and adding 3 g of deionized (>17 MΩcm) water. The vial was then agitated by hand

to produce structures. Dispersions were allowed to stand for 24 hours before examination.

To compare the thermal stabilities of $EtBO_{11}EO_{11}$ and $EtBO_{11}SO_4Na$, 1 wt % dispersions of each material were prepared by hand agitation and subsequent ultra-sonication (Ultrasonic Processor, Model 130, Cole-Parmer Instruments, Vernon Hills, IL; 3 mm probe). The $EtBO_{11}EO_{11}$ copolymer forms large MLV structures using the hand-shaking methods, so ultra-sonication was used to reduce these structures to a diameter similar to that spontaneously formed by the $EtBO_{11}SO_4Na$ oligomer. To be experimentally consistent, both dispersions were ultra-sonicated using the same conditions. The dispersions were exposed to ultra-sonication for 2 min at 10 watts using a "4 sec on/ 1 sec off" cycle, while the vials were cooled in an ice-water bath.

Prior to light-scattering measurements (Brookhaven 90Plus, Brookhaven Corporation, Holtsville, New York, USA), the 1 wt % dispersions were allowed to equilibrate in a water bath at the desired temperature for at least 16 h. The dispersions were evaluated at the equilibrium temperature, and returned to the water bath to equilibrate at a new temperature.

Light scattering data were analyzed using the CONTIN algorithm and intensity-weighted measurements. The average diameter was calculated from the mean values of at least 5 separate measurements. Structures were also examined using cryo-SEM (JEOL JSM-6320FV) as described previously in section 3.5.

5.3   *Vesicle Formation and Stability*

Vesicle formation requires that the hydrophobe length exceed some minimal value. Nakamura et al. showed that BO sulfonates with less than 3 BO units displayed no interfacial tension or film formation characteristics on water, so we felt that the combination of the ethoxide initiator and 4 BO units would be about the minimum BO block length necessary to initiate micellization.[8] We chose a maximum BO length of less than 20 units because our experience with $EtBO_{20}EO_n$ copolymers showed that spontaneous vesicle formation from materials containing such a large hydrophobe was difficult. This is likely due to the high energy needed to disperse such a large hydrophobe prior to self-assembly into an ordered structure. Therefore, the three oligomers synthesized for this study ($EtBO_4SO_4Na$, $EtBO_{11}SO_4Na$, and $EtBO_{17}SO_4Na$) were intended to represent probable minimum and maximum BO lengths for spontaneous vesicle formation as well as a composition comparable to the most common BO/EO material we previously studied ($EtBO_{11}EO_{12}$). While having low polydispersity, these materials are not monodisperse, and the formulae listed represent the average oligomeric compositions of each surfactant.

Gentle agitation was sufficient to produce structures from $EtBO_4SO_4Na$ and $EtBO_{11}SO_4Na$; however, $EtBO_{17}SO_4Na$ required sonication for complete surfactant dispersion. Light scattering showed that the $EtBO_4SO_4Na$ oligomer spontaneously produced vesicles with an intensity weighted mean particle diameter of 180 nm, with more than 95% of the particles having diameters between 88 and 263 nm. The $EtBO_{11}SO_4Na$ oligomer spontaneously formed vesicles with a mean diameter of 140 nm and greater than 95% of these particles have diameters between 62 and 188 nm. A

second dispersion of $EtBO_{11}SO_4Na$ was ultra-sonicated for 2 min to yield vesicles with diameters of 130 nm.

$EtBO_{17}SO_4Na$ produced vesicles with a mean diameter of 150 nm after 30 sec of ultra-sonication. This size, which varied by less than 30% from measurement to measurement, is on the order of that seen with BO/EO surfactants after ultra-sonication. The vesicles showed less than a 10 % change in particle size after standing at room temperature for 30 days.

Cryo-SEM images are consistent with light-scattering data taken from the same dispersion. Images such as Figure 5.2 show that $EtBO_{11}SO_4Na$ spontaneously forms
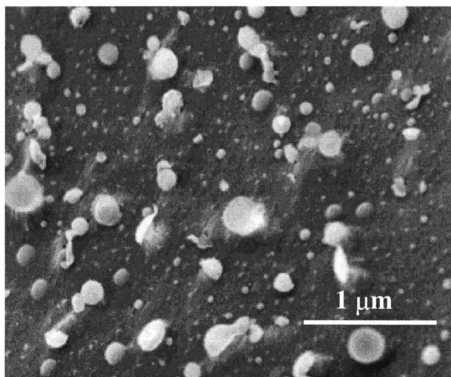
Figure 5.2. Cryo-SEM image of spontaneously-formed vesicles in a 1 wt% $EtBO_{11}SO_4Na$ dispersion.

spherical particles with 30- to 300-nm diameters, and the majority of structures are in the

50 to 150 nm range. This sample was aged for 3 weeks prior to examination.

As would be expected for an anionic surfactant, structures formed from sulfonated

copolymers are more stable at high temperatures than vesicles formed from ethoxylated

copolymers. Figure 5.3 shows the diameters of $EtBO_{11}SO_4Na$ and $EtBO_{11}EO_{12}$

structures as a function of temperature. The graph indicates that both ethoxylated and
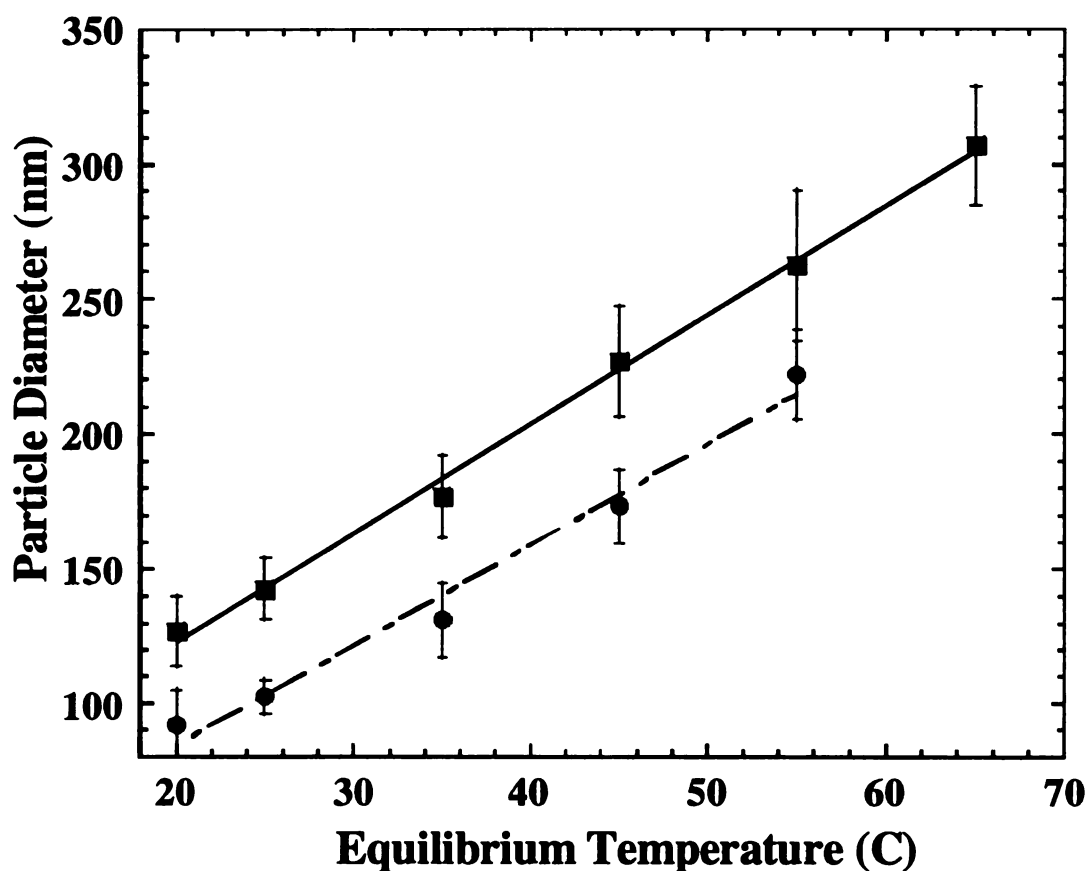
Figure 5.3. Diameters of vesicles formed from ultra-sonicated $EtBO_{11}EO_{12}$ (●) and

$EtBO_{11}SO_4Na$ (■) (1 wt %) as a function of temperature. (Error bars represent standard

deviations of the mean of 5 measurements.)

sulfonated BO structures increase in diameter at about the same rate upon heating. For both surfactants, the increase in particle size is likely due to a decrease in the head group area resulting from thermally induced dehydration.[3,9] Dehydration decreases the radius of curvature for the bilayer and increases the vesicle diameter. However, at temperatures greater than 65 °C, the ethoxylated surfactant loses its amphiphilic properties and phase separates from the aqueous medium, while $EtBO_{11}SO_4Na$ does not. (The $EtBO_{11}SO_4Na$ structures are stable enough that reproducible light-scattering data can still be collected at 75 °C, though the ability of the instrument to maintain that temperature accurately is questionable.)

To further evaluate the thermal stability of the anionic surfactant, a 1 wt % dispersion of $EtBO_{11}SO_4Na$ was sealed in a glass bottle and placed in an oven at 100 °C for 9 days. Examination of the hot sample showed that while the dispersion had become more opaque, there was no indication of phase separation or an increase in sample viscosity. The cooled sample returned to its original appearance.

Since hydrolysis of the sulfate group in an aqueous environment is a possibility, the chemical stability of the vesicles was evaluated. A 1 wt % dispersion of $EtBO_{17}SO_4Na$ was prepared with ultra-sonication and found to have a mean particle diameter of 140 nm by light scattering. The sample then stood at room temperature for 5 months with less than a 10% decrease in average particle diameter. Thus, at pH 6.8 these vesicles are extremely stable.

5.4   Conclusions

Spontaneous formation of vesicles from both sulfonated BO oligomers and BO/EO copolymers indicates that the BO hydrophobe, not the EO head group, is primarily responsible for the formation of BO/EO vesicles. Spontaneous structure formation by sulfonated BO oligomers occurs for average hydrophobe lengths of 4 and 11 BO units, and vesicles also form from sulfonated BO_{17} oligomers upon ultra-sonication. Structures of all three sulfonated oligomers were between 120 and 175 nm in diameter, which is consistent with the size expected from a surfactant geometry model.[2] Furthermore, the BO sulfate structures are stable for at least 5 months at room temperature and give no sign of phase separation after standing at 100 °C for more than a week. These structures are much more temperature stable than vesicles formed from $EtBO_{11}EO_{12}$, as the ethoxylated materials phase separate at 65 °C.

5.5   References

(1)   Israelachvilli, J. N.; Mitchell, D. J.; Ninham, B. W. *J. Chem. Soc., Faraday Trans. 2* **1976**, *72*, 1525-1568.

(2)   Crook, E. H.; Fordyce, D. B.; Trebbi, G. F. *J. Phys. Chem.* **1963**, *67*, 1987-1994.

(3)   Rosen, M. J. *Surfactants and Interfacial Phenomena*, Second ed.; Wiley-Interscience: New York, 1989, pp 70-80.

(4)   Schmolka, I. R. *J. Am. Oil Chemists Soc.* **1991**, *68*, 206.

(5)   Asinger, F.; Geiseler, G.; Muller, G. *Chem. Ber.* **1960**, *93*, 2491-2497.

(6)   Kelly, K. K.; Matthews, J. S. *J. Org. Chem.* **1971**, *36*, 2159-2161.

(7)   Colthup, N. B. *Journal of the Optical Society of America* **1950**, *40*, 397-400.

(8)   Nakamura, M.; Sakashita, T.; Mori, T.; Yano, W.; Kimura, W. *Yukagaku* **1972**, *21*, 95-99.

(9)   Corkill, J. M.; Goodman, J. T.; Tate, J. R. *Trans. Faraday. Soc.* **1966**, *62*, 979.

Chapter 6

Summary and Future Work

6.1 *Background*

This research was based primarily on the micellar model developed by

Israelachvili et al. that states that micellar shape formed during self-assembly is

dependent on surfactant geometry. Limitations on the surfactant packing configuration,

which determine the shape that the aggregate will form, are a function of hydrophobe

volume and length, and hydrophilic head group diameter. The twin tails of phospholipids

facilitate vesicle formation because the large hydrophobe volume makes packing the tail

into a micelle core unfavorable. We hypothesized that a single tail surfactant with a

similar volume to length ratio would also produce vesicles.

The BO oligomer has a much larger volume-to-length ratio than most

hydrophobes, making it a potential substitute for the two tails in phospholipids vesicles.

This hydrophobe also offers the advantage of being much more hydrophobic that the

propylene oxide monomer commonly used in nonionic surfactants. Increased

hydrophobicity enhances the driving force for self-assembly and increases the stability of

structures formed from BO containing surfactants.

Selection of an appropriate head group was not straightforward because the actual

size of surfactant head groups *in solution* is not well known. Thus, we chose to use a

nonionic head group because we could alter its size easily and to a greater extent than

with typical ionic head groups. By varying the EO block length we hoped to find the

correct hydrophile to form vesicles from the BO hydrophobe.

6.2 *Summary*

Copolymer synthesis is a two-step anionic polymerization using an alkoxide initiator. The reaction is fast and efficient with few byproducts or side reactions. However, the transition from polymerization of the BO block to initiation of the EO block does not have 100 % efficiency, and the reaction can produce hydroxy-terminated BO oligomer instead of diblock copolymer. This has two effects: copolymer contamination with a hydrophobic material and an increase in the average EO block length for the copolymers that do contain an EO segment.

After evaluating numerous BO/EO diblock compositions I found that when the EO block length is less than 16 and greater than 6, and the BO block length is less than 17 and greater than 4, the copolymer forms vesicles spontaneously upon mixing with water. For similar EO block lengths, and for BO blocks less between 17 and 25 units, vesicles could be formed using ultra-sonication of the dispersion. However, determination of composition using NMR analysis alone is not sufficient to predict vesicle formation. I found that copolymer batches that had a mean composition of $BO_{10}EO_{17}$ and a high polydispersity did not form vesicles. The physical properties of the sample indicated an average that a substantial fraction of these copolymers had an EO block length greater than 17 units. Fractionation of this material using hexane and low temperature centrifugation isolated the copolymer with shorter EO blocks to yield copolymer that did spontaneously produce vesicles. Thus, while mean BO/EO composition is important to vesicle formation, a narrow distribution of EO block lengths is also important. To more accurately determine the range of EO block lengths in a

batch, I used mass spectrometry, which provided important information concerning BO oligomer concentration and surfactant composition.

For relatively mono-disperse copolymers with a nominal composition of $BO_{12}EO_{12}$, vesicles formed at copolymer concentrations between 0.05 and 10 wt % upon simple hand-shaking. However, at concentrations greater than 25 wt %, vesicle formation required ultra-sonication. BO/EO structures were stable for more than a 24 months at room temperature with little or no discernible change in particle size distribution. Typically more than 80 % of the copolymer added was found in vesicular structures. I also discovered that while vesicle formation is spontaneous, the size distribution of the structures is a function of formation method. Simple agitation produces micron-sized vesicles, but if the copolymer/ water mixture is ultra-sonicated, the particles will have a diameter of about 70 nm. The same effect occurs if the mixture is extruded through a polycarbonate filter. Solvent exchange processes also generate structures that tend to be in the 70 – 100 nm range. If the copolymer is brought into contact with water at ~1 wt % level and allowed to hydrate without agitation, giant vesicles with diameters of 1 mm or greater can be produced. However, the process must include thermal oscillations (> 10 °C) in order for multi-lamellar giant vesicle formation to occur.

Once formed, these structures demonstrate good mechanical stability. Shear applied by mixing, sonication or shaking had no effect on mean particle size distribution when performed at room temperature. This stability is probably due in part to the liquid crystalline nature of these structures. However, plane-polarized light microscopy shows that the structures undergo a phase transition at about 40 °C that would probably reduce

this stability. Cooling the structures reformed the liquid crystalline morphology. In fact, samples heated to 80 °C for three hours, then cooled and agitated showed the same mean particle diameter as the original dispersion.

To confirm that the BO oligomer was critical to vesicle formation, I replaced the EO block with an SO_3^- group that is similar in size to the "predicted" diameter of an EO_{15} block. The sulfonated compositions also formed vesicles upon mixing with water when the BO block was 12 units long or less. The SO_3^- oligomers showed improved thermal stability versus the ethoxylated copolymers.

Because BO/EO vesicles consist of both hydrophilic and hydrophobic regions, I examined the capacity of the structures to encapsulate both hydrophilic and hydrophobic substrates. I used a fluorescein dye as the hydrophilic compound and loaded the vesicles by mixing the copolymer with 100 ppm aqueous fluorescein. The vesicles were then passed through a Sephadex column to separate the unencapsulated dye from the vesicles. Less than 20 % of the fluorescein leaked out of the vesicles over a one month period. I also found that I could add dodecane to the copolymer in a 1:1 mole ratio and produce vesicular structures. There was no evidence of leakage from these vesicles over a two month period.

6.3 *Future Research*

Because of the versatility of these materials, there are several areas that would be of interest to explore. Phase diagrams showed that the presence of a hydrophobe has an impact on structure formation. We also know from mass spectrometry data that there is typically residual BO oligomer in each batch of copolymer. It would be interesting to

develop a technique for removing the BO oligomer without extracting diblock copolymer that has short EO blocks. One solvent which is promising for such work is dimethyl sulfoxide (DMSO), which is quite effective at solubilizing EO but poor at dissolving BO.

A second area of study would be the effect of EO block polydispersity on vesicle formation. Surfactant polydispersity and its impact on vesicle formation is a controversial topic. Some have argued that polydispersity is necessary to allow those molecules on the concave portion of the structure to assume a smaller head group diameter than those on the convex side. We have shown that excessive polydispersity can hinder vesicle formation, even if the mean composition is within the desired range. One means of investigating the effect of polydispersity on structure formation would involve the synthesis of mono-disperse BO/EO diblock copolymers.

Lithium-based initiators allow for the addition of single EO units per run.[1,2] Since an EO block of only 8 or 10 units is sufficient to produce structures, making a mono-disperse batch of $BO_{10}EO_8$ would be a realistic target. This material could be used as a model to study the effects of added BO or other BO/EO copolymers on vesicle formation. Further vesicles from these materials could be used to accurately determine the mean EO head group diameter *in solution* as a function of EO block length. Preparation of a second mono-disperse copolymer with a composition of $BO_{10}EO_{25}$ would be time consuming, but mixing this with $BO_{10}EO_8$ would show the impact of EO polydispersity on vesicle formation.

Another area of interest is to use the static vesicle formation process employed with $BO_{12}EO_{12}$ to form giant vesicles with other copolymers, preferably those with larger EO blocks. Clearly identifying the conditions necessary for giant structure

formation could yield a better understanding of the mechanism of vesicle formation from these materials. This would provide additional information on the thermodynamics involved and the stability of vesicles formed from BO/EO copolymers.

The BO oligomer sulfonation also presents some research opportunities. We have shown that the anionic oligomer forms vesicles spontaneously upon hydration, and while there is no evidence to suggest that cationic materials would not do the same, it would be worth demonstrating. Others have shown that the blending of anionic and cationic single-tailed surfactants can lead to spontaneous vesicle formation, so the blending of anionic and cationic BO oligomers would also be interesting. In fact, preparation of a variety of BO oligomers with various head groups could provide some insight into the size of the head group *in solution*, an area not well understood at the moment.

Finally, ethoxylation of oligomers that have the same or similar V/l_c ratios as the BO oligomer would provide an expanded source of potential vesicle-forming hydrophobes. These new hydrophobe may offer advantages over BO in terms of cost, ease of preparation, or versatility. The resulting surfactants may provide increased structural stability, improved bio-compatibility or even enhanced biodegradation.

6.4 References

(1)   Guilbert, Y.; Brossas, J. *Polymer Bulletin (Berlin, Germany)* **1979**, *1*, 293-298.

(2)   Cabasso, I.; Zilkha, A. *Journal of Macromolecular Science, Chemistry* **1974**, *A8*, 1313-1324.

APPENDICES

Geometric Limitations Imposed by Surfactant Packing Shape

A1 *The Critical Packing Factor Model*

The critical packing factor model is based on the limitations imposed on a structure by its geometric shape. As a first example consider a sphere. Previous discussions (section 1.5) have described the number of aggregates in a spherical micelle as N. The volume of a sphere is shown in equation A1.1.

$$V = \frac{4}{3}\pi R^3$$

<div align="right">eq. A1.1</div>

The surface area of a sphere is given by equation A1.2.

$$A = 4\pi R^2$$

<div align="right">eq. A1.2</div>

Dividing A1.1 by A1.2 yields R/3 or the following relationship (equation A1.4) that is fixed for any sphere.

$$\frac{R}{3} = \frac{V}{A}$$

<div align="right">eq. A1.3</div>

Here R is the radius of the sphere which, in terms of the micelle, corresponds to the hydrophobe length, l_c. This equation can be rearranged to produce equation A1.4 which shows the relationship between v, a_o, and l_c for a spherical micelle.

$$\frac{v}{a_o l_c} = \frac{1}{3}$$

<div align="right">eq. A1.4</div>

This value of $1/3$ sets an upper limit on the ratio that these values can have and still produce a sphere. Therefore, in order to form a sphere, the ratio of the hydrophobe volume to the product of the hydrophile head group area and the hydrophobe length must lie between 0 and $1/3$. These same geometric limitations can be shown for cylindrical micelles and bilayer structures.

A2. *Aggregation number versus Head Group Size*

The volume of each surfactant molecule in the structure is that of a right circular cone (equation A2.1).

$$v = \frac{1}{3}\pi r^2 h \qquad\qquad \text{eq. A2.1}$$

Here r is the radius of the head group while h is the length of the hydrophobe, which is the same as R for the micelle. We can divide equation A1.1 by A2.1 to determine the number of surfactant molecules, N, in a given micelle.

$$N = \frac{4\pi}{3}\frac{R^3}{v} \qquad\qquad \text{eq. A2.2}$$

By substitution of a for πr^2 in equation A2.1, equation A2.2 can be re-written as equation A2.3.

$$N = \frac{4\pi R^2}{a} \qquad\qquad \text{eq. A2.3}$$

This equation shows an inverse relationship between the aggregation number, N, and the head group area, a which is consistent with Figure 1.3.

Appendix B

Processing the Mass Spectrometry Data

Detailed information such as residual BO oligomer concentration and the distribution of copolymer block lengths can be obtained by analysis of mass spectrometry data. Table B.1 presents one set of mass spectrometry (MS) raw data generated by the Analytical Lab at The Dow Chemical Company and forwarded to me for additional analysis. These data had been processed to remove contributions from multiply charged ions. Values of M_W, M_N, M_P and M_W/M_N, were calculated for the entire data set and were provided as well. Also included were graphs of each data set shown in Figure B.1.

The data were initially arranged in order of increasing mass as shown in Table B.1. In the second column, $MW - 18$, the mass of the ammonium ion (18.0344 amu) was subtracted from the detected mass to determine the actual mass of the molecule. The signal intensity for that mass was recorded in column 3, *Intensity*. I assumed that little molecular fragmentation occurred during analysis, and that all data represented intact copolymers. Thus, the ratio of the intensities of any two masses that represent specific copolymer compositions should correspond to the molar ratio of those compositions present in the sample.

I prepared a second table that lists the calculated masses of BO/EO compositions ranging from BO_3EO_0 to $BO_{28}EO_{28}$. (Table B.2 shows a portion of these data.) I used masses of 72.0575 amu for each BO group, 44.0262 amu for each EO group and 46.0419 amu for each chain initiator. These are the average masses of each unit assuming a typical distribution of the isotopes. However the masses of each composition are unique

only within a limited range. Note that the value of $BO_{14}EO_0$ is quite similar to the value of BO_3EO_{18}, differing by less than 0.20 amu. This occurs because 11 BO units have approximately the same mass as 18 EO units, so copolymers BO_xEO_y (y > 18) have a mass similar to copolymers $BO_{x+11}EO_{y-18}$. Thus, copolymer batches having narrow BO polydispersity (< 11 units) minimize the confusion over assignment of composition to a given mass by restricting the mass to a unique composition. When a specific m/z value could be assigned to more than one composition, I initially assigned it to the composition whose calculated mass was closest to the actual mass, then later made adjustments if needed when all of the intensities had been assigned. For example, if an intensity value was assigned to $BO_{14}EO_3$, but at the end of the analysis there were no other compositions having a BO length of 14, I would probably transfer that intensity value to BO_3EO_{21}, particularly if there were other long EO compositions in the batch, or if there were no intensity values for any compositions containing BO_{13}.

To begin the analysis, I sorted the raw data by decreasing intensity and inserted the column labeled *Range* (Table B.3). Using the *MW – 18* mass and the compositional masses found in Table B.2, I matched the recorded mass to a BO/EO composition and entered the intensity for that mass into a third Excel spreadsheet like the one shown in Table B.4. The differences between the recorded mass and the compositional mass usually fell into one of 4 groups. When the actual masses differed by less than 1.15 amu from the calculated mass, I labeled the accuracy *range* value "1". For *range* "2", the actual mass was ~18 amu less than the calculated compositional mass. (These materials may have lost an H_2O molecule.) A third type of data (*range* "3") had masses ~29 amu less than a calculated composition (perhaps the loss of a CH_3CH_2 group), and m/z values

that did not match an BO/EO composition were given a *range* value of "u" (unknown). The majority of the data used for compositional mapping (> 95 %) had *range* values of "1", and in general, the actual masses were between − 0.8 and + 0.5 amu of their corresponding compositions.

As an example, the actual mass ($MW - 18$) of the first entry of Table B.3 is 1162.866 dal. The corresponding composition (Table B.2), with a mass of 1162.853, is found at $EO_{10}BO_9$. Thus, on Table B.4, under composition "$BO_{10}EO_9$", an intensity value of 4830 was entered. Finally on Table B.3, in the *Range* column, a 1 is recorded to note that that the ($MW - 18$) value (1162.866) was within 1.5 amu of the calculated mass for $BO_{10}EO_9$. If another ($MW - 18$) value were found that matched $BO_{10}EO_9$, for example, 1162.861, then the intensity of that mass would also be entered under the composition "$BO_{10}EO_9$". Summation of all of the intensities for a particular composition yielded a total intensity. (The value shown for "$BO_{10}EO_9$" in Table B.4 is 4880 because the total of all of the intensities recorded for that composition is 4880.) This process was continued until the first 70 % of the total intensity, when arranged by decreasing intensity, was matched to a composition.

When all of the entries were made to Table B.4, the sum of the intensities for a given composition was plotted as a function of BO and EO block lengths. Figure B.2 is the graph for copolymer L120-15A, a material shown by NMR to have a composition of BO_6EO_4. The MS data indicate an average composition of $BO_{10}EO_6$, but they also show high levels of BO oligomer. The presence of uncapped oligomer is an important factor in explaining the phase behavior of this material.

In cases when the BO oligomer was available for analysis, MS data of this material aided in determining the copolymer compositional profile. The BO oligomer distribution for batch M1038 is shown in Figure B.3. I first plotted the BO data to determine the minimum and maximum BO oligomer lengths as well as relative amounts of each composition. This was done by subtracting the ethoxide initiator from each block (- 46.0419) then dividing the remaining mass by 72.0575. The result was the BO block length, which was generally close to integer values. (Integer values are represented by vertical lines in Figure B.3.) Isotopic compositions were typically within 1 amu of the most intense peak and appear as lower intensity points on the same line. Contaminants or byproducts appear as materials not found on an integer value and can be seen in the figure as the low intensity deviations. Note that the range of BO oligomers for BO-M1038 is about BO_6 to BO_{22}. I used these data limits to help resolve questions about matching a mass to a composition when two calculated masses were similar to the actual mass.

Table B.1. A portion of the mass spectrometry data for copolymer L1150-51A

$(BO_{11}EO_{12})$, arranged by increasing mass, after being processed to remove multiple-

charge signals.

| Molecular Weight	MW – 18	Intensity
319.1746	301.1402	3.78E+01
327.2177	309.1833	7.99E+01
335.2996	317.2652	7.26E+01
341.2262	323.1918	2.22E+01
345.3176	327.2832	1.34E+02
349.2039	331.1695	3.88E+01
358.2583	340.2239	1.01E+02
363.2011	345.1667	2.77E+01
372.2481	354.2137	5.17E+01
380.3179	362.2835	4.13E+01
381.3273	363.2929	1.88E+01
388.2802	370.2458	2.69E+01
389.2590	371.2246	5.03E+01
393.2210	375.1866	3.89E+01
402.2861	384.2517	1.94E+02
407.2470	389.2126	8.79E+01
415.2693	397.2349	3.64E+01
416.2724	398.2380	8.01E+01
424.3780	406.3436	5.48E+01
430.3210	412.2866	5.56E+01
432.2984	414.2640	1.20E+02
433.2211	415.1867	3.79E+01
437.2598	419.2254	7.08E+01
444.3050	426.2706	6.22E+01
446.3056	428.2712	1.94E+02
447.3542	429.3198	3.65E+01
451.2766	433.2422	9.00E+01
452.3735	434.3391	1.28E+02
456.9733	438.9389	4.11E+01
460.3132	442.2788	1.20E+02
465.2775	447.2431	3.59E+01
472.3450	454.3106	4.81E+01
474.3278	456.2934	9.84E+01
476.3259	458.2915	1.72E+02
477.3170	459.2826	9.49E+01
479.4138	461.3794	9.89E+01
481.1236	463.0892	7.91E+01
483.3810	465.3466	7.68E+01
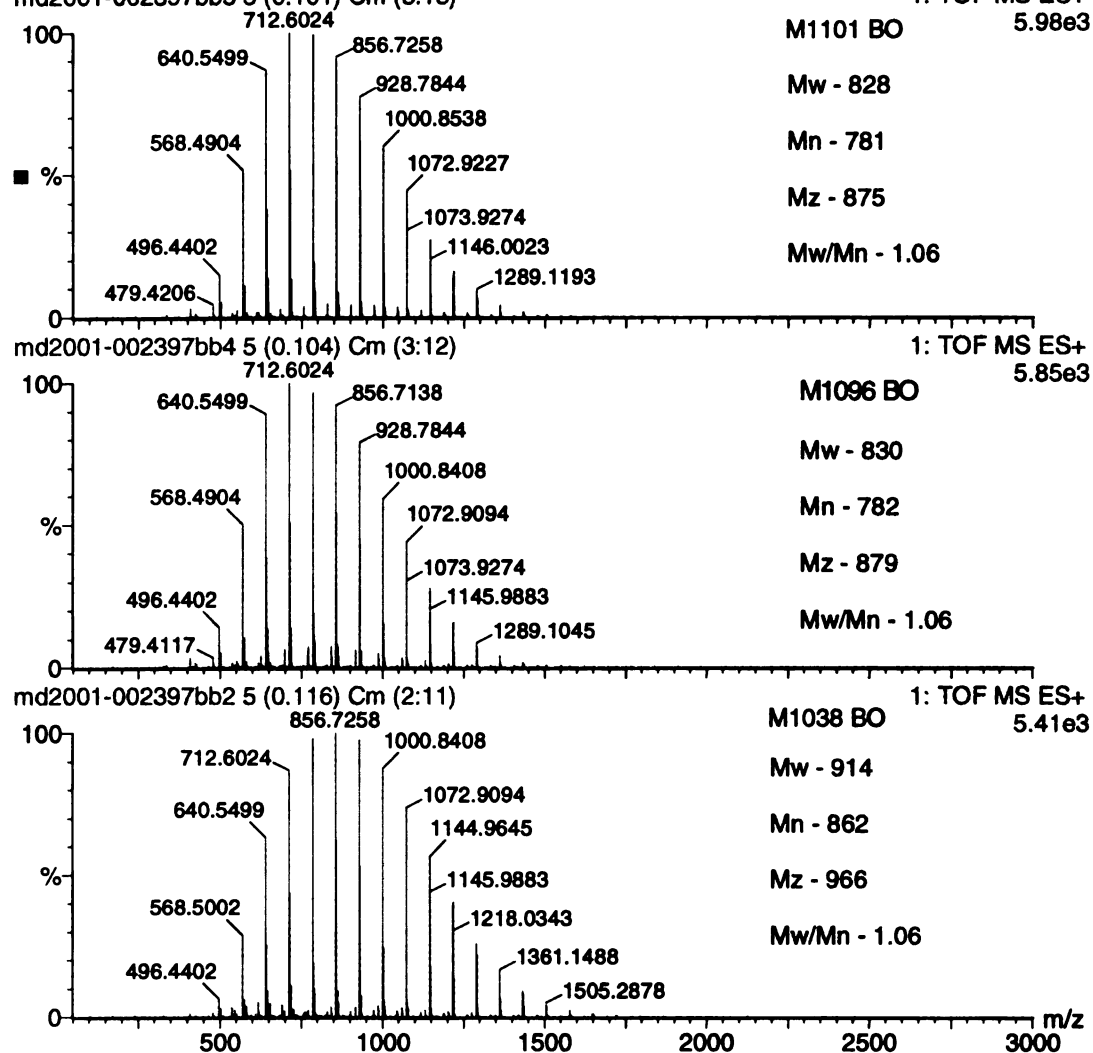
Figure B.1. Mass spectra of three BO oligomers along with calculated average molecular weights and polydispersities.

Table B.2. Calculated masses of BO/EO diblock copolymers for compositions BO_3EO_0 through $BO_{14}EO_{24}$.

	BO_3	BO_4	BO_5	BO_6	BO_7	BO_8	BO_9	BO_{10}	BO_{11}	BO_{12}	BO_{13}	BO_{14}
EO_0	262.214	334.272	406.329	478.387	550.444	622.502	694.559	766.617	838.675	910.732	982.790	1054.847
EO_1	306.241	378.298	450.356	522.413	594.471	666.528	738.586	810.643	882.701	954.758	1026.816	1098.873
EO_2	350.267	422.324	494.382	566.439	638.497	710.554	782.612	854.669	926.727	998.784	1070.842	1142.899
EO_3	394.293	466.351	538.408	610.466	682.523	754.581	826.638	898.696	970.753	1042.811	1114.868	1186.926
EO_4	438.319	510.377	582.434	654.492	726.549	798.607	870.664	942.722	1014.779	1086.837	1158.894	1230.952
EO_5	482.345	554.403	626.460	698.518	770.576	842.633	914.691	986.748	1058.806	1130.863	1202.921	1274.978
EO_6	526.372	598.429	670.487	742.544	814.602	886.659	958.717	1030.774	1102.832	1174.889	1246.947	1319.004
EO_7	570.398	642.455	714.513	786.570	858.628	930.685	1002.743	1074.800	1146.858	1218.916	1290.973	1363.031
EO_8	614.424	686.482	758.539	830.597	902.654	974.712	1046.769	1118.827	1190.884	1262.942	1334.999	1407.057
EO_9	658.450	730.508	802.565	874.623	946.680	1018.738	1090.795	1162.853	1234.910	1306.968	1379.025	1451.083
EO_{10}	702.477	774.534	846.592	918.649	990.707	1062.764	1134.822	1206.879	1278.937	1350.994	1423.052	1495.109
EO_{11}	746.503	818.560	890.618	962.675	1034.733	1106.790	1178.848	1250.905	1322.963	1395.020	1467.078	1539.135
EO_{12}	790.529	862.586	934.644	1006.702	1078.759	1150.817	1222.874	1294.932	1366.989	1439.047	1511.104	1583.162
EO_{13}	834.555	906.613	978.670	1050.728	1122.785	1194.843	1266.900	1338.958	1411.015	1483.073	1555.130	1627.188
EO_{14}	878.581	950.639	1022.696	1094.754	1166.811	1238.869	1310.926	1382.984	1455.042	1527.099	1599.157	1671.214
EO_{15}	922.608	994.665	1066.723	1138.780	1210.838	1282.895	1354.953	1427.010	1499.068	1571.125	1643.183	1715.240
EO_{16}	966.634	1038.691	1110.749	1182.806	1254.864	1326.921	1398.979	1471.036	1543.094	1615.151	1687.209	1759.266
EO_{17}	1010.660	1082.718	1154.775	1226.833	1298.890	1370.948	1443.005	1515.063	1587.120	1659.178	1731.235	1803.293
EO_{18}	1054.686	1126.744	1198.801	1270.859	1342.916	1414.974	1487.031	1559.089	1631.146	1703.204	1775.261	1847.319
EO_{19}	1098.712	1170.770	1242.827	1314.885	1386.943	1459.000	1531.058	1603.115	1675.173	1747.230	1819.288	1891.345
EO_{20}	1142.739	1214.796	1286.854	1358.911	1430.969	1503.026	1575.084	1647.141	1719.199	1791.256	1863.314	1935.371
EO_{21}	1186.765	1258.822	1330.880	1402.937	1474.995	1547.052	1619.110	1691.167	1763.225	1835.283	1907.340	1979.398
EO_{22}	1230.791	1302.849	1374.906	1446.964	1519.021	1591.079	1663.136	1735.194	1807.251	1879.309	1951.366	2023.424
EO_{23}	1274.817	1346.875	1418.932	1490.990	1563.047	1635.105	1707.162	1779.220	1851.277	1923.335	1995.392	2067.450
EO_{24}	1318.844	1390.901	1462.959	1535.016	1607.074	1679.131	1751.189	1823.246	1895.304	1967.361	2039.419	2111.476

Table B.3. A portion of the copolymer L1150-51A mass spectrometry data, arranged by increasing intensity, and including a "*range*" designation.

Range	Molecular Weight	MW – 18	Intensity
1	1180.9	1162.866	4.83E+03
1	1225	1206.966	4.74E+03
1	1108.9	1090.866	4.68E+03
1	1152.9	1134.866	4.63E+03
1	1136.9	1118.866	4.61E+03
1	1064.8	1046.766	4.45E+03
1	1253	1234.966	4.41E+03
1	1036.8	1018.766	4.40E+03
1	1269	1250.966	4.39E+03
1	1020.8	1002.766	4.39E+03
1	1208.9	1190.866	4.20E+03
1	1297	1278.966	4.16E+03
1	1080.8	1062.766	4.13E+03
1	1196.9	1178.866	4.09E+03
1	1092.9	1074.866	4.07E+03
1	992.8	974.7656	3.97E+03
1	1124.9	1106.866	3.95E+03
1	1164.9	1146.866	3.81E+03
1	1341.1	1323.066	3.81E+03
1	948.7	930.6656	3.80E+03
1	1325	1306.966	3.79E+03
1	1313	1294.966	3.76E+03
1	1048.8	1030.766	3.75E+03
1	1281	1262.966	3.70E+03
1	1120.9	1102.866	3.57E+03
1	976.8	958.7656	3.54E+03
1	1168.9	1150.866	3.53E+03
1	964.8	946.7656	3.52E+03
1	1008.8	990.7656	3.50E+03
1	1240.9	1222.866	3.48E+03
1	784.7	766.6656	3.45E+03
1	856.7	838.6656	3.42E+03
1	1052.8	1034.766	3.42E+03
1	1237	1218.966	3.34E+03
1	928.8	910.7656	3.31E+03
1	1385.1	1367.066	3.26E+03
1	712.6	694.5656	3.24E+03
1	1369.1	1351.066	3.21E+03

Table B.4. Example of copolymer compositional distribution spread sheet showing total intensity of each composition.

(150 highest intensity peaks recorded.)

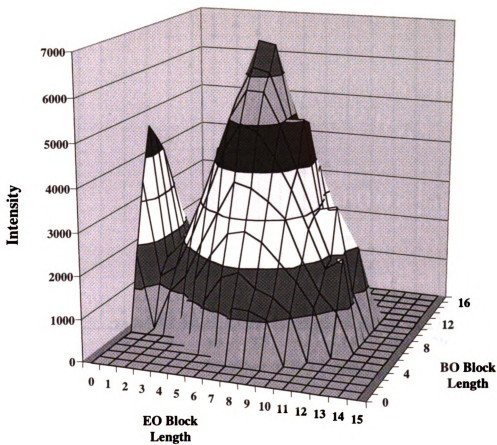|	BO_2	BO_3	BO_4	BO_5	BO_6	BO_7	BO_8	BO_9	BO_{10}	BO_{11}	BO_{12}	BO_{13}	BO_{14}	BO_{15}	BO_{16}	BO_{17}
EO_0					1770	3460	4700	4340	3940	3230	2440	1700	1190			
EO_1						1170	1510	1590	1700	1540	1270	1100				
EO_2					953	1450	1940	2170	2030	2030	1580	1490				
EO_3					1390	2260	2840	3020	3110	3988	2440	1890		962		
EO_4				1490	2260	3280	3950	4240	4270	4060	3410	2570	1690	1390		
EO_5			1170	2130	3020	4380	5080	5430	5360	4830	3970	3240	1990	1280		
EO_6			1760	2670	3770	5030	5730	6190	6750	5900	5058	3790	2230	1120		
EO_7		1230	1920	2760	3660	4860	5710	6090	6670	5980	4120	3040	1900	1320		
EO_8		1210	1590	2550	3390	4310	4960	5030	4880	4839	3280	2460	1570	945		
EO_9		1050	1430	2130	3030	3600	3950	5040	4880	3250	3650	1920				
EO_{10}			1100	1710	2080	2710	2900	2960	2590	2160	1770	2130				
EO_{11}				1150	1360	1800	1920	3050	1790	1370	1120					
EO_{12}					940	2086	1310	1030	1971	1090						
EO_{13}																
EO_{14}																
EO_{15}																
EO_{16}																

Figure B.2. Compositional profile of copolymer L120-15A (angled view). The mean composition of the above peaks is $BO_{10}EO_6$, while NMR indicated a composition of BO_6EO_4. The expected composition based on synthesis formulation was $EO_{10}BO_{10}$.
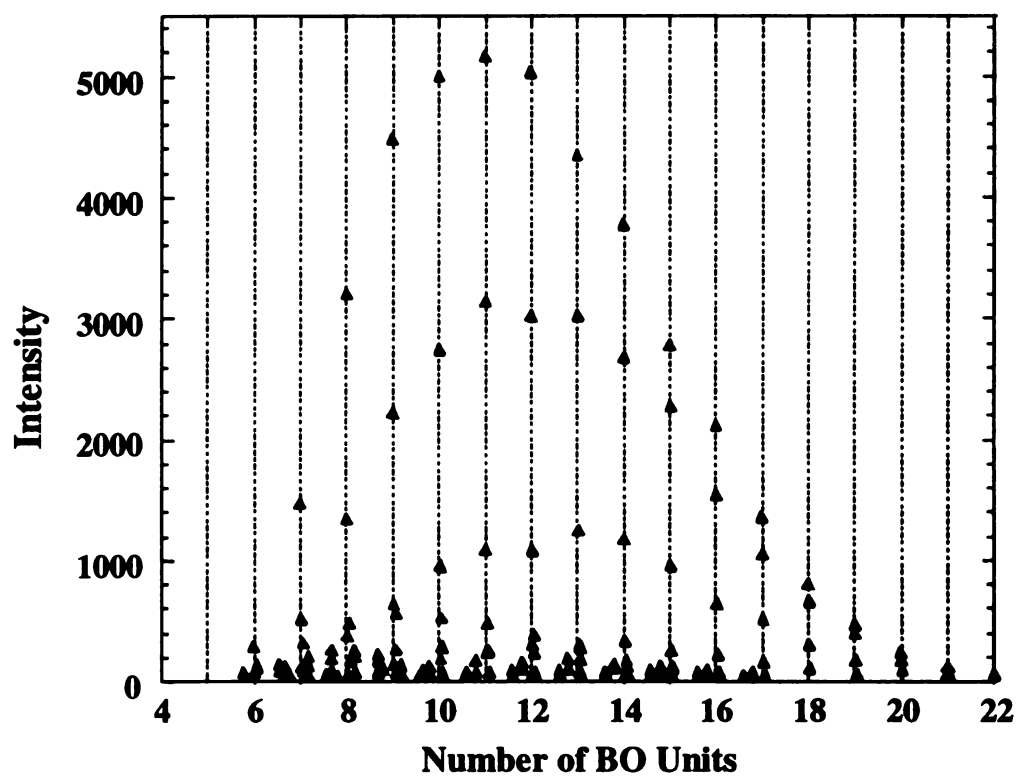
Figure B.3. The compositional distribution of the BO oligomer from Batch M1038.

Note that the majority of the material (peaks with highest intensity) lie on integer values

of BO length.